I. DIFFUSION PROCESSES IN A-PEC STARS

II. NUCLEOSYNTHESIS IN Si BURNING

Thesis by

Georges J. Michaud

In Partial Fulfillment of the Requirements

For the Degree of

Doctor of Philosophy

California Institute of Technology

Pasadena, California

1970

(Submitted September 16, 1969)

ACKNOWLEDGMENT

The author would like to thank his advisors, Drs. W. A. Fowler and W. L. W. Sargent for generously making their time and knowledge available to him. It was found that they had surprisingly large amounts of both.

The author is also indebted to Drs. W. D. Arnett, D. Bodansky, R. F. Christy, A. J. Deutsch, J. L. Greenstein, D. L. Lambert, L. Searle and J. W. Truran for very useful discussions and comments, and to Dr. E. W. Vogt for his guidance in the complex field of nuclear reactions.

I would like to thank my wife and my child for successfully keeping me from the dangers of overworking.

I would also like to thank Mrs. Alrae Tingley for the careful typing of a difficult manuscript and Ken and Susan Foster for translating some of my slang into English.

This research was made possible by fellowships from l'Hydro Québec (1965-68) and Le Ministère de l'Education du Québec (1968-69) and by grants from the National Science Foundation (GP-9433 and GP-9114) and the Office of Naval Research (Nonr-220(47)).

ABSTRACT

Two problems related to elemental abundances have been studied: the abundance anomalies in A-pec stars and the nucleosynthesis of elements between ^{28}Si and ^{59}Co.

Diffusion processes were found to lead to most of the peculiar abundances observed in A-pec stars. If it is assumed that the atmosphere is stable enough for diffusion processes to be important, gravitational settling leads to the underabundances of He, Ne and O in the stars where they are observed (that is with the θ_{eff}, log g they are observed to have). Radiation pressure leads to the overabundances of Mn, Sr, Y, Zr and the rare earths in the stars where they are observed. Si would be expected to be overabundant only if it has wide auto-ionization features. The overabundance of P is not explained.

The magnetic fields observed in A-pec stars could bring to the atmosphere the stability needed for diffusion processes to be important. They would also guide diffusion into patches leading to the periodic variation of the observed overabundances.

We have also studied the conditions necessary to generate through nuclear reactions, the abundances observed between ^{28}Si and ^{59}Co. It was found that most of the observed abundances could have been generated in a single process, Si burning.

A mixture of ^{28}Si, ^{30}Si and ^{32}S, at t = 0, in proportions leading to the observed abundance of ^{28}Si, ^{30}Si and ^{31}P was found to lead to the generation of most elements between ^{28}Si and ^{59}Co if one added up the zone where "no" Si had burned, where little had burned ...

and where all had burned.

The summation over the zones was seen to depend on essentially two parameters which most conveniently can be expressed as the lower and upper limits of integration. One then has essentially four parameters: $((N-Z)/(N+Z))_{t=0}$, $\langle A \rangle_{t=0}$, and the two limits of integration. The density was found to have no effect on our results. The temperature is more important but the range of freezing temperatures to be expected can be estimated accurately enough from the dynamic time scale. With four free parameters, one than fits the abundances of some 25 to 30 of the 41 nuclei between ^{28}Si and ^{59}Co. Some of the poorly fitted nuclei are very neutron rich nuclei (^{36}S, ^{40}A, ^{46}Ca, ^{48}Ca) which could easily have been formed by a slight exposure of the material to a neutron flux.

TABLE OF CONTENTS

I. DIFFUSION PROCESSES IN A-PEC STARS

1. INTRODUCTION

Even though peculiarities in the spectra of A stars have been known for some 60 years, and Morgan (1933) grouped the peculiar A stars together some 35 years ago, no explanation of their peculiarities has yet found general acceptance. Efforts at explaining them through unusual conditions of excitation have not been successful. Recently some authors invoked nuclear processes, but, as discussed below, these explanations also have serious shortcomings.

A-pec stars are slow rotators, and convection is of little importance for early A and late B stars. Therefore, we hypothesized that their atmospheres are stable enough for diffusion processes to become important. Radiation pressure then plays an important role. An overabundance of a given element is observed in those stars in which radiation pressure is expected to push that element into the region where lines are formed as should be expected from the diffusion hypothesis. The magnetic fields observed in those stars may help in bringing stability to the atmosphere. These fields guide diffusion in some preferred direction and may account for the observed relationships between spectral and magnetic field variations.

Briefly observational data will be reviewed noting the uncertainties in its analysis. Then we will compare the predictions of nuclear-physics models to the most reliable of the observed characteristics. We will discuss some aspects of diffusion processes: their time scales and the role of gravitational, magnetic and radiation forces. Both continuum and line absorption will be seen to be impor-

tant. Auto-ionization levels may substantially contribute to line absorption. Finally, the abundance anomalies expected from diffusion processes will be compared to the observed abundances.

2. THE OBSERVED ABUNDANCES IN A-PEC STARS

The analysis of A-pec star spectra is hampered by our ignorance of the structure of their atmosphere. The presence of strong magnetic fields and of large overabundances of certain elements may significantly alter the outer structure of the atmosphere where the lines are formed. There is however no evidence for anomalies in that part of the atmosphere where the continuum and the wing of the Balmer lines are formed. No anomalies are observed (Searle and Sargent, 1964) in the shape of the Balmer lines or in the relationship between the Balmer lines, the B-V and U-B color indices, and D, the Balmer discontinuity. However, disagreements between the abundances predicted by the infrared and visible lines of Mg and O suggest the existence of anomalies in the structure of the outer part of the atmosphere (Mihales and Henshaw, 1966). The anomalies seem to exist in both the normal and the peculiar stars. They disappear if one compares a peculiar star to a normal one. Comparative studies are then probably more reliable than "absolute" studies made with a model atmosphere of one star.

Furthermore, in determining the parameters of the atmosphere, one must be careful to use only criteria that do not depend on the abundances of elements as most elements do not have normal abundances. Not only should criteria depending on the intensity of one particular line be avoided but also those affected by line blanketing. In practice, this is not always possible. Current model atmospheres do not take into account the possibly important contri-

butions of, for instance, the overabundant metals to the total opacity. One should take into account the uncertainty introduced in θ_{eff} ($\equiv 5040/T_{eff}$ where T_{eff} is the effective temperature) and log g (g $\equiv$ gravitation constant). Therefore, to determine abundances lines must be chosen whose width is independent of θ_{eff} and log g.

We present an incomplete résumé of the data on the abundance anomalies of A-pec stars. These data have been grouped according to their reliability. One of the better established observational facts (Sargent and Searle, 1967a, Wolff, 1967) seems to be that some of the abundance anomalies depend on the effective temperature of the star. Before the systematic studies of Sargent, Searle and co-workers, it could have been argued that the apparent effective temperature dependence of the abundance anomalies is due to selection effects. However by determining the abundances of certain elements (O, Mg, Si, Mn,...) in a large number of both normal and peculiar stars, Sargent and Searle (1967a) were able to establish that certain elements (O, Si, Mn) had unusual abundances only in peculiar stars of a given range of θ_{eff}. Outside that range they measured the abundances of the same elements and they were found normal, or at least not so abnormal.

In tables 1 and 2, we have summarized the results of Sargent, Searle and co-workers. Their results for O, Si and Mn seem particularly reliable since they depend on lines whose equivalent width, for a given abundance, is relatively independent of the parameters of the atmosphere (supposing LTE). However, depending on the region of the spectrum observed, one may obtain abundances, for one element in a given star, varying by factors of up to 10. (Compare the

TABLE I

Abundance anomalies observed in A-pec stars*

	HD	Peculiarity	θ_{eff}	log g	[C/H] 1969	[O/H] 1962	[O/H] 1969	[Ne/H]	[Mg/H] 1962	[Mg/H] 1964	[Si/H] 1964	[Si/H]	[Ti/Fe]	[Cr/Fe]	[Mn/Fe]
ν For	12767	Si 4200	0.32	3.75	-0.9		-0.2	<-0.9		-1.0	+0.8	+1.1			
63 And	14392	Si 4200	0.38	3.5						-0.2	+1.7				
HR 710	15144	Sr	0.60	4.0						+0.5	+0.1		-0.02	+0.28	+0.16
21 Per	18296	Si 4200	0.45	3.0		-1.0			-0.6	-1.0	+2.0		-0.09	-0.03	+0.16
41 Tau	25823	Si 4200	0.34	3.5		-1.4	-0.1		-1.1	+0.1	+1.8	[+1.8]	-0.37	+0.04	-0.28
53 Tau	27295	Mn	0.41	4.0						-0.3	+0.1		+0.81	+0.54	+1.34
HR 1445	28929	Mn	0.40	3.5		-0.3			-0.3	+0.2	+0.5				
μ Lep	33904	Mn	0.36	3.75		-0.3	0.0		-0.5						
HR 1732	34452	Si 4200	0.27	4.0	-0.5		+0.3	<-1.3		+0.5	+2.0	+2.1			
0 Aur	38104	Eu-Cr	0.49	3.5						-0.2	<-0.8				
15 Cnc	63351	Si 4200	0.38	3.5						-0.3	+1.7				
3 Hya	72968	Sr	0.45	3.5						+0.2	<-0.9				
ν Cnc	77350	Si	0.42	3.5						+0.3	+0.4				
κ Cnc	78316	Mn	0.35	3.5		+0.3			<-0.8	-0.7	+0.1		-0.13	-0.39	+1.18
36 Lyn	79158	Weak He	0.32	3.5	0.0		-1.3	-0.2		+0.3	-0.2	+0.4			
45 Leo	90569	Eu-Cr	0.43	3.5						+0.1	+0.5				
17 Com A	108663	Eu-Cr	0.43	4.0						+0.4	+0.7		-0.13	+0.46	+0.19
α^2 Cvn	112413	Si-Eu-Cr	0.34	4.0		-1.0			-0.5	-0.6	+1.0				
78 Vir	118022	Eu-Cr	0.49	3.5		<-2.0			+0.7	+0.2	-0.6				
π Boo	129174	Mn	0.45	3.75					+0.1				-0.07	+0.38	+1.26
β Cr B	137909	Eu-Cr-Sr	0.69	3.5		<-1.8			+0.0						
i Cr B	143807	Mn	0.42	3.75		+0.3			-0.3	+0.1	+0.1		-0.21	-0.03	+0.15
ϵ Her	144206	Mn	0.37	3.75		-0.3	-0.9		+0.0	-0.1	+0.1	-0.3			
ϕ Her	145389	Mn	0.40	3.5			-0.1			-0.3	-0.2	0.0			
ω Her	148122	Eu-Cr	0.47	3.5						+0.2	-1.1				
ω Oph	148898	Sr	0.53	4.0		<-1.6			+0.5						
HR 6176	149822	Si-Eu-Cr	0.34	4.0						+0.3	+2.1	+1.1			
45 Her	151525	Eu-Cr	0.44	3.5		-1.0			-0.1						
52 Her	152107	Sr	0.54	4.0		<-1.6			0.0						
112 Her	174933	Mn	0.36	3.75		-0.4			-0.2	-0.4	-0.5				

TABLE I (Concluded)

	HD	Peculiarity	θ_{eff}	log g	[C/H] 1969	[O/H] 1962	[O/H] 1969	[Ne/H]	[Mg/H] 1962	[Mg/H] 1964	[Si/H] 1964	[Si/H]	[Ti/Fe]	[Cr/Fe]	[Mn/Fe]
10 Aql	176232	Eu-Cr-Sr	0.68	3.5		-0.9			+0.2						
21 Aql	179761	Normal	0.38	3.0		-0.1			-0.5	+0.3	+0.1		-0.73	-0.77	
γ Equ	201601	Eu-Cr-Sr	0.67	3.5		<-1.7			+0.6				+0.05	+0.10	-0.16
Hr 8216	204411	Eu-Cr	0.55	3.0						+0.6	+0.8		+0.22	+0.39	+0.29
Hr 8240	205087	Si-Sr	0.30	4.0			0.0			-0.3	+1.3	+0.5			
Hr 8348	207840	Si-Normal	0.38	3.5		<-2.0				+0.5	+0.2				
κ Psc	220825	Eu-Cr	0.49	3.75					+0.5	+0.8	-0.1		+0.12	+0.28	-0.15
108 Agr	223640	Si 4200	0.27	4.0	-0.6	-0.4	-0.2	-0.5	-0.4	+0.2	+1.8	+1.4			
β Ari	11636		0.59	4.0		+0.2			+0.3						
π Cet	17081		0.32	4.0						-0.1	+0.3				
γ Gem	47105		0.47	4.0											
α Cmi	61421		0.75	4.0											
95 Leo	103578		0.58	3.0						+0.2	-0.1				
η Vir	107259		0.50	3.75						-0.2	+0.1				
γ Vir (A+B)	110378-9		0.71	4.0											
τ Her	147394		0.28	4.0	-0.2		-0.1	[0.0]		+0.0	-0.2	0.0			
ν Cap	193432		0.41	4.0		+0.1	+0.1		+0.2	+0.2	-0.1	0.0			
ο Peg	214994		0.45	4.0		-0.2			-0.5						

*Includes only the stars analyzed by Sargent and Searle (1962 and 1964) and by Mihalas and Henshaw (1966). We have tabulated the logarithm of the ratio of the peculiar to the usual abundances.

TABLE 2

Abundance anomalies observed in A-pec stars*

	HD	Peculiarity	θ_{eff}	[C/H]	[O/H]	[Ne/H]	[Si/H]
α Scl	5737	Wk He	0.34	+0.4	-1.1	-0.2	-0.1
3 Cen A	120709	Wk He	0.32	-0.2	-0.7	+0.3	-0.4
ρ Her A	157778	Si	0.50	-	-0.9	-	-0.5

*Includes the stars analyzed by Sargent, Greenstein and Sargent (1969) but not by Mihalas and Henshaw (1966). We have tabulated the logarithm of the ratio of the peculiar to the usual abundances.

two values for Si/H and for Mg/H in a few stars). If one wishes to compare the abundances of two elements in a number of stars, one should use, for both elements, lines in the same part of the spectrum.

For most elements there is no available line whose equivalent width is insensitve to θ_{eff} and log g. Then the results obtained are more dependent on the parameters of the atmosphere. However, the underabundances of He, C and Ne seem well established at least in the Si 4200 stars.

The behavior of the iron peak elements is more open to question. The Mn overabundance, both with respect to H and the rest of the iron peak, seems well established. Whether or not Ti, Cr, and Fe have normal abundances is not established. Detailed analyses of some stars point to their being anomalous, contrary to the findings of Searle, Lungershausen and Sargent (1966).

In addition to "systematic" studies of a few elements, there now exist detailed studies of the spectra of a few peculiar stars. Now we will discuss briefly the three different analyses that have been made of the same observational material on 53 Tau. Then we will summarize the data on the abundances of A-pec stars recently compiled by Hack (1968). We will use that résumé, along with the systematic studies of Sargent, Searle and co-workers, to judge the success of theoretical models.

One can estimate how accurately the model atmosphere fits a given atmosphere by comparing the analyses of Strom (1969) to that

of Auer et al. (1966) for the same observational material on 53 Tau (table 3). Differences by a factor of 4 are frequent. They seem to stem mainly from a different choice for the turbulent velocity. Whereas Auer et al. (1966) took $v_T = 0.0$, Strom (1969) chose $v_T = 10.0$ km/sec in the UV and $v_T = 3.0$ km/sec in the visible. Strom (1969) found that a turbulent velocity was necessary to obtain, on the average, the same abundances from strong as from weak lines. However, in spite of her using one turbulent velocity for the visible and one for the UV, she still gets differences by factors as large as seven between abundances obtained from lines in the ultraviolet and in the visible. Arguing in the same way, Hardorp (1966) used $v_T = 4.0$ km/sec for 3 cen A. Hardorp et al. (1968) found, however, by analyzing line profiles, that $v_T \leq 2.0$ km/sec. It then seems that, until one understands what "turbulent velocity" stands for it will not be possible to choose a turbulent velocity unambiguously. Uncertainties in the abundances by factors of 5 to 10 can be expected.

The differences between the results obtained by the two curves of growth analyses probably can be related to the Searle, Lungershausen and Sargent (1966) use of lines in the UV whereas Aller and Bidelman (1964) give lines in the visible the greatest weight. Because the UV and the visible form at different heights in the atmosphere, they are probably influenced by different "turbulent velocities." Disagreements are again likely to disappear only when "turbulent velocities" are better understood.

Considering the uncertainties associated with the detailed

TABLE 3

Abundance Analyses of 53 Tau**

	Auer et al. 1966 "Fine"	Aller et al. 1964 "Grosse"	Strom 1969 "Fine"	Sargent and Searle "Grosse"	Cosmic
C	+1.93	+2.70	+2.72		+2.03
Mg	+0.83	+0.44	+1.29	+0.53*	+0.83
Si	+0.99	+0.66	+1.46	+1.03*	+0.93
Ca	-0.09	-1.67	-0.50		-0.38
Ti	-0.12	-0.80	-0.64	-0.87	-1.68
Cr	-1.16	-1.84	-0.55	-0.65	-1.19
Mn	+0.77	+0.65	+0.58	-0.10	-1.45
Ga	-0.28	-1.45	-0.49		-4.12
Sr	-2.70	-2.13	-2.09		-3.87
Y	-2.34	-2.59	-2.63		-4.12
Zr	-1.36	-2.13	-1.92		-4.07

*Fe supposed normal.

**We have tabulated the logarithm of the abundances on an arbitrary scale.

analyses, we do not feel it worthwhile to compare the predictions of theories to the abundances obtained for individual stars. It seems preferable to group stars into a few categories, the better established properties of which the theories should be expected to predict. Such an attempt at grouping peculiar stars has recently been made by Hack (1968). She separates the stars into four categories: Si, Mn, Sr-Eu-Cr and Sr (table 4). Using the results of Sargent and Searle (1967a), we can say that the Si stars have $0.28 \leq \theta_{eff} \leq 0.38$, the Mn stars $0.34 \leq \theta_{eff} \leq 0.48$ and the Sr-Eu-Cr and Sr stars have $0.42 \leq \theta_{eff} \leq 0.6$. In our opinion the studies of Sargent, Searle and co-workers have best established the dependence of abundances on atmospheric parameters. Hacks then fills in, from other people's observations, the abundances of elements not observed by Sargent and Searle.

The main points that we should retain from table 4 are:

a) The general overabundances of the rare earths and the relatively smaller ones of Ba.

b) The temperature dependence of the overabundances of the elements Sr, Y and Zr. Sr is most overabundant in the cooler stars, $\theta_{eff} \geq 0.4$, Zr is most overabundant in the hotter stars and Y is in between. We think a systematic study of the kind done for O, Si, ... would yield interesting results if done for Sr, Y and Zr.

c) Contrary to table 4, Sargent and Searle (1967a) concluded that the abundances of C was normal in Mn stars, unknown in the cooler A-pec stars and only smaller than normal in the Si stars.

TABLE 4

Composition of Ap Stars*

	Si	Mn	Sr-Eu-Cr	Sr
He	-	-		
C	-	-	-	-
O	-	o + **	- --	
Na				
Mg	o	o	o +	o -
Al	o	o	-	
Si	+	o	o	o
S				
K				
Ca	--	-	o	o +
Sc	o	-	o -	- ?
Ti	o +	o +	o +	o + ++
V	o +	-	o	
Cr	+	o +	+	o -
Mn	+ ++	+ ++	+ ++	o ++
Fe	+	+ +	o +	+
Co			+	(-)
Ni	+		o +	(-)
Cu				
Zn				
Sr	+	+ ++	++	++
Y	+	+ ++	+	++
Zr	++	++	o	+
Ba	o	+	- o +	(++)
Eu	+++		++ +++	+++
Re	++ +++	++	++ +++	+++

*(Hack, 1968).

** + indicates an overabundance by one order of magnitude, ++ by two orders of magnitude, ...

Finally the relationship between the atmospheric parameters and the peculiarities was strikingly confirmed when Sargent and Searle (1967b) found that the same peculiarities occurred at the same (θ_{eff}, log g) in Pop II stars as they did in A-pec stars.

3. COMPARISON OF NUCLEAR MODELS TO OBSERVATIONS

We will now compare the observations to a few theoretical models which have been proposed to explain A-pec stars. Because nucleo-synthesis theory succeeded in explaining the normal abundances observed in stars, it was tempting to hypothesize that the peculiar abundances were also due to nuclear processes and to postulate whatever astrophysical situation necessary to generate the observed peculiarities through those processes. The abundances that could be expected from nuclear reactions in the atmosphere were studied by Fowler, Burbidge and Burbidge (1955) and more recently by Brancazio and Cameron (1967). The astrophysical history necessary to explain the abundances through nuclear reactions in the interior of the stars has been discussed by Fowler, Burbidge, Burbidge and Hoyle (1965). They mention that possibly the evolution took place in a companion that threw the abundances to the observed A-pec star in an explosion. Van den Heuvel (1968a, b) further developed this idea. We will mention objections to each of those models before proceeding to discuss the possibility of explaining the abundance anomalies by diffusion processes.

First, there is a general property of the A-pec stars as noted by Sargent and Searle (1967a) and Deutsch (1966) that none of the nuclear physics models explains in a natural way; i.e., the dependence of the anomalies on the parameters of the atmosphere. In this respect the model developed by Van den Heuvel (1968a, b) fares most poorly. How can the nuclear processes inside the companion of the A star be in-

fluenced by the atmospheric parameters of the A-star? Equally hard to imagine is how the effective temperature and the gravity could change appreciably the end results of the magnetic acceleration of particles in the atmosphere. In Fowler et al. (1965) model, the produced abundances could be related to atmospheric parameters only by the dependence of atmospheric parameters and abundances on the mass of the stars. This link seems rather tenuous for the striking relationships observed.

The most serious difficulty faced by the interior model of Fowler et al. (1965) is the discovery of A-pec stars in young clusters. Their model requires that the A-pec stars should be A or late B stars returning to the main sequence after the red giant phase. This seems inconsistent with the observation of peculiar stars in clusters whose turning point in the H-R diagram is higher than the position of the A-pec stars (Kraft, 1967; Hyland, 1967; Garrison, 1967; and Adelman, 1968).

The difficulty faced by the "atmosphere-nuclear-reactions" model with element conservation has been discussed by Searle and Sargent (1963). We will discuss it here relative to the specific model proposed by Brancazio and Cameron (1967). In Si stars they assume the whole surface material of the star has been exposed to little bombardment by He ions (small values of their parameter W). However, since He is underabundant by a factor of 10 or so in those stars, He must have been "consumed" to a large extent over the whole surface of the star. The transformation of O to Si requires a mass fraction

of 10^{-2}. He ions represent a mass fraction of 0.4 in normal stars. The transformation of O to Si requires only 3% of it. Where did the rest go?

This model faces other difficulties when one compares it to the details of the observations. It predicts, for instance, that Cr and Mn should behave in a similar manner. However observationally, they seem to behave differently (Sargent and Searle, 1967a). The nuclear physics models predict that Sr, Y and Zr should all three be overabundant in the same stars. Observationally, however, they behave differently with θ_{eff}.

In our opinion all the nuclear physics models that have been proposed up to now face serious difficulties. Rather than discuss all the difficulties related to the details of the observations, we have tried to limit discussion to the best observed difficulties. The problems they face are numerous and serious enough to warrant looking in another direction for an explanation of the abundance anomalies. Now we will discuss the consequences of making the hypothesis that the atmosphere of the A-pec stars is stable.

4. DIFFUSION PROCESSES

We postulate that the outer atmosphere of the A-pec stars is stable enough for diffusion processes to be important there. This is reasonable since the A-pec stars are known to be slow rotators and convection zones are not expected to be important in B and early A stars. The magnetic fields may also add to the stability of the atmosphere as magnetic fields are observed to reduce convection in sun spots. Also the ability of the rigid rotator hypothesis (Deutsch, 1958) to explain a large fraction of the observed magnetic field variations argues for their stability.

We will now describe the physics of diffusion processes, their time scale in the atmospheres of A and B stars, the relative importance of forces due to gravitation, to magnetic field gradients and to differential radiation pressure from photo-ionization and line absorption. We found that diffusion processes naturally lead to the abundance anomalies observed in the A-pec stars and to their observed dependence on atmospheric parameters.

Diffusion processes in stars have been discussed by Aller and Chapman (1960), Babcock (1947, 1958b, 1963), Greenstein, Truran and Cameron (1967) and Praderie (1968). Aller and Chapman studied the possibility that gravitational settling has reduced the abundances of the heavier elements in the atmosphere of the sun. Babcock's studies are related to the A-pec stars and will be discussed below. Greenstein, Truran and Cameron showed that the underabundances of He, in old halo B stars, could be explained by gravitational settling.

Praderie discussed the possibility that the metallic line stars could be the normal stars. Gravitational settling would have reduced the abundances of heavy elements in the other stars including the sun.

First we will discuss the diffusion equation proposed by Aller and Chapman (1960). We shall then use it to calculate diffusion velocities and hence diffusion time scales in A-pec stars. The time scale turns out to be of the order of 10^4 years; much smaller than the expected life times of these stars. To oppose gravity, a force must be of the same order as the gravitational force. Diffusion due to a magnetic gradient will then be seen to be negligible. Then we will discuss how a continuous force like gravity compares to a discreet force like the absorption of photons. Both bound-free transitions (continuum) and bound-bound ones (lines) contribute substantially to the transfer of momentum from the radiation field to certain elements.

Starting from the diffusion equation for a binary mixture, Aller and Chapman (1960) argued for the following equation for a mixture of ionized hydrogen, electrons and an ionized gas of charge Z, and atomic mass A:

$$w_{12} = D_{12}\left[-\frac{1}{c_2}\times\frac{\partial c_2}{\partial r}+\frac{2A-Z-1}{p}\frac{\partial p}{\partial r}\right.$$
$$\left.+\frac{2.65\,Z^2+0.805(A-Z)}{T}\frac{\partial T}{\partial r}+\frac{A(F_1-F_2)}{kT(c_1+c_2A)}\right] \qquad (1)$$

where

c_1 = mass fraction of hydrogen

Ac_2 = mass fraction of the gas (Z,A).

w_{12} = relative velocity of the gas (Z,A) with respect to hydrogen

r = a measure of distance (supposing plane symmetry) in cm

T = temperature in ^{o}K

p = pressure (cgs units)

F_1 = force on hydrogen (dynes)

F_2 = force, per unit atomic mass, on the gas (Z,A) (dynes)

$$D_{12} = 1.947 \times 10^{9} T^{5/2} [NZ^2 A_1(2)]^{-1} \qquad (2)$$

$$A_1(2) = \log_e(1 + x_o^2)$$

$$x_o^2 = 2.73 \times 10^{8} T^3/(Z^2 N)$$

N = number density of hydrogen

To evaluate equation 1 for the stars of interest, we used the model atmospheres of Mihalas (1965). Before giving the numerical results, we will briefly discuss the relative importance of each term and obtain, as a by-product, the force needed to counter gravity and a determination of the distribution with height of diffused elements. It is found numerically that in the atmospheres of A and B stars, the term containing $\partial T/\partial r$ is generally less than 10% of the term containing $\partial p/\partial r$; we may then neglect the term containing $\partial T/\partial r$. If the gas (Z,A) has not diffused yet, $\partial c_2/\partial r = 0.0$, we are left with the term containing $\partial p/\partial r$ and that containing $(F_1 - F_2)$. But we know: $\partial p/\partial r = \overline{nm}g$ and $p = nkT$. Since hydrogen is completely ionized and since one assumes $c_2 << c_1$,

$$\overline{m} \simeq (m_p + m_e)/2 \simeq m_p/2$$

Then

$$\frac{1}{p}\frac{\partial p}{\partial r} \simeq \frac{1}{2}\frac{m_p g}{kT}$$

(note that in deriving equation 1, it was assumed that H was completely ionized and that He was not present. If one wishes to apply equation 1 when those two conditions are not satisfied, it must be modified slightly.) For diffusion to occur towards the top of the atmosphere, one then requires (if $Ac_2 \ll c_1$)

$$W m_p |F_1 - F_2| > \frac{2A-Z-1}{2} m_p g = \left(A - \frac{Z}{2} - \frac{1}{2}\right) g m_p$$

If $F_1 \ll F_2$ and $\left(\frac{Z}{2} + \frac{1}{2}\right) \ll A$ (here this is always a reasonable approximation, since for the ions of interest $Z \lesssim 2$ and $A \gtrsim 15$), one requires the other force on (Z,A) to be larger than the gravitational force on (Z,A). The terms $\left(\frac{1}{c_2}\frac{\partial c_2}{\partial r}\right)^{-1}$ and $\left(\frac{1}{p}\frac{\partial p}{\partial r}\right)^{-1}$ represent respectively the scale height of settling due to diffusion (R_D) and the scale height of pressure variations in the atmosphere. If due to gravity diffusion stops when

$$\frac{1}{c_2}\frac{\partial c_2}{\partial r} = \frac{2A-Z-1}{p}\frac{\partial p}{\partial r} \simeq \frac{Agm_p}{kT} \simeq 3.5 \times 10^{-7}$$

then (for $A \simeq 30$)

$$R_D \simeq 3 \times 10^6 \text{ cm}$$

A radiation force twice as large as the gravitational force would lead to the same R_D as the pressure gradient term. For diffusion to cause observable effects, it has to take elements from the zone where lines are formed to a zone one can not observe from the outside (or

vice versa). This corresponds to a $\Delta\tau \gtrsim 1$. The corresponding ΔR is of the order of 10^8 cm in A stars. The atmosphere will then have to be stable for at least 10^8 cm. There are 30 diffusion scale heights over that distance. Diffused elements will then either be floating at the top of the stable zone or lying at its bottom.

For diffusion to be of any importance, it is at least necessary that the diffusion time scale be shorter than the life time of the star. To determine the diffusion time scale, we have used equation 1 (with $\partial c_2/\partial r = 0.0$ and $F_1 = 0 = F_2$), along with Mihalas' (1965) models. The results are shown on Fig. 1, for Mn III ions, for log g = 4, and different values of θ_{eff}. One reads directly the time to diffuse from $\tau = 5 \times 10^{-4}$ to $\tau = \tau_1$. One can use Fig. 1 to calculate time scales for other elements and other ions by remembering that (equations 1 and 2)

$$w_{12} \propto A/Z^2 \tag{3}$$

or

$$t_o \propto Z^2/A \tag{4}$$

It is seen that the time scales are of the order of 10^4 years for the ions of interest to move from $\tau = 0.1$ to $\tau = 10.0$ under the influence of the gravitational force. If the radiation force on an element is twice the gravitational force, that element will diffuse towards the top of the atmosphere on the gravitational settling time scale. These time scales are much shorter than the expected main sequence life times ($\simeq 10^8$ years) of A or B stars (Iben, 1965 and 1966).

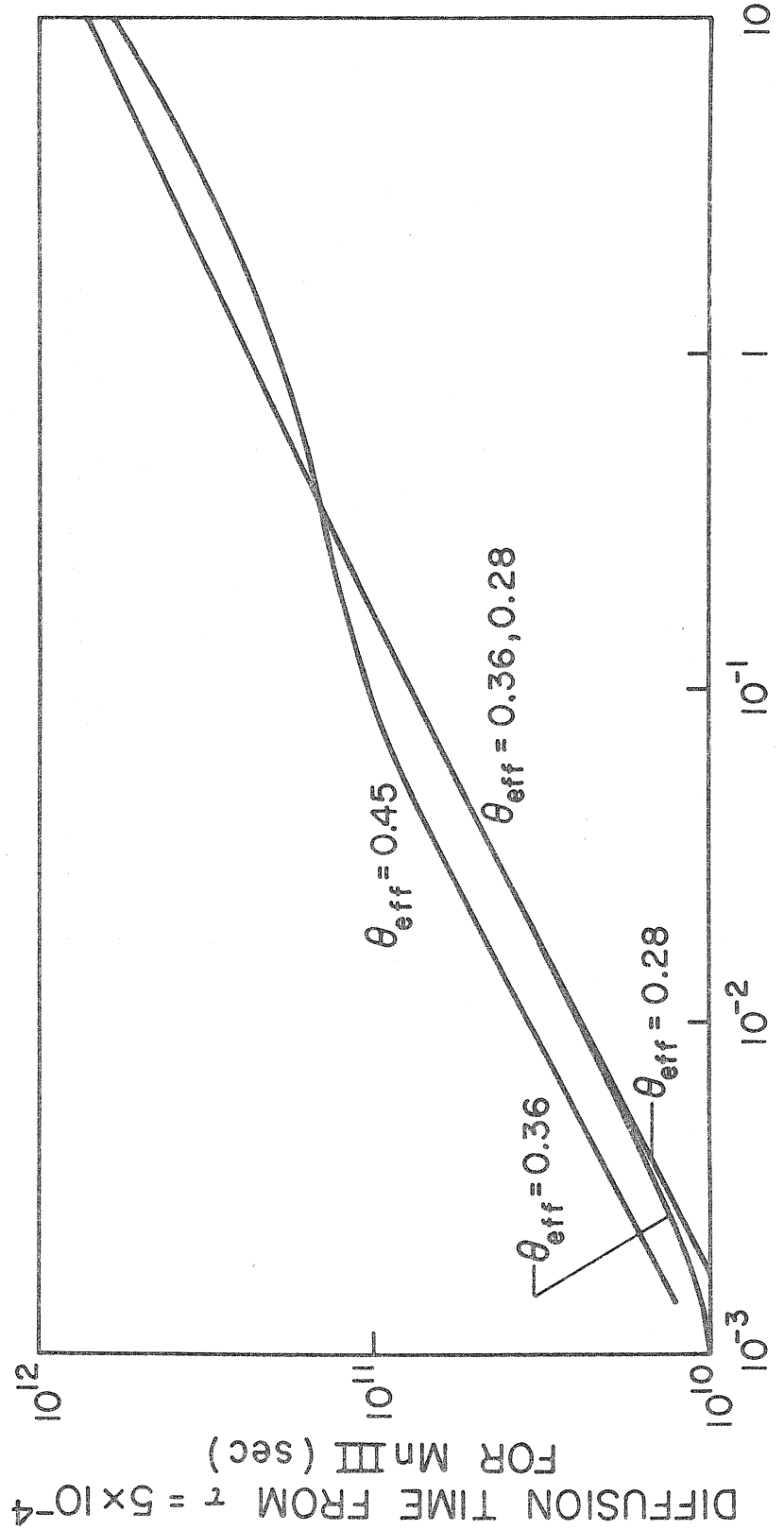
DIFFUSION TIME FROM $\tau = 5\times10^{-4}$ FOR Mn III (sec)
10^{12}
10^{11}
10^{10}
10^{-3}
10^{-2}
10^{-1}
1
10
OPTICAL DEPTH
$\theta_{eff} = 0.45$
$\theta_{eff} = 0.36, 0.28$
$\theta_{eff} = 0.36$
$\theta_{eff} = 0.28$

Fig. 1

Fig. 1. The time needed for Mn III ions to diffuse from $\tau = 10.0$ to $\tau = 0.2$ is seen to be of the order of 10^4 years, much shorter than the expected main sequence life times of A or B stars. If the atmosphere is stable enough diffusion processes should then be important.

To determine how stable the atmosphere has to be for diffusion to be important, we have plotted the diffusion velocities as a function of τ for Mn III ions, for log g = 4.0 and a few values of θ_{eff}. For diffusion to be important, convection and rotational circulation currents would have to be slower than 10^{-3} cm/sec or so in the atmosphere of the star (Fig. 2).

We have also calculated the diffusion speed for unionized O, in the approximation $w = \frac{1}{2} g t_A$, where t_A is the average time between two collisions and g is the gravitational acceleration. For the collision frequency of a non-ionized gas, we have used (Loeb, 1934)

$$\nu = t_A^{-1} = \pi \sigma^2 N v \tag{5}$$

where N is the number density of H, σ is the mean diameter of the two colliding atoms ($\simeq$ 3 Å) and v is the average thermal velocity ($v = (8kT/\pi m)^{1/2}$). If one uses $p_G = p - p_e$ where p is the total pressure and p_e the electron pressure, then t_A becomes:

$$t_A \simeq 4.2 \times 10^{-6} \frac{\sqrt{AT}}{p_G} \tag{6}$$

The diffusion velocity in a gravitational field is then approximately:

$$w \simeq \frac{1}{2} g T_A = 2 \times 10^{-6} g \frac{\sqrt{AT}}{p_G} \tag{7}$$

Since the diffusion velocity of once ionized O is about the same as the diffusion velocity of twice ionized Mn, the ionization of O is seen, from Fig. 2, to reduce its diffusion velocity by a factor of

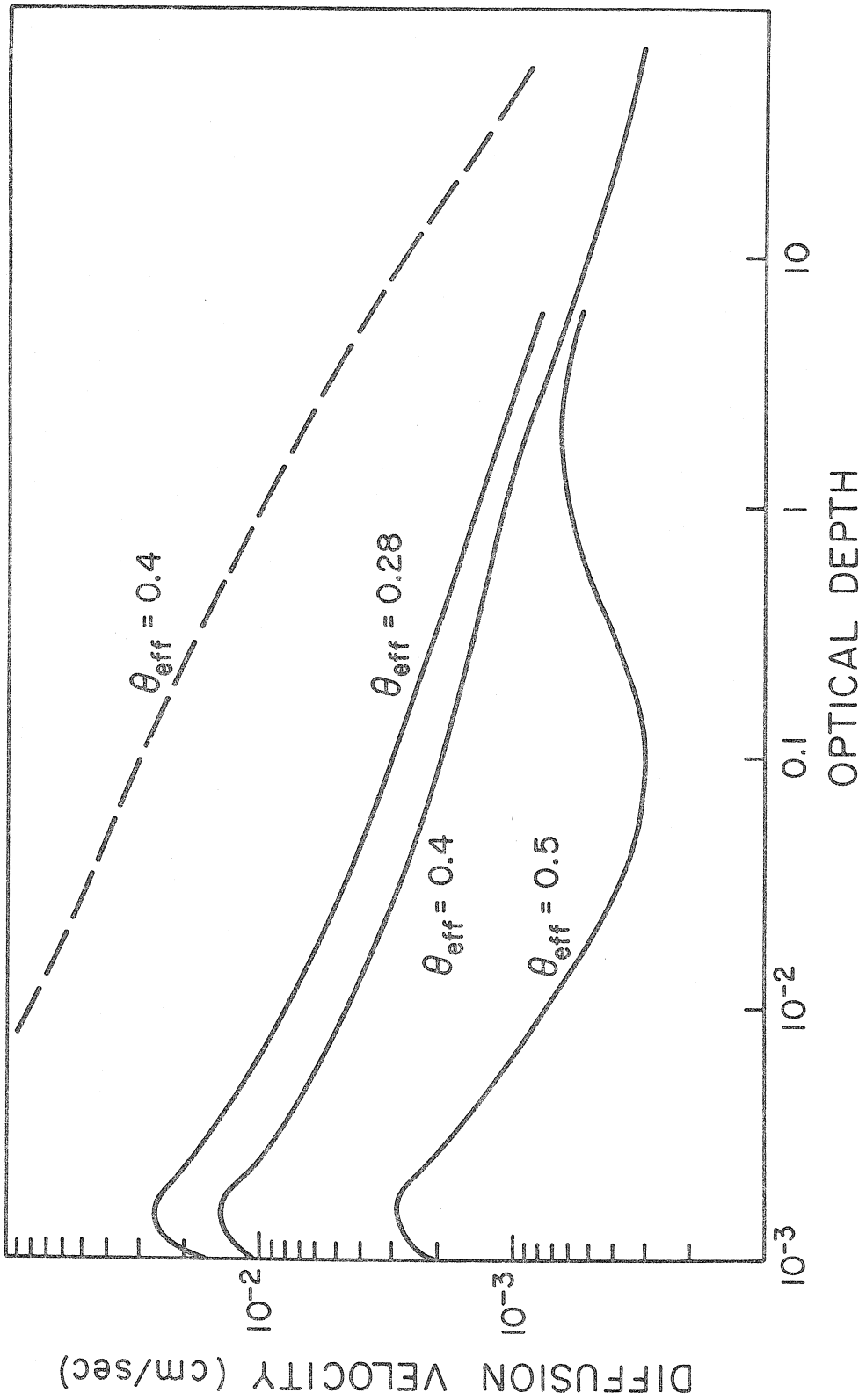
DIFFUSION VELOCITY (cm/sec)
10^{-2}
10^{-3}
10^{-3}
10^{-2}
0.1
1
10
OPTICAL DEPTH
$\theta_{eff} = 0.4$
$\theta_{eff} = 0.28$
$\theta_{eff} = 0.4$
$\theta_{eff} = 0.5$

Fig. 2

Fig. 2. The diffusion velocity shows that there must be no currents faster than 10^{-3} cm/sec for the diffusion of ions (full line) to be important in the atmosphere of A or B stars. Unionized elements would diffuse ten times as fast (dashed line). Diffusion could not be important when there is convection.

about 10.

In the sun, convection leads to granules whose speed is observed to be 10^5 cm/sec. However, the sun is known to have an important convection zone close to the surface, whereas late B and early A stars have only weak convection zones (Mihalas, 1965). We have not found any reliable estimates of turbulent velocities in A-pec stars; however, the abundance anomalies appear in those stars in which convection becomes relatively unimportant and therefore where diffusion processes are most likely to be important.

A-pec stars have recently been shown to be slow rotators (Sargent and Searle, 1967a; Abt, 1967; Deutsch, 1967). Their rotational velocity is about a quarter that of normal main-sequence stars. At the moment, there are no reliable estimates of the velocities of rotational circulation. Assuming a star uniformly rotates, Sweet (1950) has calculated the velocity of the rotational currents. We have used the $3M_\odot$ model of Iben (1965) to obtain ρ_c and T_c needed to calculate $v_{rotation}$ from Sweet's calculation. Wolff (1968) found that the observations were consistent with the A-pec stars being all those A stars having equatorial rotational velocities of 90 km/sec or less. Using Sweet's calculations, this implies meridional currents of 10^{-3} cm/sec. The normal A-stars rotating faster would then have currents too rapid to allow diffusion. This agreement may well be a coincidence however. Mestel (1966) has shown that Sweet's calculations should not be applied outside the surface whose density is defined by $\bar{\rho} = \Omega^2/2\pi G$ where G is the gravitational constant. For a period of five days, we obtain

$\bar{\rho} = 6 \times 10^{-4}$ g/cm^3. At $\tau = 1$, in the atmosphere of a star with $\theta_{eff} = 0.4$ and log g = 4, Mihalas (1965) obtains $\rho = 3 \times 10^{-9}$ g/cm^3 which is much smaller than $\bar{\rho}$. Outside of that zone, the circulation velocities should be increased by $\rho/\bar{\rho}$. Mestel, however, neglects the influence of magnetic fields. Magnetic fields may be important in increasing stability both against convection and against rotational currents. One can expect stability against convection, if $\rho g \frac{|\nabla T|}{T} < \pi H^2/\lambda^2$ (Cowling, 1953) where λ is the size of the instabilities. Here:

$$\frac{\nabla T}{T} \simeq 10^{-10} \text{cm}^{-1}, \quad H \simeq 10^4 \text{ gauss}$$

so that

$$\lambda \leq 10^{11} \text{ cm}$$

Since the radius is approximately 10^{11} cm (Iben, 1965), one expects that the magnetic field will increase the stability against convection. Similarly for stability against rotation one should replace $\rho g \frac{|\nabla T|}{T}$ by $\rho \Omega^2$. For rotational periods of 0.5 days, one obtains $\lambda \lesssim 10^{12}$ cm (if $\rho \simeq 10^{-9}$ g/cm^3, $H \simeq 10^4$ gauss).

Even though it cannot be shown quantitatively that A-pec stars have stable enough atmospheres for diffusion processes to take place, they are expected to be among the stars having least convection and the smallest meridional circulation due to rotation. Furthermore, the magnetic fields observed in their atmospheres (Babcock, 1958a) may very well reduce convection and rotational currents. It seems reasonable then to make the working hypothesis that the atmospheres of A-pec stars are stable and to study what diffusion processes are

then likely to be important.

4.1. Magnetic Fields

We discussed above the possible importance of magnetic fields in increasing the stability of the atmosphere of A-pec stars. Magnetic fields might also be important in slowing the diffusion of ions and their gradients may cause diffusion (Babcock, 1947, 1958b, 1963).

The effect of a magnetic field on diffusion velocities may be approximated (Spitzer, 1962; Chapman and Cowling, 1953) by multiplying the component perpendicular to the magnetic field by $(1+\omega_c^2 t_c^2)^{-1}$

$$\omega_c = 2\pi\nu_c = 9.5 \times 10^3 \, ZB/A \quad (\text{sec}^{-1})$$

ν_c is the cyclotron frequency of the ion of charge Z and atomic mass A in a magnetic field of strength B gauss. t_c is the average collision time of ions in the ionized gas; it is approximately equal to:

$$t_c \simeq \frac{3 \times 10^{-16} A T^{5/2}}{Z^2 p_G} \quad (\text{sec}) \qquad (9)$$

Then:

$$\omega_c t_c = 3 \times 10^{-12} \frac{B T^{5/2}}{Z p_G}$$

The magnetic field will start having appreciable effect in slowing down diffusion when $\omega_c t_c \sim 1$ or:

$$B = 3 \times 10^{11} \frac{Z p_G}{T^{5/2}} \qquad (10)$$

If $\tau = 0.2$ in the atmosphere of a star with $\log g = 4.0$ and $\theta_{eff} = 0.4$, one obtains for O II:

$$B \simeq 4 \times 10^3 \text{ gauss}$$

Effective magnetic fields of 1000 to 6000 gauss are frequently observed in A-pec stars (Babcock, 1958a). Assuming that the star has a uniform dipolar field, H_p, one obtains:

$$H_p = H_e/(0.303 \cos i) \qquad (11)$$

where i is the inclination of the magnetic axis to the line of sight. It is reasonable to expect that H would be five times as large as H_e. The observed H_e corresponds then to fields from 5000 to 30,000 gauss in the star. Magnetic fields could then be expected to slow down diffusion perpendicular to the $\vec{H}$ field by a factor from 2 to 50.

Babcock (1947, 1958b, 1963) has discussed the possible importance of magnetic field gradients in causing diffusion in A-pec stars. Assuming $H \simeq 10^5$ gauss and H to vary over a distance of 10^7 cm (10^7 cm can be calculated from Mihalas' models to be the minimum thickness in the atmosphere of A or B stars corresponding to variations of τ from $\tau = 0.1$ to $\tau = 1.0$), then $|\nabla \cdot \vec{H}| \simeq 10^{-2}$ gauss/cm and the force on the ions is

$$\mu \nabla \cdot \vec{H} \simeq 5 \times 10^{-22} \text{ g-cm/sec}^2$$

(taking $\mu = 5\mu_B$, where μ_B is the Bohr magneton). The gravitational force, however, is 1.6×10^{-18} g-cm/sec for an ion with $A = 100$.

Since, as seen above, to cause diffusion upwards the force opposing gravity has to be at least as large as the gravitational force, it seems unlikely that the magnetic field gradient could cause diffusion leading to the observed abundance anomalies in A-pec stars.

5. RADIATION PRESSURE

We will now discuss the importance of the radiation field in causing diffusion. We first show that in spite of its discrete nature, the radiation force can be treated in the same way as the gravitational force. We then calculate the momentum transferred to the ions of interest by bound-free transitions (continuum) and bound-bound ones (lines). The radiation pressure force is frequently larger than the force of gravity. It can then push elements outwards and cause overabundances in the outer part of the atmosphere. The strength of the radiation pressure force in the outer atmosphere of A-pec stars is related to the overabundances observed in these stars.

One might argue that the momentum received by an ion from the radiation field is rapidly transferred through collisions to all species present and therefore cannot cause diffusion. Under the hypothesis that the time scale for this transfer is approximately the same as the time for an ion to be scattered through 90^{o}, t_c, it will be seen that a given radiation force causes diffusion velocities equal to those produced by the same gravitational force.

For simplicity suppose that all photons are streaming in the same direction. (In general one should consider only the anisotropic part of the radiation field, i.e., the radiation flux.) Let t_p be the average time between the absorption of two photons. The momentum transferred from the radiation field per second (the force) is then $h\nu/(t_p c)$. The distance travelled per second $h\nu t_c/(2t_p cM)$ (introducing the factor $t_c/2$, since the push is remembered for a time t_c, but over

the time $t_c/2$ the strength of the push is reduced by a factor 0.5). M is the mass of the ion. Similarly the distance travelled per second under the influence of gravity is approximately $0.5\,gt_c$. Comparing the two expressions it is easily seen that a radiation force as large as a gravitational force causes diffusion through the same distance as the gravitational force. The direction in which the ions will diffuse will be determined by the relative size of the gravitational and radiation forces, independently of t_c. In the diffusion equation, one can introduce the radiation force in the same way as a continuous force, in spite of the discrete nature of the photons. The collision frequency will only affect the diffusion velocity. The diffusion velocity due to radiation pressure should then be expected to be of the same order as the one calculated above for gravitational settling.

We now calculate radiation forces from bound-free and bound-bound transitions in the usual way and expect that when the radiation force is larger than the gravitational force, the ions will diffuse towards the top of the atmosphere. One then observes overabundances.

5.1. Continuous Absorption

The force exerted on an atom by a radiation flux ϕ_ν (physical flux) in a wave length interval $d\lambda$, through absorption of photons by the level n, when the fraction N_n/N_{tot} of the given element are in the level n, is given by (Pecker and Schatzman, 1959)

$$F_\lambda\, d\lambda = 10^8 \frac{N_n}{N_{tot}} \sigma_n \phi_\nu \frac{d\lambda}{\lambda^2} \quad \text{(cgs)} \tag{12}$$

where σ_n is the cross section for absorption of the photon by level n,

in the wave length interval $d\lambda$ (λ in Å).

We calculated the partition function from:

$$U = \sum_i g_i \exp(-W_i/kT) \tag{13}$$

where the weights $g_i = (2J_i+1)$ and the excitation energies W_i are obtained from NBS tables. We then used Saha's and Boltzmann's equations to obtain N_n/N_{tot} for all the levels of interest.

We estimated the contribution of the continuum by calculating the bound-free transition cross section in the classical hydrogenic approximation

$$\sigma_n^{(c)} = 7.9 \frac{n}{Z_n^2} \frac{1}{Y^3} \times 10^{-18} \text{ cm}^2 \tag{14}$$

where Z_n is the charge of the ion after ionization, n is the principal quantum number of the level and $Y = h\nu/\text{I.E.}$ (I.E. = ionization energy of the level n).

For photoionization, equation 12 has to be slightly modified since not all the momentum of the ionizing photon is transferred to the ion. Some of it is given to the electron. Far away from the atom, the distribution of electrons after photoionization is given by (Sommerfeld, 1939):

$$J \simeq \sin^2\theta \cos^2\varphi \, (1 + 4\beta \cos\theta) \tag{15}$$

where θ is the angle between the direction of the light quantum and of the electron and φ is the angle between the plane containing the

electron, the photon and the ion and the plane containing the photon and its polarization vector ($\beta \equiv v/c$). The fraction F of the momentum given to the electron is then:

$$F = \frac{\int mv \cos\theta \, J \, d\Omega}{\int \frac{h\nu}{c} J \, d\Omega} \tag{16}$$

Since $d\Omega = \sin\theta \, d\theta \, d\varphi$, one obtains:

$$F = \frac{4}{5} \frac{mv^2}{h\nu} = \frac{8}{5} K \tag{17}$$

where:

$$K = \frac{\frac{1}{2} mv^2}{h\nu} = \frac{h\nu - I.E.}{h\nu} \tag{18}$$

As $K \rightarrow 1$, the electrons go away with more momentum than the photons brought in; the ions are then pushed back by the photoionization. However, in the cases of interest to us $K \lesssim 15\%$, so that most of the momentum is transferred to the ion and not to the ejected electron. In our calculations of the radiation force due to photoionization, we subtracted the momentum transferred to the electron by multiplying the right-hand side of equation 12 by $(1 - 1.6K)$.

Equation 15 was obtained by Sommerfeld for the ionization of the ground state of the hydrogen atom. To our knowledge, J has not been calculated for any case but hydrogen when K is appreciably smaller than 1. When K is close to 1, the effect becomes measurable. For krypton the anisotropy has been measured and, on the average, less momentum would be transferred to the electron than in the case of

hydrogen (Krause, 1969). However, the experiment was carried out at photon energies much larger than those of interest here. It seems impossible to observe the $4\beta \cos\theta$ term at low energy. It would be nice to have J determined theoretically for cases other than hydrogen. If for some ions of interest the correction term went as $12\beta \cos\theta$, say, it would have an important effect on our conclusions.

We have calculated for a number of model atmospheres the force transferred through photoionization from the radiation field to different elements of interest. The results for the force at $\tau = 0.1$ are shown in Figs. 3 to 8 as a function of θ_{eff}, log g = 4. The special cases of O and Si will be discussed below in a section on auto-ionization.

To calculate the forces, we used Mihalas' (1965) models. The main feature in his calculated outgoing flux, insofar as our calculations are concerned, is the Lyman continuum. Below the Lyman continuum, hardly any flux is coming out. Photoionization will only occur then for those levels in which the ionization potential is less than 13.6 ev.

The elements with ionization potentials larger than 10.5 ev but smaller than 13.6 ev will be pushed out by large radiation forces in the cooler peculiar stars. C, P, Cl, Ca, Sc, As, Br, Sr, Y, Zr, Xe, Rn and the rare earths fall in this category. The elements with ionization potentials smaller than 10 ev or greater than 18 ev will not absorb enough radiation to counter gravity in the A-pec stars. He, Li, Be, B, Ne, Na, Al, K, Ni, Cu, Ga, Se, Rb, In, Sb, Te, Cs, fall in this category. Those with an ionization potential between 13.6 and

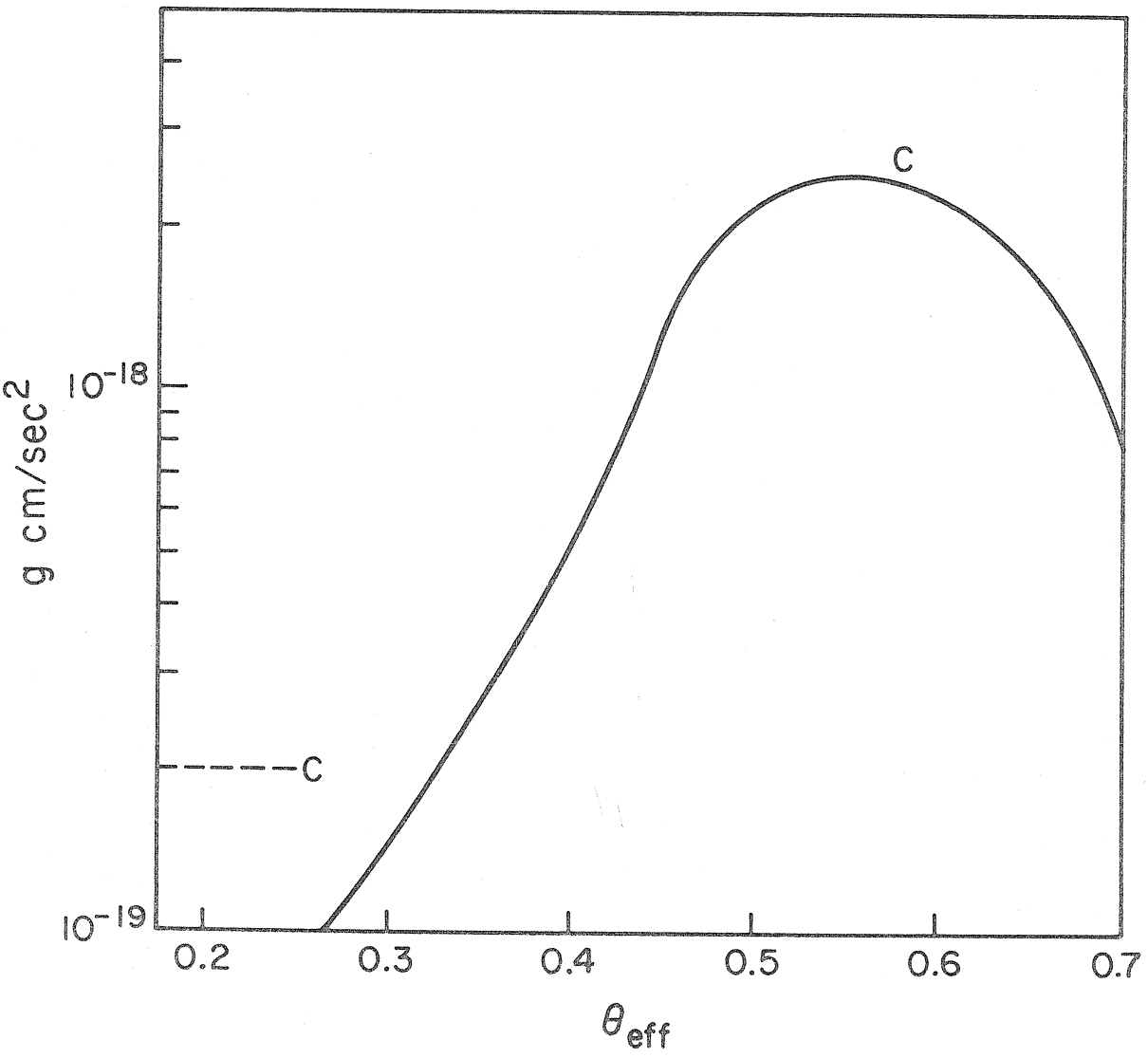

Fig. 3

Fig. 3. Radiation force from the photoionization of C. The dashed line indicates the gravitational force if log g = 4.

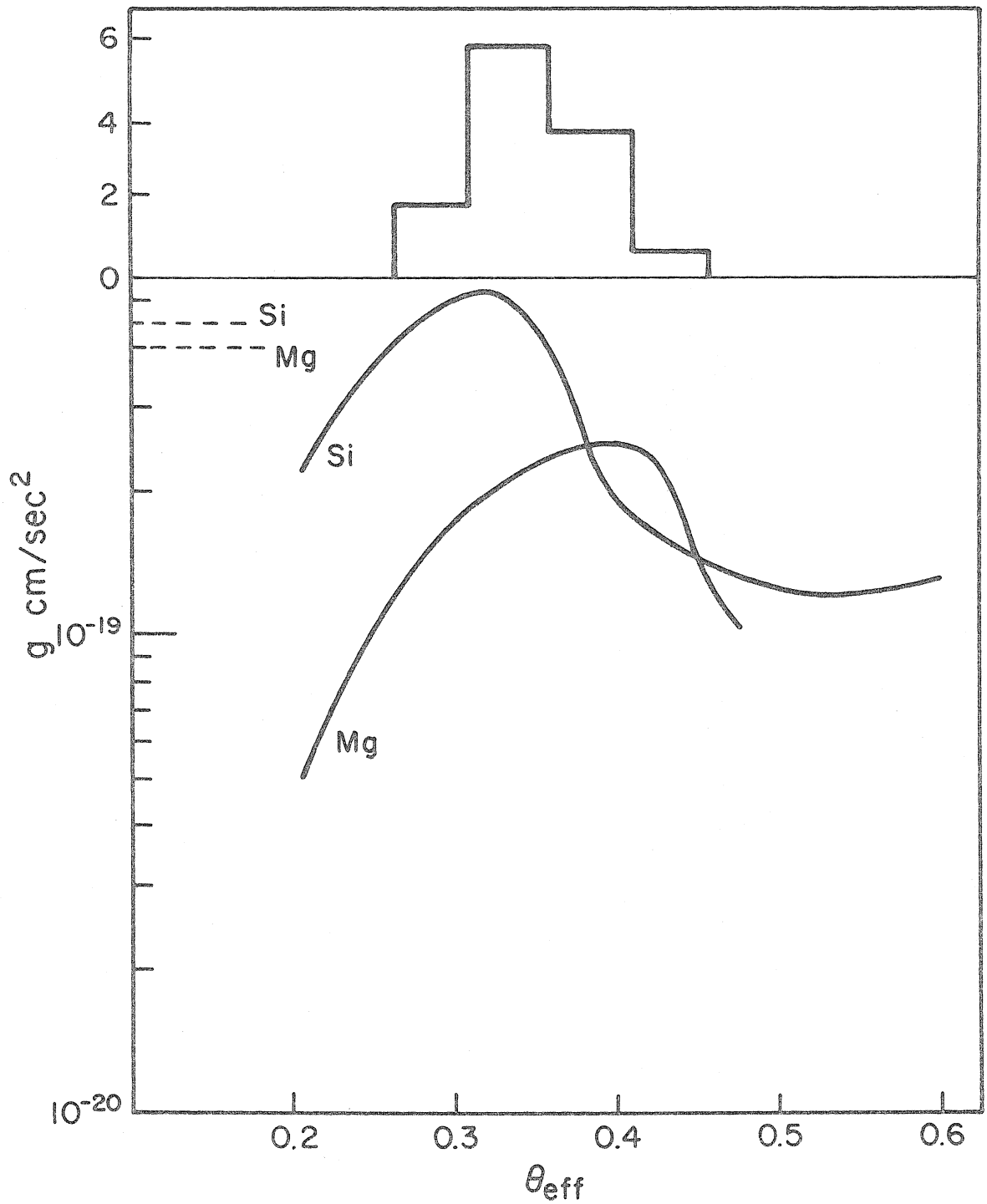

Fig. 4

Fig. 4. Radiation force transferred through photoionization to Si and Mg. The dashed line indicates the gravitational force. The histogram shows the number of Si stars as a function of θ_{eff} (from Sargent and Searle, 1967a). Wide auto-ionization levels would have to exist in Si II, for the radiation force to be able to push Si into the outer atmosphere.

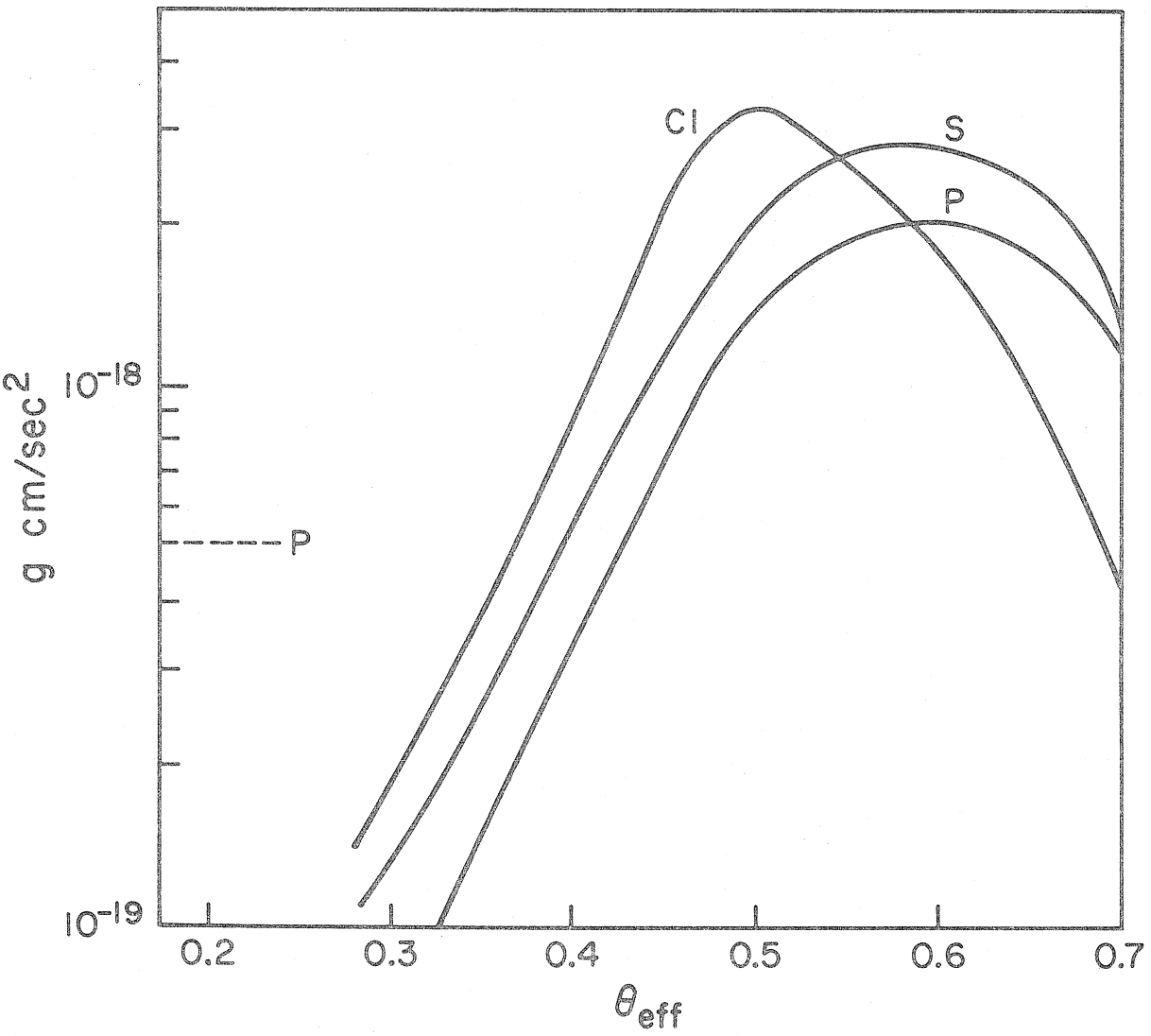

Fig. 5

Fig. 5. Radiation force transferred through photoionization to P, S and Cl. The dashed line indicates the gravitational force on P.

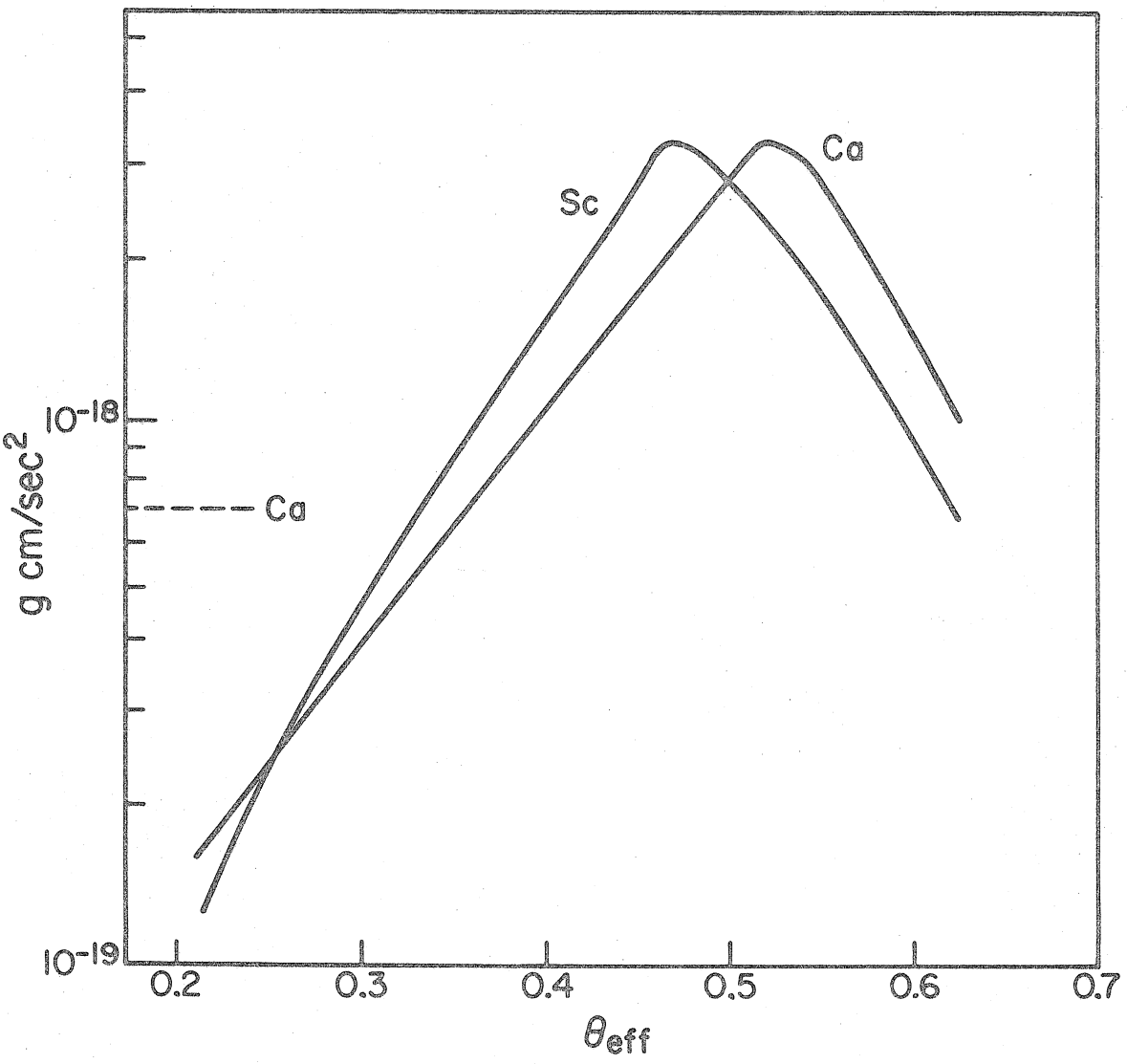

Fig. 6

Fig. 6. Radiation force transferred through photoionization to Ca and Sc. The dashed line indicates the radiation force on Ca.

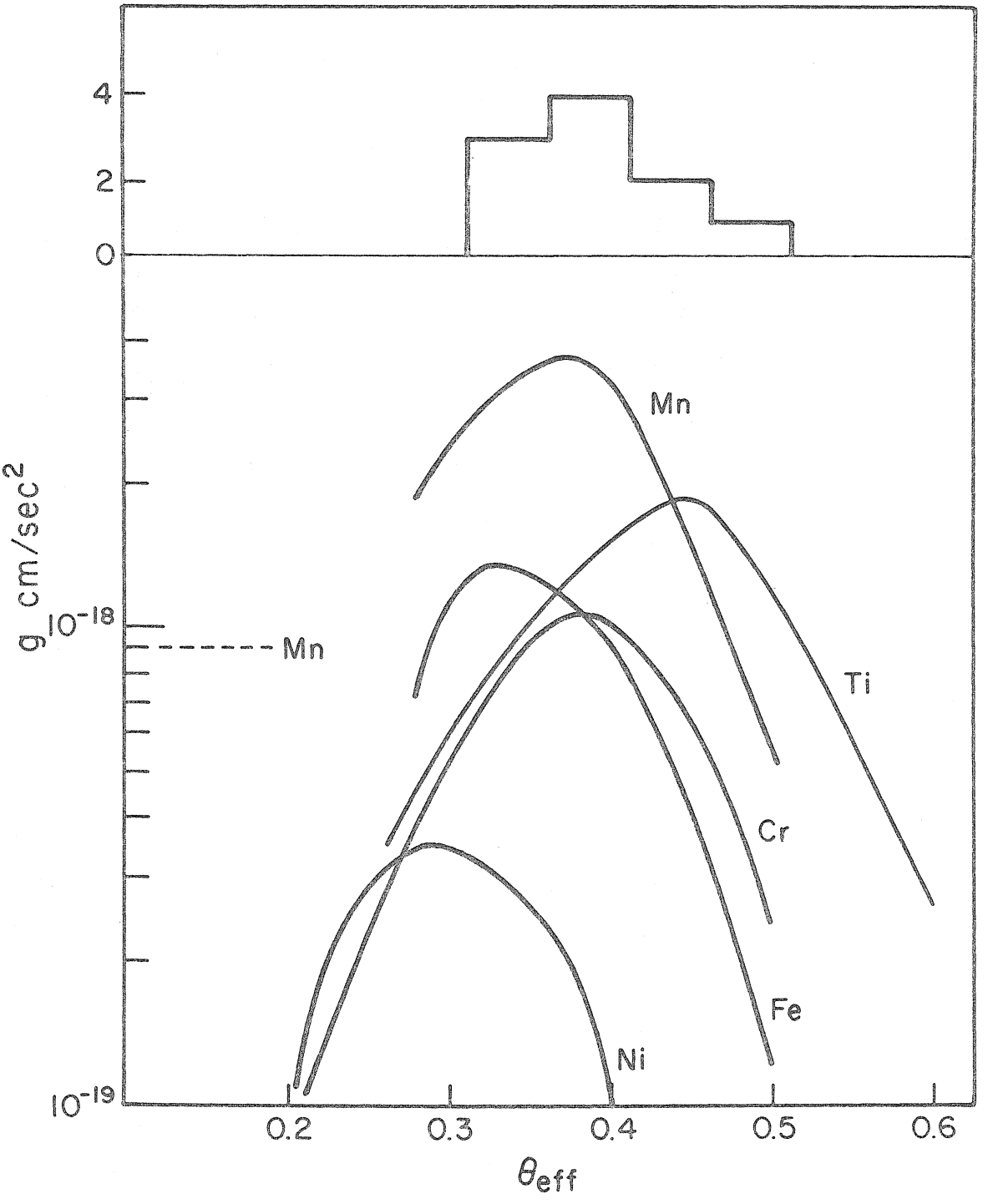

Fig. 7

Fig. 7. Radiation force from the photoionization of iron peak elements. The dashed line indicates the gravitational force on Mn. The histogram shows the number of Mn stars as a function of θ_{eff} (Sargent and Searle, 1967a). The radiation force from the continuum appears related to the Mn overabundance in A-pec stars.

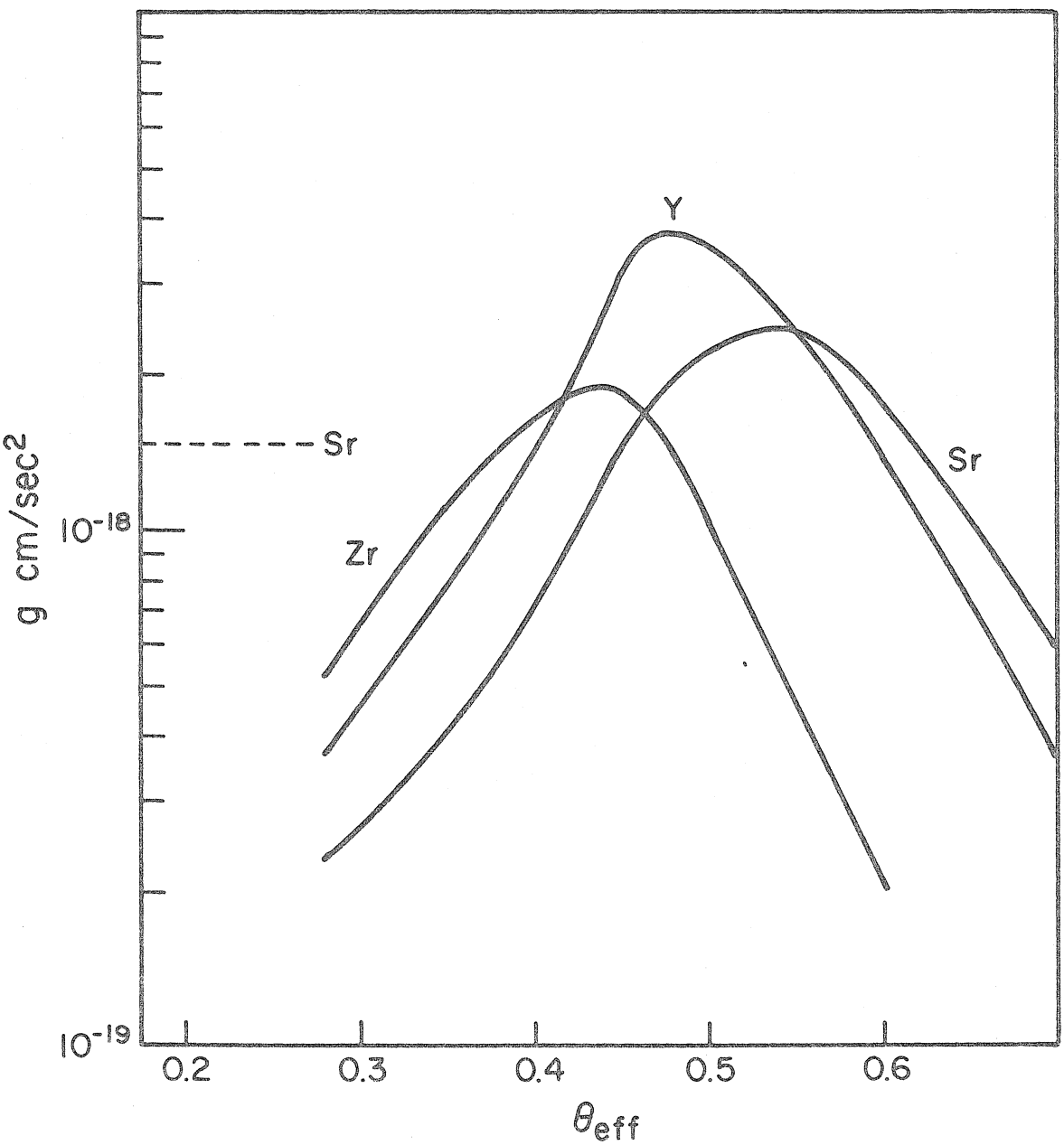

Fig. 8

Fig. 8. Radiation force from the photoionization of Sr, Y and Zr. The dashed line indicates the gravitational force on Sr.

18 ev may or may not be pushed outwards by the radiation field in the warmer A-pec stars. Whether or not they are pushed out depends on the details of the atomic structure. Compare Mg, Mn, Fe and Cr.

In Fig. 9 is plotted the variation with τ of the force transferred through photoionization on Si, Mn, P and Cl for the model atmosphere $\theta_{eff} = 0.4$ and log g = 4. The behavior with τ depends on the excitation energy of the levels from which photoionization occurs. The special case of Si will be discussed at greater length below. The radiation force on Si does not decrease as rapidly when τ increases as that on Cl or P.

One may wonder why hydrogen, the lightest element, should not be thrown out. The answer is simple. There is too much H or not enough light. The radiation pressure in these stars is only a few per cent of the total pressure (Mihalas, 1965). The flux at the proper wave length to push hydrogen up (below the Lyman continuum) is very small. Compare, for instance, H to Mn in a model atmosphere with $\theta_{eff} = 0.4$ and log g = 4. There is about the same fraction of hydrogen which is not ionized as there is Mn in those levels of Mn II which can be ionized by the radiation flux above the Lyman continuum. Because Mn is 50 times as heavy as H and the radiation force on Mn is four times the gravitational force, there has to be 200 times less flux below the Lyman continuum as above, for hydrogen not to be thrown out. An estimate of the relative flux below the Lyman continuum to the flux above can be obtained from:

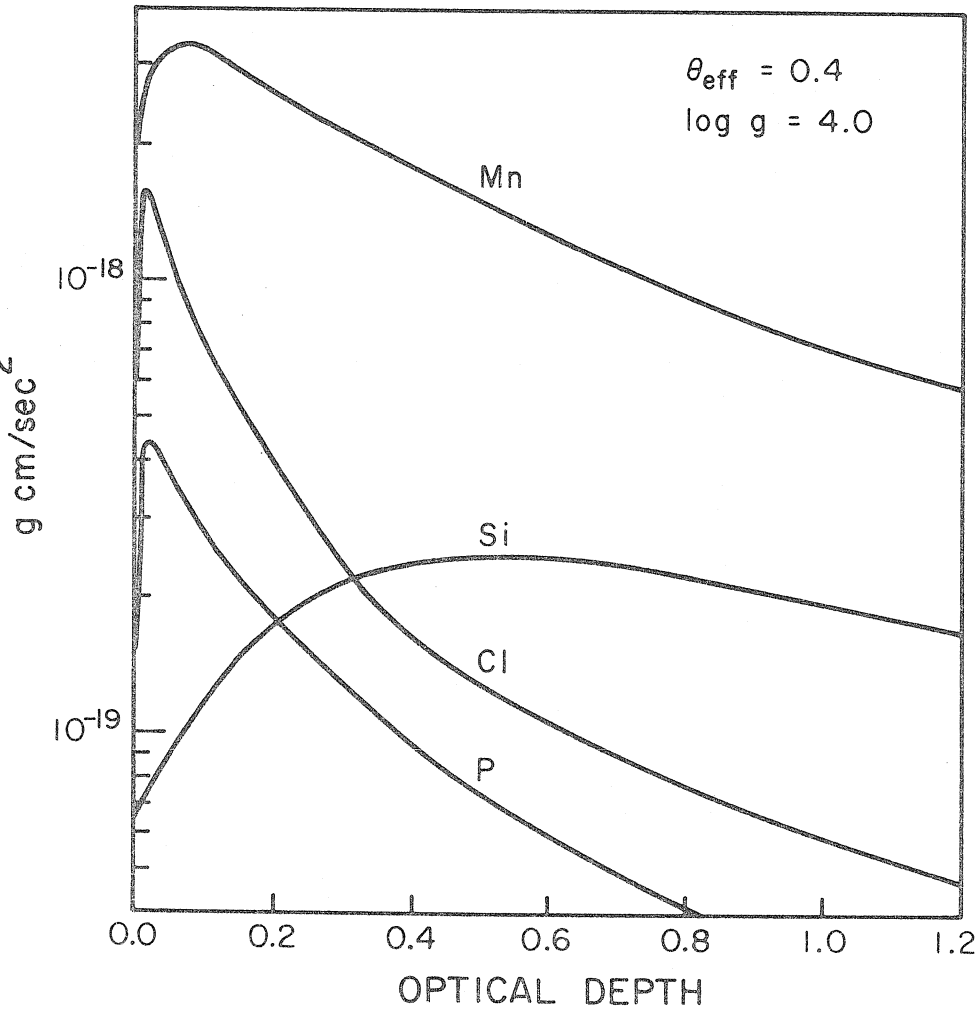
θ_{eff} = 0.4
log g = 4.0
Mn
Si
Cl
P
10^{-18}
10^{-19}
g cm/sec^2
0.0
0.2
0.4
0.6
0.8
1.0
1.2
OPTICAL DEPTH

Fig. 9

Fig. 9. Variation with τ of the force transferred through photoionization to certain elements. Notice that the different behavior with τ of the force from element to element may have important effects in causing overabundances.

$$\frac{F_\nu(\lambda = 910)}{F_\nu(\lambda = 912)} = \frac{\kappa_\nu(\lambda = 912)}{\kappa_\nu(\lambda = 910)} \simeq 10^{-5}$$

We obtained the ratio of opacities from tables prepared by Mihalas for his model atmosphere calculations. H is then not expected to be thrown out by the radiation flux.

5.2. Line Absorption

The possible influence of lines in pushing elements outwards can first be seen by comparing to the gravitational force the momentum per second a line would transfer from the radiation field to the element of interest. For one line, $\int \sigma_n \, d\nu = \frac{\pi e^2}{mc} f$. Equation 12 then becomes (keeping ϕ_ν constant over the width of the line; N_{tot} is the number density of the element of interest):

$$F_{rad} = \frac{\pi e^2}{mc^2} \frac{N_n}{N_{tot}} \phi_\nu f$$

$$\simeq 3 \times 10^{-16} \frac{N_n}{N_{tot}} f \quad (\text{g-cm/sec}^2) \qquad (19)$$

if you assume $\phi_\nu = 3 \times 10^{-3}$ (cgs) (as is typical in the atmospheres of A and B stars, Mihalas, 1965). This force compares with $1.7 \times 10^{-20} A$ (g-cm/sec^2), the gravitational force on an element with atomic mass A, if log g = 4. Saturation could reduce the flux by a factor of $2 \times 10^4/A$, and the radiation force from one line could still be as strong as the gravitational force. If the flux in the line can be approximated by

$$\phi_{line} = \phi_{\nu_{cont}} (\kappa_\nu / \kappa_{\nu_{nm}}) \qquad (20)$$

saturation can be estimated by comparing $\kappa_{\nu_{nm}}$ in the line to κ_ν in the continuum. In the line

$$\kappa_{\nu_{nm}} = \frac{\pi e^2 \lambda}{m_e c^2 n_H} \left(\frac{f_{nm} N_n \lambda}{N \Delta\lambda} \right) = 10^7 \left(\frac{f_{nm} N_n}{N} \frac{\lambda}{\Delta\lambda} \right) \tag{21}$$

We require, in order to take saturation into account:

$$F_{rad} \frac{\kappa_\nu}{\kappa_{\nu_{nm}}} = F'_{rad} = F_{grav} \tag{22}$$

This leads to:

$$\text{mass fraction that one line can support} = \frac{A N_{tot}}{N_H}$$

$$= \frac{10^4 \phi_\nu \kappa_\nu}{\lambda} \frac{\Delta\lambda}{\lambda}$$

$$= 0.1 \phi_\nu \kappa_\nu / \lambda \tag{23}$$

if $\Delta\lambda/\lambda = (1/c)\sqrt{2kT/M} = 10^{-5}$, as would be the case for an ion with A = 100 at a temperature of 10^4 °K. We calculated, for different values of λ, $0.1 \phi_\nu \kappa_\nu / \lambda$ at $\tau = 0.2$, in a model atmosphere with log g = 4 and $\theta_{eff} = 0.4$. The results are shown in Fig. 10. Depending on where it is in the spectrum, a line of thermal Doppler width can support a mass fraction anywhere from 10^{-7} to 10^{-6}. Note that $N_n f_{nm}$ has dropped out of the expression for AN_{tot}/N_H. This is because we assumed the line saturated so that the product $\phi_{\nu_{nm}} \kappa_{\nu_{nm}}$ is independent of the value of $\kappa_{\nu_{nm}}$.

The line width could be defined as the width over which the

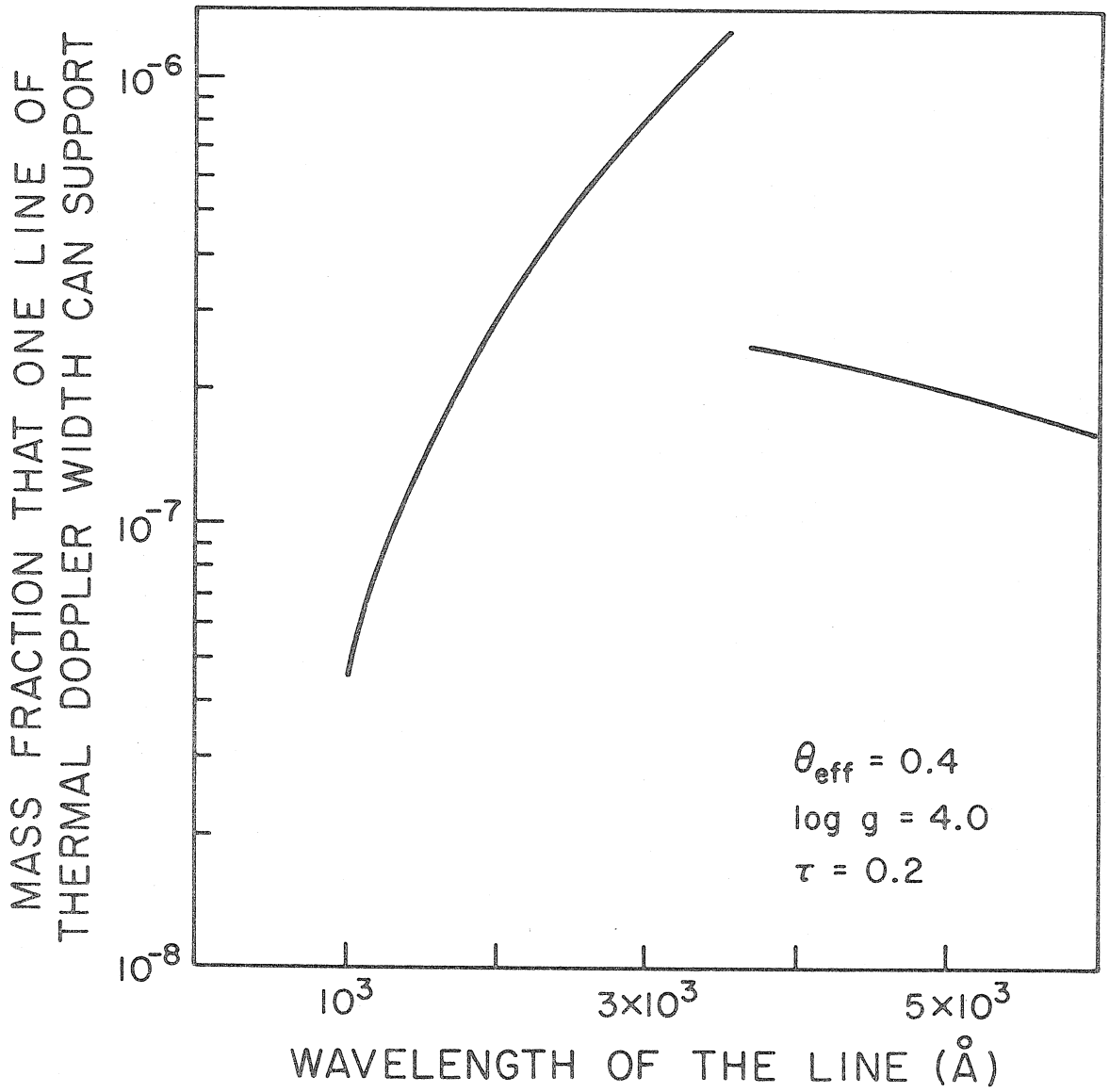
MASS FRACTION THAT ONE LINE OF THERMAL DOPPLER WIDTH CAN SUPPORT
10^{-6}
10^{-7}
10^{-8}
10^3
3×10^3
5×10^3
WAVELENGTH OF THE LINE (Å)
θ_{eff} = 0.4
log g = 4.0
τ = 0.2

Fig. 10

Fig. 10. Mass fraction that one line of thermal Doppler width can support in an atmosphere with $\theta_{eff} = 0.4$, $\log g = 4.0$. On the average it can support approximately 3×10^{-7} of the mass.

product $\phi_{\nu_{nm}} \kappa_{\nu_{nm}}$ is independent of $\kappa_{\nu_{nm}}$. If $\kappa_{\nu_{nm}}/\kappa_{\nu} \simeq 200$ in the center of a line, and if $\kappa_{\nu_{nm}} \propto \exp - [(\lambda - \lambda_o)/\Delta\lambda_o]^2$ where $\Delta\lambda_o$ is the thermal Doppler width, then $\exp -[(\lambda - \lambda_o)/\Delta\lambda_o]^2 = 0.005$ for $|\lambda - \lambda_o| \simeq 2.5$. The total width of the line is then approximately $5\Delta\lambda_o$. If a given element has a resonant line at 4000 Å, that line alone could support a mass fraction of 10^{-6}. If in addition to that line, the element has 10 lines from the ground state with $f \simeq 0.01$, the lines could support a mass fraction of 3×10^{-6}. One could similarly add the contribution of other levels, of multiplets, etc. One could go through tables of lines for elements of interest and derive a formula to estimate their f values. One could then estimate how many lines of a given width an element could be expected to have. However, as we shall see below it is generally clear whether or not the lines could support the observed overabundances of given elements. Si certainly does not have the 10^5 lines necessary to support its observed overabundances. But Eu does have the 1 to 10 lines found necessary to support its overabundances. In what follows, we compare our results above for what mass fraction a line can support, to what one obtains supposing LTE in the formation of the line (Milne, 1927). The two approximations give approximately the same results. We then calculate how the mass fraction supported by one line varies with τ, λ and from one model atmosphere to another. Comparing the calculated with the observed mass fractions, we determine which element can be supported by the radiation pressure transferred through lines to an element.

According to Milne (1927) when $\exp(-\tau_{\nu_{nm}})$ is small, one

line of width $\Delta\nu$ would transfer $4\pi\Delta\nu(dB_\nu/d\tau)\Delta\tau/(3c)$ from the radiation pressure to the pressure supporting one element in a shell of thickness $\Delta\tau$. The number of atoms of an element per cm^2 of that shell is:

$$N(A)\, dr = \frac{X(A)\Delta\tau}{Am_p\overline{\kappa}} \tag{24}$$

The force one line exerts on one atom is then:

$$F_{line} = \frac{4\pi}{3c}\Delta\nu \frac{dB_\nu}{dT} \frac{Am_p\overline{\kappa}}{X(A)} \frac{dT}{d\tau} \tag{25}$$

Equating F_{line} to the gravitational force, one obtains the mass fraction $X(A)$ of a given element one line can support:

$$X(A) = 4 \times 10^4 \frac{\Delta\lambda}{\lambda^2} \frac{h\nu}{kT} \frac{\exp(h\nu/kT)}{1-\exp(h\nu/kT)} B_\nu(T)\overline{\kappa} \frac{dT/T}{d\tau} \tag{26}$$

(cgs units except for λ in Å). Using Mihalas (1965) models we calculated the mass fraction a line of thermal Doppler width can support. The results are shown in Figs. 11 to 13 as a function of λ, for different θ_{eff}, and at different τ. The Doppler width is the appropriate one for an element with $A \simeq 30$. Since $\Delta\lambda_o \propto A^{-1/2}$, the plotted results can be extended to an element with any A.

Listed in table 5 are the number of "average" lines of thermal Doppler width needed to support normal abundances of a few elements of interest. Each line is assumed to support a mass fraction of 3×10^{-7}. Note from table 5 that overabundances of elements heavier than the iron peak can be supported by line absorption. However,

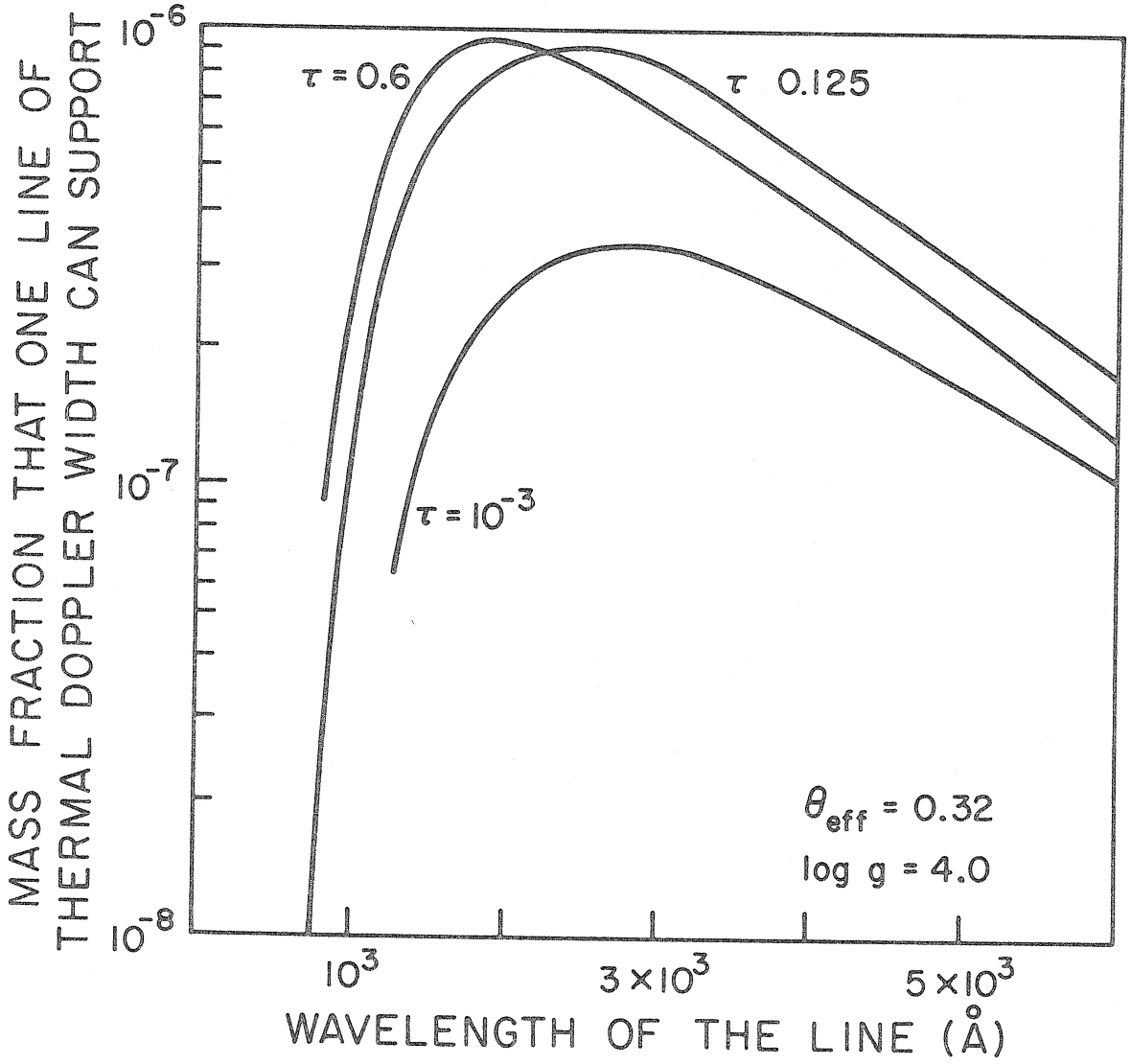
MASS FRACTION THAT ONE LINE OF THERMAL DOPPLER WIDTH CAN SUPPORT
10^{-6}
10^{-7}
10^{-8}
$\tau = 0.6$
τ 0.125
$\tau = 10^{-3}$
$\theta_{eff} = 0.32$
log g = 4.0
10^3
3×10^3
5×10^3
WAVELENGTH OF THE LINE (Å)

Fig. 11

Fig. 11. Mass fraction that one line of thermal Doppler width can support as a function of the wave length of the line. It was calculated at $\tau = 10^{-3}$, 0.125 and 0.6 in an atmosphere with $\theta_{eff} = 0.32$, log g = 4.0. Note that on the average, it tends to increase as τ increases, contrary to the radiation force transferred through photoionization (see Fig. 9).

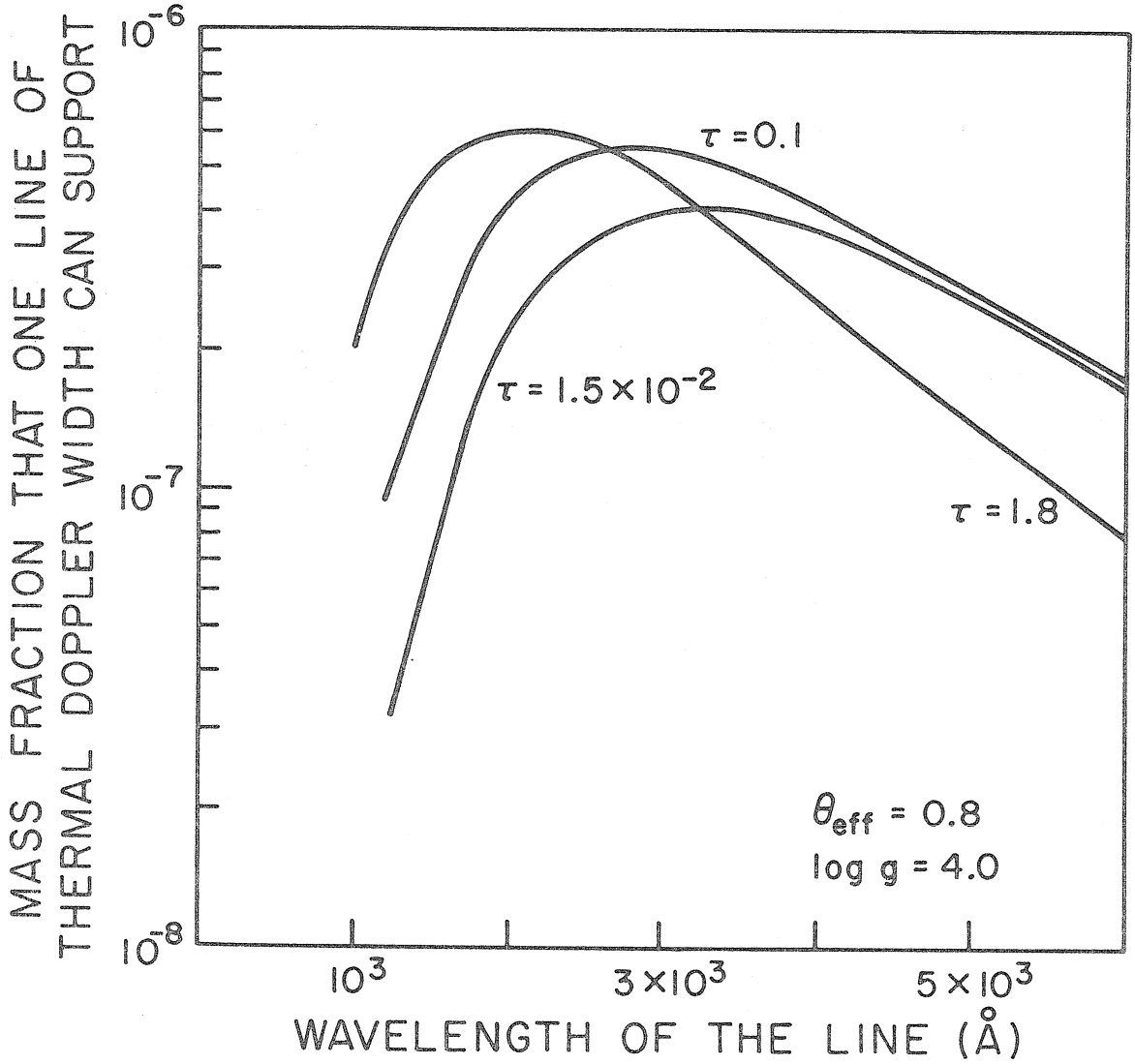
MASS FRACTION THAT ONE LINE OF THERMAL DOPPLER WIDTH CAN SUPPORT
10^{-6}
10^{-7}
10^{-8}
$\tau = 0.1$
$\tau = 1.5 \times 10^{-2}$
$\tau = 1.8$
$\theta_{eff} = 0.8$
log g = 4.0
10^3
3×10^3
5×10^3
WAVELENGTH OF THE LINE (Å)

Fig. 12

Fig. 12. Same as Fig. 11 except that it was calculated at different τ, in a different atmosphere.

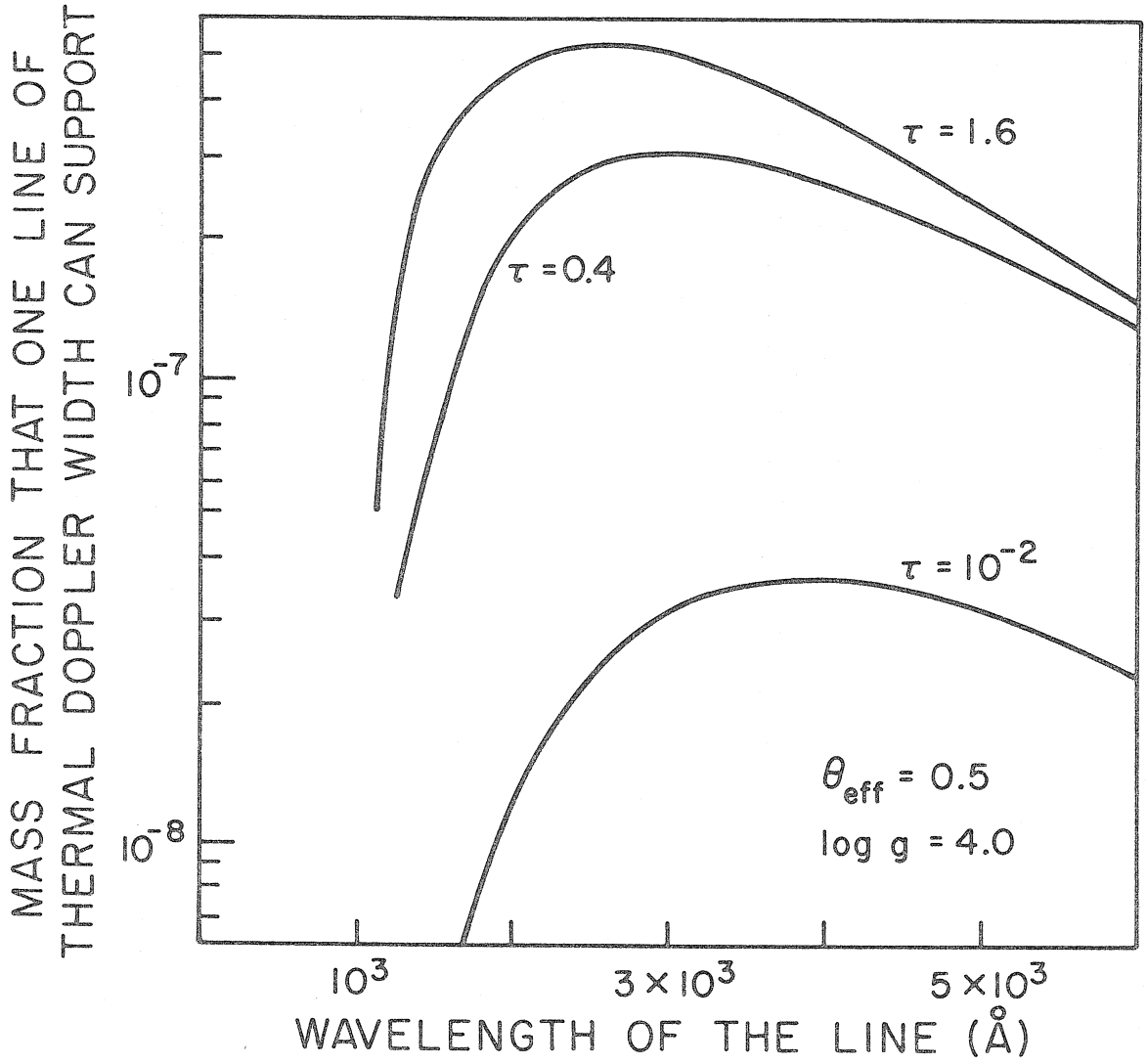
MASS FRACTION THAT ONE LINE OF THERMAL DOPPLER WIDTH CAN SUPPORT
10^{-7}
10^{-8}
$\tau = 1.6$
$\tau = 0.4$
$\tau = 10^{-2}$
$\theta_{eff} = 0.5$
log g = 4.0
10^3
3×10^3
5×10^3
WAVELENGTH OF THE LINE (Å)

Fig. 13

Fig. 13. Same as Fig. 11 except that it was calculated at different τ in a different atmosphere.

TABLE 5

The Effect of Lines

	Number* of lines required	Abundance
O	$5. \times 10^4$	2.5×10^7
Ne	1.5×10^3	$8. \times 10^5$
Mg	$2. \times 10^3$	9.1×10^5
Si	$3. \times 10^3$	10^6
Cl	10.	2.6×10^3
Ca	250.	$5. \times 10^4$
Cr	40.	7.8×10^3
Mn	35.	6.9×10^3
Fe	500.	8.5×10^4
Ga	0.1	9.
Sr	.5	61.
Y	.1	8.9
Zr	.1	14.2
Ba	.05	2.6
La	.01	.5
Eu	.002	.115

*Number of lines required to counter gravity for the observed normal abundances of some elements of interest. Each line was taken as supporting a mass fraction of 3×10^{-7}. The abundances are taken from Bashkin, 1963. The number density of silicon is normalized to 10^6. The number density of hydrogen is then 3.0×10^{10}.

large overabundances of the iron peak elements or of the lighter metals (except Li, Be and B) have to be supported by continuum absorption.

5.3. Auto-Ionization Levels

The force transferred from the radiation field to elements might be increased for two elements of interest, O and Si, by an unusual type of levels, the auto-ionization levels. Those of interest here are levels in which two electrons are excited. The total excitation energy of the two electrons is greater than the energy needed to ionize the ground state. At the same energy then there exists a continuum of states. There is a finite probability that after the two electrons have been excited, the system will ionize without collision or absorption of a photon; hence the name given to these states.

If the parity and the quantum numbers J, L and S of the excited states are the same as those of the continuum for one value of ℓ of the emitted electron, the probability for auto-ionization is large. The levels are then much wider than the usual excited levels. For instance, auto-ionizing levels have been observed in Ca as wide as 0.07 ev (Newson, 1966, Ditchburn and Hudson, 1960), and in Cd and Hg as wide as 0.3 ev (Berkowitz and Lifshitz, 1968).

Calculation of what mass fraction a line related to such a level can push upwards shows how important it might be. At $\lambda = 1000$ Å for an atmosphere with $\theta_{eff} = 0.32$ and $\log g = 4$, Mihalas (1965) obtains for the physical flux: $\phi_\nu = 10^{-3}$ (cgs). The pressure upwards transferred to such a level from the flux is then

$$\phi_\nu \Delta\nu/c = 3 \text{ gr cm}/(\text{sec}^2\text{cm}^2)$$

($\Delta\nu = 0.3$ ev or $\Delta\nu/c = 3000\ \text{cm}^{-1}$). If X is the mass fraction that can be supported by such a level:

$$X = \phi_\nu \Delta\nu/(cp_G) \simeq 0.6\ \%$$

where we took $p_G = 5 \times 10^2$ (cgs) from Mihalas calculations, at $\tau = 0.1$.

One single line ending at such a level could support nearly 1% of the mass (an overabundance of Si by a factor of 10) of the elements above $\tau = 0.1$, if that element is concentrated above $\tau = 0.1$, as would be expected for an element being pushed upwards by such a continuum-like level.

When an element has an ionization potential smaller than 13.6 ev it can be ionized from the ground state by continuum radiation above the Lyman continuum. The photoionization cross section is affected by the presence of auto-ionization levels, however it is not expected to change the integrated value over the spectrum by an order of magnitude. It could make significant changes, by factors of about 2 to our calculations. If there were enough information on those levels, it would be interesting to include them in our calculations. The same remarks apply for elements having numerous excited levels contributing to the photoionization opacity, like the iron peak elements and Zr. The auto-ionization levels cannot contribute substantially here to the transfer of momentum to ions, like Mg II, having only one electron outside of a closed shell: the excitation

of two electrons then always involves more energy than is available above the Lyman continuum.

Both O and Si are special cases. There is only one level of O which is properly placed to transfer an appreciable amount of momentum from the continuum: the $2p^4\ ^1D$ level which is 2.0 ev above the ground state (ionization from the ground state would require radiation from below the Lyman continuum). However, it is a ^1D term and, in Russel-Saunders coupling, the $\Delta S = 0$ selection rule does not allow it to be photoionized to the ground state of O II, a ^4S term. Allowed photoionization from that excited level requires light from below the Lyman continuum. Furthermore, in such a light element as O, Russel-Saunders coupling holds as exemplified by the small energy difference between terms of different J in a multiplet. Transitions to auto-ionization levels might then be the main source of absorption. However, in the case of O, either transitions from the ^1D level have to go to ^3P or ^3F levels and thus are expected to be weak transitions (forbidden by the $\Delta S = 0$ selection rule) or they go to ^1P and ^1F levels and are not expected to be broadened by auto-ionization because the available continuum of states has $S = 3$. The same argument applies to the second excited level, a ^1S level; however, it is never populated enough to contribute substantially to the absorption, even if there were no selection rules against it. One then expects only a little momentum to be transferred from the radiation field to oxygen. The experimental results of Rudd and Smith (1968) agree with the preceding discus-

sion: they have found no evidence of the auto-ionization of ^1D or of ^1S levels to the continuum involving the ground state of O II (a ^4S level). The force transferred from the radiation field to O is then calculated to be smaller than 10%of the gravitational force on O. It could not impede gravitational settling.

The case of silicon is different, mainly because of the break down of Russel-Saunders coupling. Si II has two excited levels that are properly placed: a $3p^2\ ^4P$ level and a $3p^2\ ^2D$ level. The $3p^2\ ^2D$ level is perturbed by a $3d\ ^2D$ level. Froese and Underhill (1966) calculated that the wave function for the level of interest was actually:

$$0.84\ 3s3p^2\ ^2D + 0.54\ 3s^23d\ ^2D$$

The photoionization of the $3s\ 3p^2\ ^2D$ configuration to the ground state of Si II is prohibited, but that of the $3s^23d\ ^2D$ is not. Furthermore that level has permitted transitions to levels which are known to be strongly auto-ionizing (Shenstone, 1961). Their width is however unknown.

The photoionization of the $3p^2\ ^4P$ level to the ground state of Si III is forbidden. It is a two electron jump. However, this level has permitted transitions to quadruplet levels which, in spite of the $\Delta S = 0$ selection rule, show auto-ionization effects to the continuum involving the ground state of Si III (Shenstone, 1961). These auto-ionization levels would not be expected to be very wide, but it seems, in spite of the $\Delta S = 0$ selection rule, that the transitions to the strongly auto-ionizing doublet terms may not be so strongly prohibited

because of the break-down of the $\Delta S = 0$ selection rule in the auto-ionizing of the ^4P levels.

The available information on Si II does not allow us then to say whether auto-ionization will be important or not in transferring momentum from the radiation field to Si. However, it is quite possibly important. Because we ignore the width of auto-ionizing levels and the f values of the lines connecting them to the $3p^2\ ^4P$ and $3p^2\ ^2D$ levels, one cannot calculate with any degree of certainty the radiation force the auto-ionization levels may transfer to Si. An upper limit is obtained by assuming an auto-ionization level is 0.5 ev wide and is connected to the levels of interest by lines with $f \simeq 1$. The radiation force on Si is then found to be 20 times the gravitational force in an atmosphere with $\theta_{eff} = 0.32$, $\log g \simeq 4$ and taking saturation into consideration for an overabundance of Si by a factor of 20.

Whether radiation pressure is transferred to Si through photo-excitation to auto-ionization levels or through photoionization, the lower levels are always the same and the radiation comes from the same part of the spectrum. Both processes then give the same dependence of the radiation force on the effective temperature of the star. Plotted in Fig. 4 are the results for photoionization in the hydrogenic approximation. This could be an overestimate if Russel-Saunders coupling is a good approximation. It would be an under-estimate if the auto-ionization levels which are known to exist were wide enough, $\Gamma \gtrsim 0.05$ ev, and if they were connected to the levels of interest by strong lines.

6. COMPARISON WITH OBSERVATIONS

We are now in a position to discuss what abundance anomalies can be expected from diffusion processes in A-pec stars and to compare these to the observed abundance anomalies. Given the diffusion hypothesis, most well-established abundance anomalies would be expected. The most important difficulty comes from the Si overabundance. Its explanation requires the auto-ionization levels known to exist at the proper energy in Si II to be unusually wide features.

If the atmosphere of the star is stable, abundance anomalies should manifest themselves on a time scale of 10^4 years. Those elements not contributing enough to the opacity in the outer atmosphere of the star will settle down. To observe large underabundances, elements have to settle over the whole surface of the star. For instance to observe an underabundance by a factor of 100, the elements must have settled down over 99% of the surface. Ionized elements will settle down ten times more slowly than the non-ionized ones. Furthermore, when they have to cross magnetic field lines, they will be slowed down by another factor of 10. An element is then expected to be most underabundant when it is not ionized.

Diffusion upwards will also be slower for ionized than for nonionized elements. However, the magnetic field is now expected to channel elements into patches and not to slow appreciably the flow of elements upwards when the magnetic field is parallel to the gravitational field. In those stars with magnetic fields, over-

abundances of ionized elements should be expected to occur in patches and to vary with a period related to that of the magnetic field.

The transfer of momentum through bound-bound transitions (lines) is expected to be efficient in pushing outwards the less abundant elements. Each line of thermal Doppler width can, on the average, support a mass fraction of 3×10^{-7}. Since the mass fraction of a typical normally abundant rare earth is only 10^{-8} to 10^{-9}, lines could easily cause overabundances of rare earths. As seen from Figs. 11 to 13 the force exerted by lines is not dependent on τ, so long as the element remains in an ionization state where there are lines, i.e., does not take the configuration of a rare gas. Lines cannot only maintain overabundances in the upper part of the atmosphere, they can also push elements from below.

Lines cannot support overabundances of the more abundant elements, like Si, in the upper part of the atmosphere. Overabundances of the light elements are possible only when the radiation force transferred through photoionization or through auto-ionization levels is larger than the gravitational force. However, lines can still push elements from below to fill the upper part of the atmosphere where the continuum takes over. Note that an overabundance by a factor of ten requires only that the elements from above $\tau = 1$ be pushed up.

The diffusion hypothesis predicts that the abundant, light, nonionized elements, which have no properly placed continuum and which do not have enough lines to be kept up by lines, should be most

underabundant. This is confirmed by the results of Sargent and Searle (1962). When O and Mg are both once ionized one expects both to have settled down by the same amount. On the average this happens around $\theta_{eff} = 0.4$ (see Fig. 14). When O is not ionized, one expects O to be much more underabundant than Mg. This is confirmed at $\theta_{eff} \gtrsim 0.45$. When Mg is twice ionized and O is once ionized, one would expect O to be slightly more underabundant than Mg. This would occur for $\theta_{eff} \lesssim 0.36$. The data are not good enough yet to confirm this trend; in any case, the difference should be relatively small. Whereas O not being ionized increases its diffusion velocity by a factor of about 100, Mg being twice ionized changes the diffusion velocity by a factor of only 4.

Similarly Ne and He would be expected to be most underabundant when they are not ionized. The data are not as conclusive for Ne as for O (see Fig. 15). Note that Ne can be observed only when it is starting to be ionized. We have compared Ne to C because, for a given abundance, the observed lines of Ne and C behave similarly with θ_{eff} (Sargent et al., 1969). He seems to be underabundant in the stars in which it is not ionized in the upper atmosphere as would be expected.

Si will be pushed up only if there exist wide auto-ionization states in Si II, as mentioned above. If they do exist, the radiation force on Si will be largest in the temperature range in which the Si stars are observed.

P, S, Cl, Ca, and Sc can be expected to be overabundant

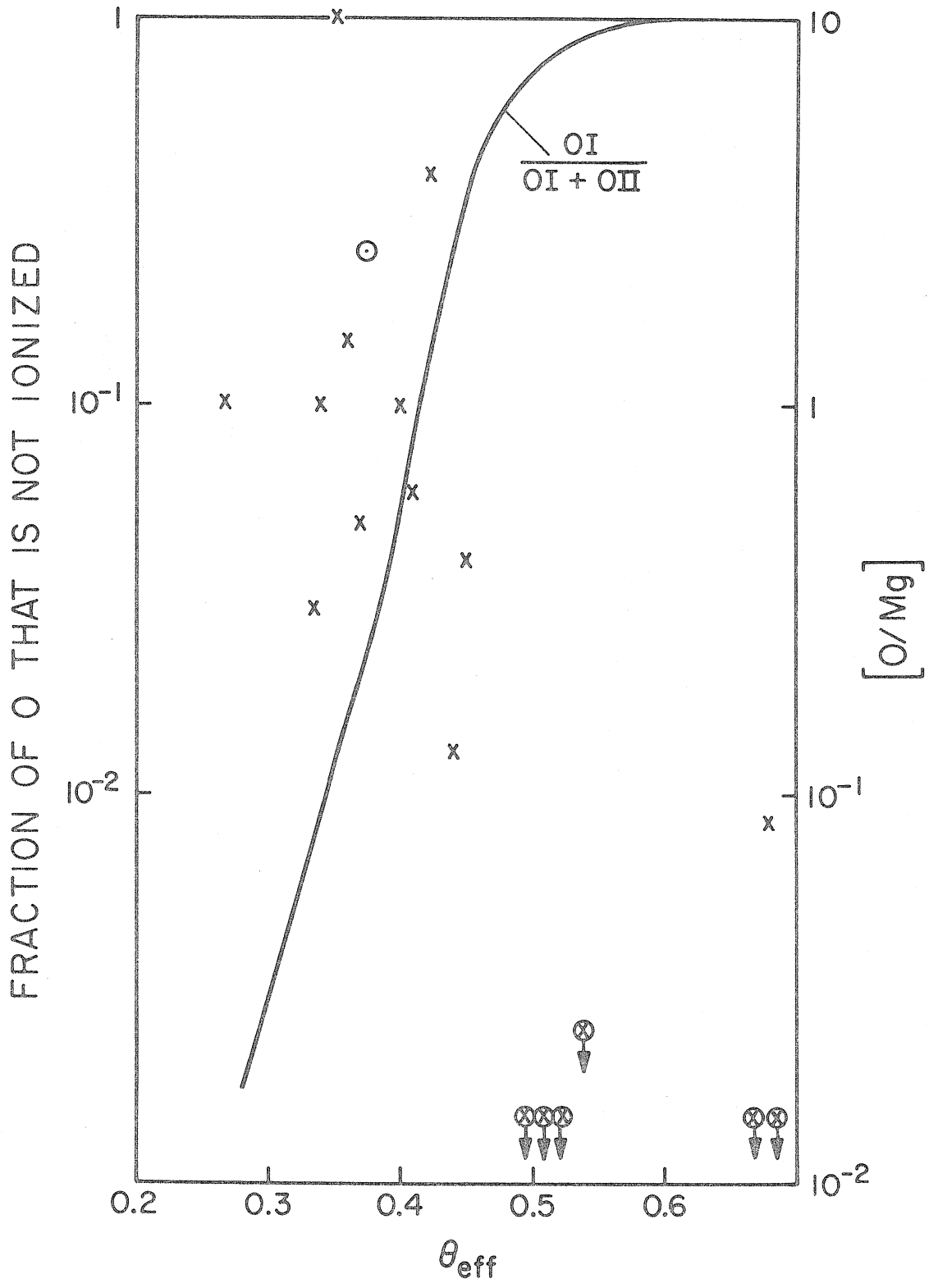
FRACTION OF O THAT IS NOT IONIZED
1
10^{-1}
10^{-2}
10
1
10^{-1}
10^{-2}
[O/Mg]
OI / OI + OII
0.2
0.3
0.4
0.5
0.6
θ_{eff}

Fig. 14

Fig. 14. The line indicates what fraction of O is not ionized at $\tau = 0.3$ in model atmospheres with log g = 4.0 and different θ_{eff}. The points show the abundance of O in a number of stars. The unfilled circle represents an He weak star and the crosses represent A-pec stars (from Sargent and Searle, 1962). The greater underabundances of O occur only in stars where O is not ionized in the outer atmosphere as would be expected from the diffusion hypothesis.

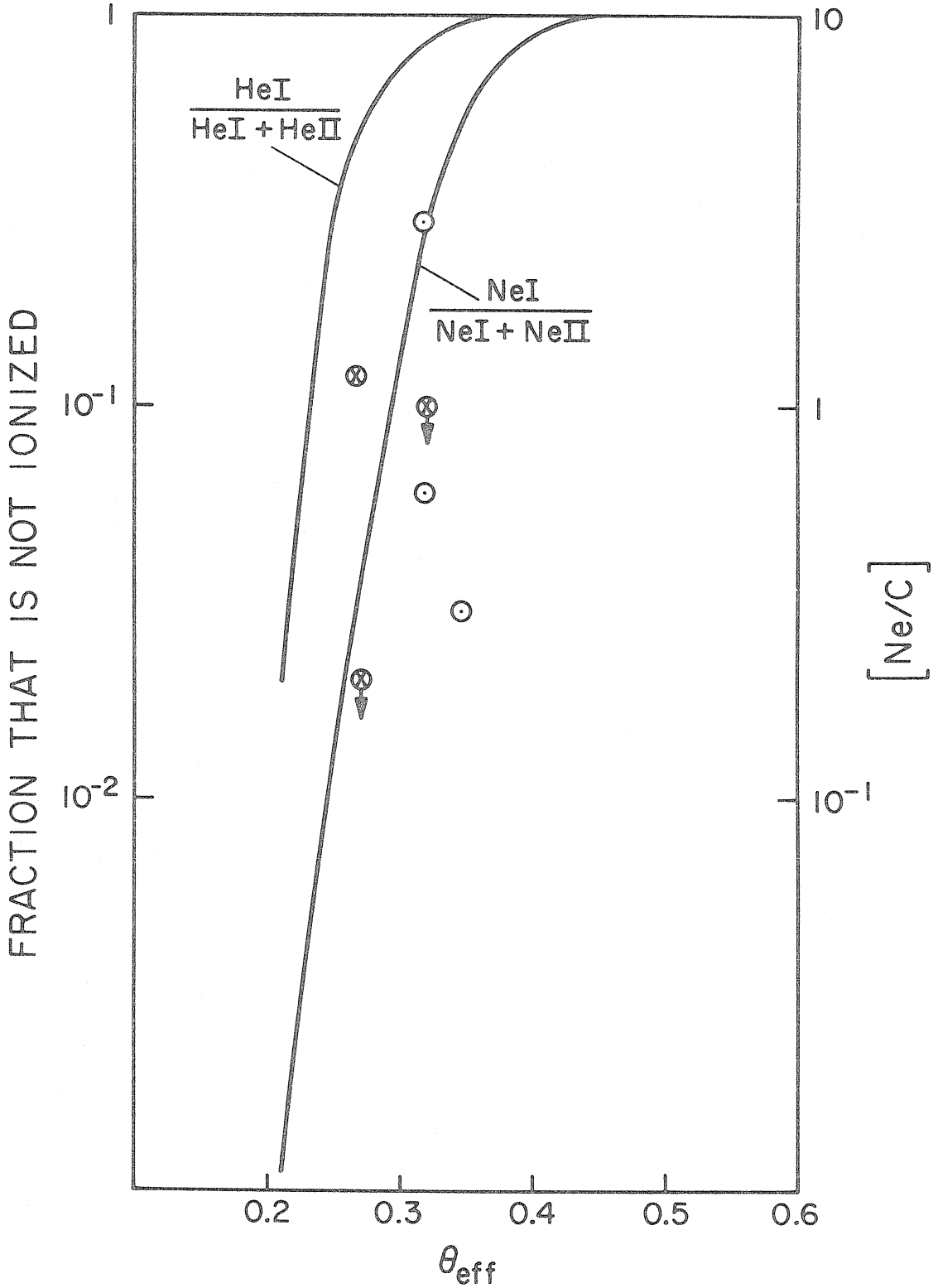
FRACTION THAT IS NOT IONIZED
1
10^{-1}
10^{-2}
HeI / (HeI + HeII)
NeI / (NeI + NeII)
10
1
10^{-1}
[Ne/C]
0.2
0.3
0.4
0.5
0.6
θ_{eff}

Fig. 15

Fig. 15. The lines indicate what fraction of He and Ne is not ionized at $\tau = 0.3$ in model atmospheres with $\log g = 4.0$ and different θ_{eff}. The points show the abundance of Ne in a number of stars (from Sargent, Greenstein and Sargent, 1969). The unfilled circles represent He-weak stars and the crosses represent A-pec stars. The data are not as conclusive as for O, since Ne has been observed only in stars where it is getting ionized in the atmosphere.

in the cooler A-pec stars, but neither A nor K should be. Sargent and Searle have made no systematic studies of these elements. The observational data is not conclusive except for P. Compare the different values obtained for the abundance of Ca in 53 Tau (table 3). The overabundances of P observed in 3 Cen A and a few Mn stars for instance κ Cnc are not explained here. In κ Cnc the ratio of O to Mg does not seem to follow the same trend as in the other A-pec stars.

In the iron peak, Fig. 7 shows that the diffusion hypothesis explains naturally the overabundance of Mn. The occurrence of Mn stars in the θ_{eff}, log g plane is also explained naturally. There is excellent agreement between the observations and the overabundances predicted by the diffusion hypothesis. Line absorption could explain slight overabundances of the other elements of the iron peak. Ti and Fe may also be affected by continuum radiation, but not as much as Mn. One would not expect from diffusion large overabundances of Cr. In fact Searle, Lungershausen and Sargent (1966) conclude that Cr was not as overabundant as generally believed.

Lines can be expected to cause overabundances of most elements heavier than the iron peak. They are so underabundant that they generally are observed to have more lines than is necessary to push them upwards. As can be seen from table 4, they are observed to be overabundant. Comparing Fig. 8 and table 4, it seems that Sr, Y and Zr are most overabundant in those stars where the radiation pressure transferred to them through the continuum is

largest.

The rare earths are observed to be overabundant as expected. Ba is not expected to be as overabundant as the rare earths, since in the atmosphere of the A-pec stars, it is mainly in the form of Ba III which has the same atomic configuration as the preceding noble gas. It must have very few lines if any.

However, Sr will also take the configuration of the preceding noble gas in the atmospheres of the A-pec stars, and it is observed to be overabundant. It should first be mentioned that the maximum of the radiation pressure force on Sr is in stars with $\theta_{eff} \simeq 0.55$. The maximum on Ba would occur in stars with $\theta_{eff} \simeq 0.61$, because the ionization potential of Ba II is smaller than that of Sr II. At that temperature, the convection zone is becoming more important and diffusion processes are probably unimportant. Similar remarks apply to the contribution of lines. Sr is then expected to be more overabundant than Ba, however the observed difference between the two is perhaps bigger than would be expected.

Thus the diffusion hypothesis predicts the better established abundance anomalies in the A-pec stars. In particular it predicts the dependence of the anomalies on θ_{eff}, unlike any nuclear model. It also predicts that in a given star, Sr, Y and Zr should behave differently, which again no nuclear models predict. It also predicts the existence of patches leading to periodic variation of the overabundances. However, explaining the overabundance of P and the existence of both Si and Mn stars at the same θ_{eff} is difficult.

In our calculation, we had no free parameter to play with. However, if we suppose that the atmospheres are not stable in their uppermost part but only below a given value of τ, which may vary from star to star, we would expect to have both Si and Mn stars at the same θ_{eff}. We see on Fig. 9 that the radiation force on Si does not decrease as rapidly when τ increases as that on Mn. If the relevant τ for a given star were 1.0 or 2.0 it might become a Si star, whereas it would be a Mn star if the relevant τ were 0.1. Some of the characteristics of the metallic line stars can probably be explained in the same way. However, it is not clear how one could explain the underabundances of Sc and Ca observed in some metallic line stars. Because of the uncertainty as to the value of τ one should use, we have not pursued the matter any further.

REFERENCES

Abt, H. A. 1967, in The Magnetic and Related Stars, Edited by R. C. Cameron (Baltimore, Mono Book Co.), 173.

Adelman, S. J. 1968, Pub. A.S.P. 80, 329.

Aller, L. H. and Bidelman, W. P. 1964, Ap. J. 139, 171.

Aller, L. H. and Chapman, A. 1960, Ap. J. 132, 461.

Auer, L. H., Mihalas, D., Aller, L. H. and Ross, J. E. 1966, Ap. J. 145, 153.

Babcock, H. W. 1947, Pub. A.S.P. 59, 112.

Babcock, H. W. 1958a, Ap. J. Suppl., 3, 141.

Babcock, H. W. 1958b, Ap. J. 128, 228.

Babcock, H. W. 1963, Ap. J. 137, 690.

Berkowitz, J. and Lifshitz, C. 1968, J. Phys. B (Proc. Phys. Soc.), 1, 438.

Brancazio, P. J. and Cameron, A. G. W. 1967, Can. J. Phys. 45, 3297.

Chapman, S. and Cowling, T. G. 1953, The Mathematical Theory of Non Uniform Gases, Cambridge, University Press.

Cowling, T. G. 1953, in The Solar System V-I The Sun, Edited by G. P. Kuiper (Chicago, University of Chicago Press), 532.

Deutsch, A. J. 1958, Handbuch der Phys. LI, (Berlin, Springer-Verlag), 689.

Deutsch, A. J. 1966, I.A.U. Sym. No. 26, 268.

Deutsch, A. J. 1967, in The Magnetic And Related Stars, Edited by R. C. Cameron (Baltimore, Mono Book Co.), 181.

Ditchburn, R.W. and Hudson, R. D. 1960, Proc. Roy. Soc. 256, 53.

Fowler, W. A., Burbidge, G. R. and Burbidge, E. M. 1955, Ap. J. Suppl., 2, 167.

Fowler, W. A., Burbidge, E. M., Burbidge, G. R. and Hoyle, F. 1965, Ap. J., 142, 423.

Froese, C. and Underhill, A. B. 1966, Ap. J. 146, 301.

Garrison, R. F. 1967, Ap. J. 147, 1003.

Greenstein, G. S., Truran, J. W. and Cameron, A. G. W. 1967, Nature, 213, 871.

Hack, M. 1968, Sky and Telescope, 36, 92.

Hardorp, J. 1966, Z. Astrophys. 63, 137.

Hardorp, J., Bidelman, W. P. and Prolss, J. 1968, Z. Astrophys., 69, 429.

Hyland, A. R. 1967, in The Magnetic and Related Stars, Edited by R. C. Cameron (Baltimore, Mono Book Co.), 311.

Iben, I. 1965, Ap. J. 142, 1447.

Iben, I. 1966, Ap. J. 143, 483.

Kraft, R. P. 1967, in The Magnetic and Related Stars, Edited by R. C. Cameron (Baltimore, Mono Book Co.), 303.

Krause, M. O. 1969, Phys. Rev., 177, 151.

Ledoux, P. and Renson, P. 1966, Ann. Rev. of Astron. and Astroph., 4, 293.

Loeb, L. B. 1934, The Kinetic Theory of Gases, McGraw Hill (Reedited 1961, Dover Publications, Inc., New York).

Mestel, L. 1966, Zeits. f. Astrophys., 63, 196.

Mihalas, D. 1965, Ap. J. Suppl. 9, 321.

Mihalas, D. and Henshaw, J. L. 1966, Ap. J. 144, 25.

Milne, E. A. 1927, MNRAS, 87, 697.

Morgan, W. W. 1933, Ap. J. 77, 330.

Newson, G. 1966, Proc. Phys. Soc. (London) 87, 975.

Pecker, J. and Schatzman, E. 1959, Astrophysique Générale, Dunod, Paris.

Praderie, F. 1968, private communication.

Rudd, M. E. and Smith, K. 1968, Phys. Rev., 169, 79.

Sargent, W. L. W. and Searle, L. 1962, Ap.J. 136, 408.

Sargent, W. L. W. and Searle, L. 1967a, in The Magnetic and Related Stars, Edited by R. C. Cameron (Baltimore, Mono Book Co.), 209.

Sargent, W. L. W. and Searle, L. 1967b, Ap. J., 150, L33.

Sargent, A. I., Greenstein, J. L., and Sargent, W. L. W. 1969, Ap. J. (in press).

Searle, L., Lungershausen, W. G., and Sargent, W. L. W., 1966, Ap. J., 145, 141.

Searle, L. and Sargent, W. L. W. 1964, Ap. J. 139, 793.

Shenstone, A. G. 1961, Proc. Roy. Soc. A261, 153.

Sommerfeld, A. 1939, Atombau und Spektrallinien, V-2, 5th ed., Braunschweig.

Spitzer, L. 1962, Physics of Fully Ionized Gases, Interscience, New York.

Strom, K. M. 1969, Astronomy and Astrophysics, 2, 182.

Sweet, P. A. 1950, MNRAS, 110, 548.

Van den Heuvel, E. P. J. 1968a, BAN, 19, 326.

Van den Heuvel, E. P. J. 1968b, BAN, 19, 432.

Wolff, S. C. 1967, Ap. J. Suppl., 15, 21.

Wolff, S. C. 1968, Pub. A.S.P., 80, 281.

II. NUCLEOSYNTHESIS IN Si BURNING

1. INTRODUCTION

It has been realized for some time that the observed abundances of the iron peak elements closely matched those to be expected from nuclear equilibrium for some value of temperature, density and neutron enrichment (Hoyle, 1946; Burbidge, Burbidge, Fowler and Hoyle, 1957). More recently, Bodansky, Clayton and Fowler (1968) found that, if equilibrium is reached between ^{28}Si and the iron peak but not between ^{28}Si and ^{4}He, it is possible that the observed abundances from ^{28}Si to the iron peak would have been generated in a single process. However their comparison with observations was made for one zone of the star, in which there is a well defined fraction of ^{28}Si. In a given star, there will be a superposition of zones, each with a different dynamic history and with a different value of left over ^{28}Si.

In what follows, we shall find that the superposition of zones in a Si burning star leads, with little arbitrariness, to the observed abundances between ^{28}Si and the iron peak. The iron peak elements may have been generated in complete equilibrium, but elements like ^{29}Si, ^{30}Si, ^{31}P, ^{32}S ... were generated in zones where little ^{28}Si had burned. The generated abundances will be seen to depend mainly on the neutron enrichment and the extent of ^{28}Si photodisintegration in the coolest and hottest ejected zones. With those three parameters, it is possible to obtain agreement within a factor of 3 between the observed abundances and those expected from these calculations for some 25 of the 41 elements between ^{28}Si and ^{58}Ni. The

generated abundances of only a few elements will depend on a fourth parameter, the ratio of ^{32}S to ^{28}Si after C or O burning. Some of the poorly fitted nuclei (^{36}S, ^{40}A, ^{46}Ca and ^{48}Ca) are unabundant neutron rich nuclei, which could easily have been produced by a slight exposure of the material to a neutron flux. The freezing process will be found relatively unimportant for most nuclei, but some of the poorly fitted nuclei will be found to be the most affected by it. Inclusion of the freezing process improves agreement with the observations, in many of those cases.

We shall first discuss the reaction rates which we shall use and mention the other physical constants of importance. We shall then describe our method of solution of the evolutionary equations and justify our assumptions a posteriori. We shall finally present our main results and compare them to the observations. We shall also discuss the limitations that the observed abundances put on the astrophysical conditions for their generation.

2. PHYSICAL CONSTANTS; REACTION RATES

There are four groups of physical constants which are important to the calculations of the transformation of ^{28}Si into the iron peak: the nuclear partition functions, the binding energies, the beta decay rates and the nuclear reaction rates. For the first three, we have used values already available in the literature.* The nuclear reaction rates needed for our calculations can be separated into two groups: those related to the photodisintegration of ^{28}Si (that is ^{24}Mg $(\gamma\alpha)$, ^{20}Ne $(\gamma\alpha)$, ^{16}O $(\gamma\alpha)$, ^{12}C $(\alpha\alpha\alpha)$ and a group of 15 reaction rates (and their reverse) at masses A = 41 to 48. Those in the first group have been measured experimentally (Fowler et al., 1967). Uncertainties of the order of 50 % are to be expected in this case. Those in the second group have not. They have been estimated theoretically by Truran et al. (1966). In order to determine more precisely which of those rates were important to the evolution calculations, how uncertain they were, and which experiments should be carried out to reduce the uncertainties, we have recalculated them using a semi-empirical formula for Γ_γ/D (Appendix 1) and the equivalent square well introduced by Vogt et al.

---

*Most of the partition functions were taken from Truran, Cameron and Gilbert (1966). Those not available there were taken from the estimates of Clifford and Tayler (1965). Most of the binding energies were taken from Mattauch, Thiele and Wabstra (1965). When not available there, we used those of Harchol, Jaffe, Miron, Unna and Zionni (1967) or, when not available there either, we used those of Clifford and Taylor (1965). For all the beta decay rates, we used the numerical fits presented by Hansen (1966).

(1965) and discussed in detail by Michaud et al. (1969). Comparing our results to other calculations and to the available experimental data points to uncertainties of a factor of two or so in the nucleon channel, of five in the alpha channel (or perhaps more due to uncertainties in the applicability of the optical model as discussed in Michaud et al., 1969), and of five in the gamma ray channel. Uncertainties due to the excited levels may also introduce a factor of five. These factors will be seen not to be additive in general.

We shall start from the results of the evaporation theory for reaction cross sections averaged over the compound nucleus resonances:

$$\bar{\sigma}_{\alpha\alpha'} = \frac{\pi}{k_\alpha^2} \sum_{I,\Pi} \frac{2J+1}{(2I+1)(2i+1)} \left\{ \sum_{s,\ell} T_\ell(\alpha) \right\} \left\{ \frac{\sum_{s'\ell'} T_{\ell'}(\alpha')}{\sum_{\alpha''s''\ell''} T_{\ell''}(\alpha'')} \right\} \quad (1)$$

where α represents the pair of particles and their state of excitation, I and i are the intrinsic spins of the pair of particles α, s is the channel spin, ℓ the orbital angular momentum of the pair, J is the angular momentum of the compound nucleus (or equivalently the total angular momentum $\vec{J} = \vec{\ell} + \vec{s} = \vec{\ell} + \vec{I} + \vec{i}$), Π is the intrinsic parity. The unprimed quantites refer to the incoming channel, the primed quantites should be summed over all open channels in the compound nucleus including excited states of the residual nucleus. It is assumed that all $T_{s\ell}(\alpha) = T_\ell(\alpha)$ and similarly in the primed and

---

*For a justification and a discussion of the evaporation theory see Vogt (1968).

double-primed cases.

As shown in Michaud et al. (1969), the equivalent square well is an excellent approximation to Saxon-Woods potentials:

$$V_{SW}(r) = (V_0 + iW_0)/(1 + e^{+(r-R_0)/a}) \tag{2}$$

where a is the surface thickness, R_0 the radius of the well, V_0 and W_0 the real and imaginary parts of the potential close to $r = 0$ (since $R_0 >> a$). The equivalent square well is defined by:

$$V = (V_1 + iW_1) \qquad r < R_1$$

$$V = 0 \qquad r > R_1$$

$$R_1 = R_0 + \Delta R$$

$$W_1 \simeq W_0$$

and V_1 determined from:

$$V_0 R_0^2 \simeq V_1 R_1^2$$

The value of ΔR is given in Michaud et al. Using the equivalent square well to replace the Saxon-Woods potential, the transmission function can be written:

$$T_\ell = \tau_\ell/(1 + \tau_\ell/4)^2 \tag{3}$$

$$\tau_\ell = 4\pi P_\ell s_\ell f \tag{4}$$

where P_ℓ $(= kr/[F_\ell^2 + G_\ell^2])$ and s_ℓ are the usual square well

nuclear penetrability and strength functions respectively, and where f is the reflection factor. We have used the black nucleus strength function throughout. Vogt (1962) has shown, for neutrons, that, on the average, the black nucleus strength function multiplied by the reflection factor should be equal to the Saxon-Woods strength function. The same is expected to be true for protons. For ^{4}He projectiles, the black nucleus strength function multiplied by f is equal to the diffuse well strength function since the large W_0 used for ^{4}He smooths out any giant resonance effects. Finally in 3, we have neglected terms like PR^{∞}, SR^{∞} and πSs.* The terms containing R^{∞} will be, on the average 0. They will change sign at resonance. For alpha particles, they will always be zero, since the large size of W_0 guarantees no resonance effects. For protons and neutrons, numerical calculations can prove them small. The $\pi S_\ell s_\ell$ term is also small. It is zero on a giant resonance since S_ℓ is zero there (see Vogt, 1962). Away from a giant resonance, s_ℓ becomes small (by definition of a giant resonance). Using the black nucleus strength function to calculate $\pi S_\ell s_\ell$ would then give an overestimate. Even then, numerical calculations have shown that the $\pi S_\ell s_\ell$ term would contribute less than 5% of the value of the denominator.

For the cases considered here, only the terms with transmission functions with $(\ell, \ell', \ell'') \leq 3$ will contribute more than 20% to the cross section. They will be the only ones considered below.

---

*These terms are defined by Vogt (1962) and are contained in the expressions from which our equation 3 originates.

We have calculated the transmission functions for all particle channels using the square wells equivalent to the Saxon-Woods wells with the parameters indicated in table 1.

For $T(\gamma)$, we have used

$$T(\gamma) = 2\pi\Gamma_\gamma/D \tag{5}$$

where Γ_γ/D was calculated as explained in Appendix 1.

Granting that the optical model is a good model, four physical parameters are needed to calculate the cross sections: the radii of the different channels, the diffuseness parameter a, and the spins and parity of the available states of the target and residual nuclei.

For the nuclei of interest here, the spin and parity of the ground state of unstable nuclei are frequently uncertain. Those of the excited levels are usually unknown.* Those nuclei whose ground state has a spin different from zero frequently have low energy excited levels that could easily be heavily populated at the temperatures of interest here $(3 \leq T_9 \leq 6)$.** We shall neglect the excited levels because of our ignorance of their spins. We shall discuss below what uncertainties this introduces.

Using equation 1, transmission functions for ^{4}He, p and n channels, Γ_γ/D from the appendix, and the spins and parities of the ground states as given in the Nuclear Data sheets, we have calculated reaction cross sections for the cases of interest to us. The

*See for instance the Nuclear Data sheets.

**We will use $T_9 \equiv T/10^9$ where T is in ^oK.

TABLE 1

Parameters of the Saxon-Woods Well

	R (fermis)	V_o (MeV)	W_o (MeV)	a (fermi)	f	ΔR
Nucleons	$1.25\ A_T^{1/3}$	50	4	0.5	2.7	0.1
^4He	$1.09\ A_T^{1/3} + 1.6$	60	10	0.5	4.8	0.7

A_T: atomic number of the target nucleus

reaction rates were then obtained from (Fowler and Hoyle, 1964):

$$\langle \sigma v \rangle = \frac{2.1 T_9 \times 10^{14}}{M} \int \left(\frac{E}{kT}\right) \sigma \exp(-E/kT)\, d(E/kT) \ \text{cm}^3/\text{sec} \qquad (6)$$

(if σ is in cm^2). The reaction cross section was evaluated for about 15 values of the energy around the maximum value of the integrand, which was then integrated using a simple sum of rectangles (i.e. $\sum \Delta(E/kT) \times$ value of the integrand at the center of ΔE).

The reaction rates were fitted to the formula:

$$N_A\langle \sigma v \rangle = A_1 \times 10^{(A_2(0.25 - 1/T_9))} \ \text{cm}^3/\text{sec g})$$

N_A is Avocadro's number. $A_1 = N_A\langle \sigma v \rangle$ at $T_9 = 4$ in the middle of the range of interest and A_2 is an effective threshold temperature. The fitted values of A_1 and A_2 are in table 2. The fitting formula reproduces the theoretical results to approximately 20% over the range $3 \leq T_9 \leq 6$. In table 3 we have compared the reaction rates we calculated to available experimental rates (Fowler, 1968) and to those calculated by Truran et al. (1966). Our calculated rates involving only particle channels are within a factor of 2 of the observed rates whereas those involving γ-rays are within a factor of 3. It seems to us that the main uncertainty in the (p, γ) rates comes from the γ-channels since the proton channels are not very sensitive to the radius used.

In table 4 we have compared the rates we calculated around atomic mass number 44 to those calculated by Truran et al.

TABLE 2

Constants for the Reaction Rates
(reaction rates in $cm^3/sec/g$)

Reaction	A_1	A_2	$A_2/5.04$ (MeV)	Q of the Reaction (Mev)
$^{41}Ca(\alpha\gamma)$	6.6	17.6	3.0	6.3
$^{42}Ca(\alpha\gamma)$	1.14×10	16.7	3.0	8.0
$^{42}Ca(\alpha p)$	1.76×10	20.6	4.0	-2.3
$^{42}Ca(\alpha n)$	7.9	27.0	5.4	-5.2
$^{43}Ca(n\gamma)$	7.8×10^6	0.0	0.0	6.7
$^{44}Ca(p\gamma)$	5.7×10^4	5.35	1.0	6.9
$^{44}Ca(pn)$	3.7×10^3	22.	4.4	-4.4
$^{44}Sc(p\gamma)$	3.2×10^4	6.14	1.2	8.5
$^{44}Sc(n\gamma)$	1.3×10^7	0.0	0.0	11.3
$^{44}Sc(pn)$	4.4×10^5	8.3	1.6	-0.9
$^{44}Ti(\alpha p)$	8.9	23.	4.6	-0.5
$^{44}Ti(n\gamma)$	6.6×10^6	0.0	0.0	9.4
$^{45}Sc(p\gamma)$	1.3×10^5	6.	1.2	10.4
$^{45}Sc(pn)$	9.2×10^4	14.3	2.8	-2.8
$^{45}Ti(n\gamma)$	1.5×10^7	0.0	0.0	13.2

TABLE 3

Comparison of Calculated and Measured Rates ($cm^3/sec/g$)

Reaction	T_9	Exper.*	These Calcu.	Turan et al. 1966
$^{27}Al(p\alpha)$	3	1.1×10^5	9.6×10^4	9.6×10^4
	5	4.7×10^5	7.8×10^5	4.1×10^5
$^{31}P(p\alpha)$	3	1.6×10^5	1.7×10^5	1.5×10^5
	5	7.8×10^5	1.6×10^6	7.2×10^5
$^{31}P(p\gamma)$	3	2.6×10^3	5.2×10^3	9.0×10^3
	5	5.9×10^3	1.7×10^4	2.4×10^4
$^{34}S(p\gamma)$	3	2.4×10^3	7.6×10^3	9.0×10^3
	5	6×10^3	2.1×10^4	3.4×10^4
$^{52}Cr(p\gamma)$	3	1.5×10^3	5.4×10^3	6.0×10^3
	5	1.1×10^4	3.9×10^4	5.4×10^4

*Fowler (1968).

TABLE 4

Comparison of Calculated Rates ($cm^3/sec/g$)

Reaction	T_9	These Calcu.	Turan et al. 1966	Turan et al. $\times \omega_T/(2\overline{I}_T+1)$
$^{41}Ca(\alpha\gamma)$	3	2.4×10^{-1}	1.3×10^{-1}	1.3×10^{-1}
	5	$5.4 \times 10^{+1}$	3.5×10	3.5×10
$^{42}Ca(\alpha\gamma)$	3	3.9×10^{-1}	2.5×10^{-1}	2.5×10^{-1}
	5	9.6×10	5.0×10	6.0×10
$^{42}Ca(\alpha p)$	3	2.7×10^{-1}	1.3×10^{-1}	1.3×10^{-1}
	5	2.5×10^{2}	1.2×10^{2}	1.5×10^{2}
$^{42}Ca(\alpha n)$	3	4.2×10^{-2}	1.6×10^{-2}	1.6×10^{-2}
	5	1.9×10^{2}	8.5×10	1.0×10^{2}
$^{43}Ca(n\gamma)$	3	7.4×10^{6}	1.4×10^{6}	1.8×10^{6}
	5	8.2×10^{6}	1.4×10^{6}	2.2×10^{6}
$^{44}Ca(p\gamma)$	3	2.0×10^{4}	2.2×10^{4}	2.4×10^{4}
	5	1.1×10^{5}	1.2×10^{5}	1.7×10^{5}
$^{44}Ca(pn)$	3	5.0×10	2.2×10	2.4×10
	5	5.0×10^{4}	2.1×10^{4}	3.1×10^{4}
$^{44}Sc(p\gamma)$	3	1.04×10^{4}	3.1×10^{3}	9.6×10^{3}
	5	7.0×10^{4}	1.3×10^{4}	6.3×10^{4}
$^{44}Sc(n\gamma)$	3	1.1×10^{7}	3×10^{6}	9.0×10^{6}
	5	1.2×10^{7}	3×10^{6}	1.5×10^{7}
$^{44}Sc(pn)$	3	8.4×10^{4}	2.2×10^{4}	6.6×10^{4}
	5	1.3×10^{6}	1.9×10^{5}	9.6×10^{5}
$^{45}Sc(p\gamma)$	3	3.8×10^{4}	2.8×10^{4}	3.6×10^{4}
	5	2.7×10^{5}	1.4×10^{5}	2.4×10^{5}
$^{45}Sc(pn)$	3	1.4×10^{3}	3.0×10^{3}	3.6×10^{3}
	5	5.5×10^{4}	2.2×10^{5}	3.6×10^{5}
$^{44}Ti(\alpha p)$	3	1.2×10^{-1}	1.1×10^{-1}	1.1×10^{-1}
	5	1.5×10^{2}	8.0×10	1.0×10^{2}
$^{44}Ti(n\gamma)$	3	6.1×10^{6}	2.9×10^{6}	2.9×10^{6}
	5	6.9×10^{6}	3.5×10^{6}	4.4×10^{6}
$^{45}Ti(n\gamma)$	3	1.4×10^{7}	6.6×10^{6}	1.1×10^{7}
	5	1.6×10^{7}	6.6×10^{6}	1.3×10^{7}

(1966). In their calculations Truran et al. (1966) approximated the effect of the existence of excited states in the target nucleus by multiplying the right-hand side of equation 1 by $(2I_T+1)/\omega_T$ where I_T is the spin of the ground state of the target nucleus and ω_T is the partition function for the target nucleus (including the excited states). They imply that inelastic scattering can be approximated by the partition function. The approximation is expected to be good only if the denominator of equation 1 is dominated by the entering channel. If it is dominated by any other channel, the factor $(2I_T+1)/\omega_T$ will be an overcorrection. This correction is seen to introduce a factor of up to 5 when ^{44}Sc is the target nucleus. When this is taken into account, the two sets of calculations seem to agree very well except for ^{45}Sc (pn) and ^{43}Ca (nγ). In the latter case the difference is probably mainly due to Γ_γ/D. In the ^{45}Sc (pn) case however, the source of the disagreement is harder to trace. Most of the present calculations give larger reaction rates, mainly because of the inclusion of the reflection factor.

Another effect of the uncertainty of the spin and parity can be studied by calculating reaction rates supposing that the target and residual nuclei, and the incoming and outgoing particles all have zero spin and the required parity Equation 1 then becomes

$$\overline{\sigma}_{\alpha\alpha'} = \frac{\pi}{k_\alpha^2} \sum_\ell (2\ell+1) \frac{T_\ell(\alpha) T_\ell(\alpha')}{\sum_{\alpha''} T_\ell(\alpha'')} \qquad (7)$$

In most cases equation 7 is a very good approximation

to equation 1. However, when neither α nor α' are the main open channels, equation 7 gives for the $\ell = 0$ term:

$$\frac{T_0(\alpha)T_0(\alpha')}{T_0(\alpha) + T_0(\alpha') + T_0(\text{main channel})} \simeq \frac{T_0(\alpha)T_0(\alpha')}{T_0(\text{main channel})} \tag{8}$$

If there were a large spin difference between the residual nucleus for the main channel compared to the α and α' channels, equation 1 would give:

$$\frac{T_0(\alpha)T_0(\alpha')}{T_{I+\frac{1}{2}}(\text{main channel})} \tag{9}$$

For neutron channels, one usually obtains:

$$T_{I+\frac{1}{2}} << T_0 \tag{10}$$

so that in these cases, equation 7 could be an underestimate by a large factor (see Fig. 1). This is what happened for ^{41}Ca $(\alpha\gamma)$ ^{45}Ti and for ^{44}Sc $(p\gamma)$ ^{45}Ti, for which the rates obtained from the approximation 6 are too small by a factor 3 and 10 respectively. If low-lying excited levels had a spin different from the ground state by $\Delta I \simeq 2$, such inaccuracies could have resulted from our neglecting them.

Suppose, for instance, that we are looking at a ^{A}Z (αp) reaction on an even Z, even N nucleus ($J = 0$ for the target nucleus). Suppose further that the $^{A+3}(Z+1)$ nucleus (the residual nucleus) has a spin $J = 7/2$. The conservation of total spin will

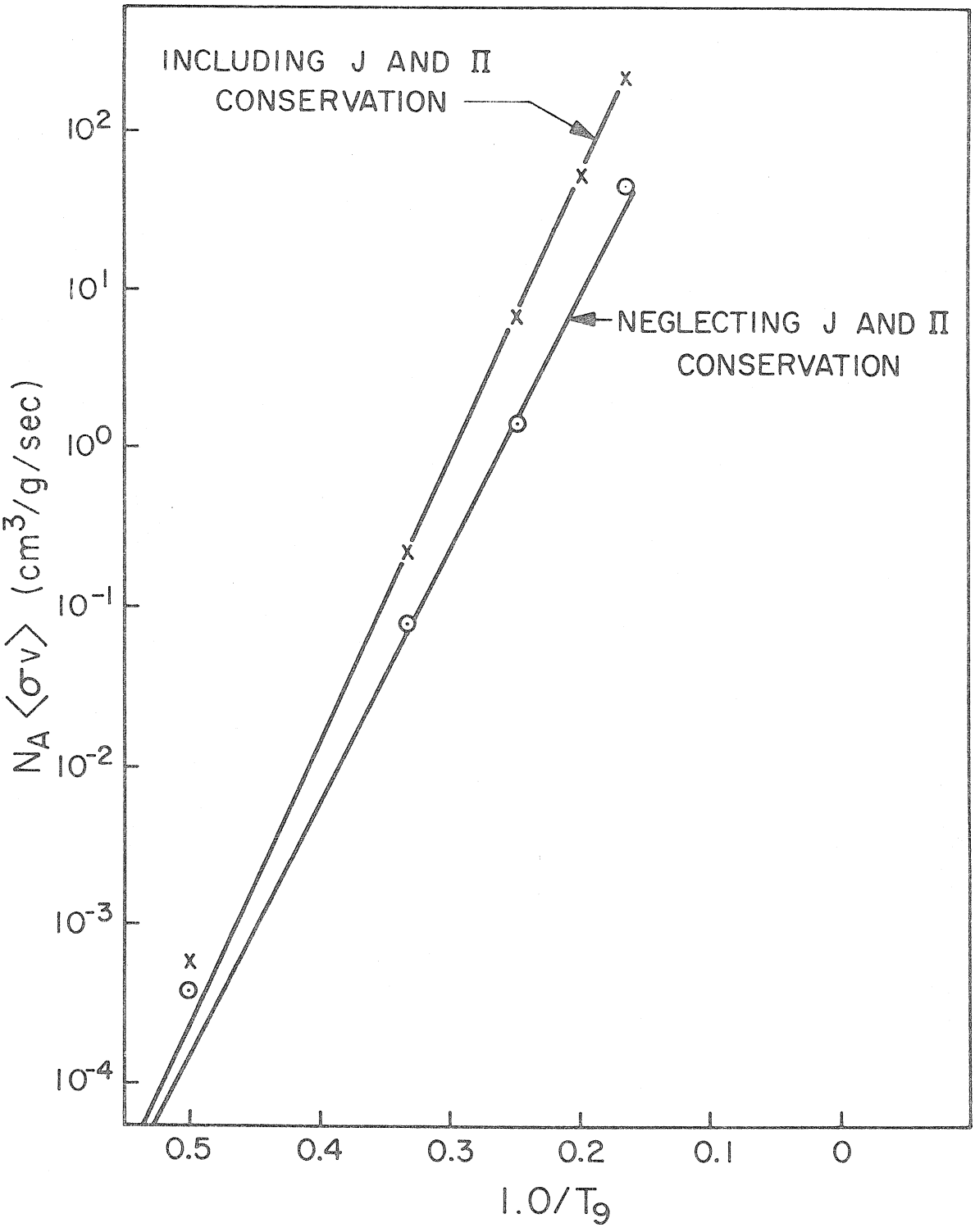
INCLUDING J AND Π
CONSERVATION
NEGLECTING J AND Π
CONSERVATION
$N_A\langle\sigma v\rangle$ (cm^3/g/sec)
10^2
10^1
10^0
10^{-1}
10^{-2}
10^{-3}
10^{-4}
0.5
0.4
0.3
0.2
0.1
0
$1.0/T_9$

Fig. 1

Fig. 1. Reaction rate for the reaction $^{41}Ca(\alpha\gamma)^{45}Ti$. The conservation of spin and parity is seen to increase the cross section by a factor of three or so. This will be the case only when there are large differences between the spins of the ground states of the nuclei involved. Our fitting formula (straight line) fits the calculated points when $T_9 \gtrsim 2.5$.

then eliminate all combinations like $T_0(\alpha)T_0(p)$ or $T_1(\alpha)T_1(p)$ and allow only the smaller $T_0(\alpha)T_4(p)$ combinations. However, if the first excited level of $^{A+3}(Z+1)$ is a low-lying state with $J = 1/2$, combinations like $T_0(\alpha)T_0(p)$, $T_1(\alpha)T_1(p)$ would be allowed again and could enhance the cross sections by one order of magnitude. From shell model calculations* levels with $J = 7/2$ are expected to occur in the mass range of interest here ($A \simeq 44$). However, no $J = 1/2$ level is expected to be too close. The enhancement is then not expected to be large (probably smaller than 30%). This effect could be much more important for nuclei with around 80 or 120 neutrons or protons, where ground states with $J = 11/2$ and $J = 13/2$ are found.

*See for instance Preston (1962).

3. THE METHOD OF CALCULATION

Our aim is to follow, in time, the evolution of nuclear matter after ^{12}C and/or ^{16}O burning. We neglect the dynamics of the problem and consider the evolution at different temperatures and densities with an eye on the observed abundances between ^{28}Si and Cu, in order to find out under what circumstances of temperature and density the evolution could have taken place.

Calculations can be considerably simplified once it is recognized that, when ^{28}Si burning occurs, one of the slowest links in the system is the disintegration of ^{28}Si. It is not that $^{28}Si\ (\gamma\alpha)\ ^{24}Mg$ is a slow reaction but rather that $X(^{24}Mg) << X(^{28}Si)$ (in what follows, we shall use $X(^{A}Z)$ to represent the mass fraction of ^{A}Z) under the circumstances considered here. Since the photo-disintegration flow is proportional to the number density of ^{24}Mg, the small ^{24}Mg abundance slows the disintegration flow by orders of magnitude.

Another slow link is found at atomic mass 44. It is again caused by the low abundance of elements which have to carry the flux to the more abundant iron peak nuclei.

The equilibrium equations will tell us what we need to know relating the nuclei that are in equilibrium. All that the time evolution needs to tell us is how much mass is available from ^{28}Si disintegration and how many nuclei have crossed the $A \sim 45$ bottle neck. One also needs to follow how many beta decays have had time to occur since the neutrinos and antineutrinos are expected

to escape and so make a complete equilibrium impossible. Instead of following with time each and every reaction rate in the system, it is then sufficient to count how much mass has disintegrated, how much has beta-decayed and how much has crossed the $A \simeq 45$ bottleneck. One is left with three time-dependent equations to solve, instead of a few hundred. The "constants" in the equations are themselves time dependent however, and their time variation determines the maximum acceptable time step for a given required accuracy. In what follows, we shall try, a posteriori, to justify quantitatively the numerous hypotheses contained in the preceding general remarks, after presenting the details of the adopted method of solution.

During the ^{28}Si photodisintegration, the nuclei separate themselves into three groups: the ^{16}O group comprises ^{12}C, ^{16}O and ^{20}Ne whose abundances are determined by the disintegration flow from ^{28}Si; the ^{28}Si group in which there is "equilibrium" among elements between ^{24}Mg and mass 45 and n, p and ^{4}He; and the iron group, where the elements are "in equilibrium" with each other and n, p and ^{4}He but not with elements of the ^{28}Si group; there is a break in the "equilibrium" at $A \simeq 45$. The term "partial-quasi-equilibrium" could be used meaning that given a certain fraction of ^{28}Si having disintegrated, given a certain value of neutron enrichment and given a certain number of nuclei having crossed into the iron peak, the nuclei are in the most likely statistical configuration. In "quasi-equilibrium" there would be no break

at A ~ 45 (Bodansky et al., 1968). In what follows we shall use for simplicity "quasi-equilibrium" instead of "partial-quasi-equilibrium."

Once the abundances of ^{4}He, p and n are determined by the quasi-equilibrium above ^{24}Mg, one can calculate the disintegration rate of ^{24}Mg. We shall consider only the main route: $^{24}\mathrm{Mg}(\gamma\alpha)^{20}\mathrm{Ne}(\gamma\alpha)^{16}\mathrm{O}(\gamma\alpha)^{12}\mathrm{C}(\gamma, 3\alpha)$ as justified by Bodansky et al. (1968). We shall also follow Bodansky et al. (1968) in supposing:

$$\frac{d\,^{20}\mathrm{Ne}}{dt} \ll \text{flux through } ^{20}\mathrm{Ne}$$

$$\frac{d\,^{16}\mathrm{O}}{dt} \ll \text{flux through } ^{16}\mathrm{O}$$

$$\frac{d\,^{12}\mathrm{C}}{dt} \ll \text{flux through } ^{12}\mathrm{C}$$

The number of ^{24}Mg nuclei disintegrating per second then forms a "conserved current" J_- down to the alpha particles. It is given by

$$J_- = \frac{\lambda_{\gamma\alpha}(^{24}\mathrm{Mg})n(^{24}\mathrm{Mg}) - \eta(^{20}\mathrm{Ne})\eta(^{16}\mathrm{O})\eta(^{12}\mathrm{C})r_{3\alpha}}{1 + \eta(^{20}\mathrm{Ne})\{1 + \eta(^{16}\mathrm{O})[1 + \eta(^{12}\mathrm{C})]\}} \tag{11}$$

where

$$\eta(^{A}\mathrm{Z}) = \frac{\lambda_{\alpha\gamma}(^{A}\mathrm{Z})}{\lambda_{\gamma\alpha}(^{A}\mathrm{Z})} \tag{12}$$

$$\lambda_{\alpha\gamma} = n_\alpha \langle \sigma(\alpha, \gamma)v \rangle$$

The abundances of ^{12}C, ^{16}O and ^{20}Ne are then given by:

$$n(^{12}C) = \frac{J_- + r_{3\alpha}}{\lambda_{\gamma\alpha}(^{12}C)} \tag{13}$$

$$n(^{16}O) = \frac{J_- + \lambda_{\alpha\gamma}(^{12}C)n(^{12}C)}{\lambda_{\gamma\alpha}(^{16}O)} \tag{14}$$

$$n(^{20}Ne) = \frac{J_- + \lambda_{\alpha\gamma}(^{16}O)n(^{16}O)}{\lambda_{\gamma\alpha}(^{20}Ne)} \tag{15}$$

The assumption $dX(^{A}Z)/dt \ll J_-$ for ^{12}C, ^{16}O and ^{20}Ne holds well through most of the ^{28}Si disintegration. However, it does not hold well at the beginning, when the ^{4}He particle density is very low. It is then preferable to also calculate J_-':

$$J_-' \equiv \lambda_{\gamma\alpha}(^{24}Mg)n(^{24}Mg)/[1 + \eta(^{20}Ne)]$$

that is, the conserved current, if all the current were absorbed in ^{16}O. We then use, for the abundances of ^{12}C, ^{16}O and ^{20}Ne, $n'(^{A}Z)$:

$$n'(^{A}Z) \equiv \frac{n(^{A}Z)}{n(^{12}C)+n(^{16}O)+n(^{20}Ne)} \left\{ \int J_-' \, dt - \int r_{3\alpha} n'(^{12}C, t) \, dt \right\}$$

$$= \frac{n(^{A}Z)\{\int [J' - r_{3\alpha} n'(^{12}C, t)] \, dt\}}{n(^{12}C) + n(^{16}O) + n(^{20}Ne)}$$

until

$$\int [J' - r_{3\alpha} n'(^{12}C, t)] \, dt = n(^{12}C) + n(^{16}O) + n(^{20}Ne)$$

We shall now indicate how we calculated the flow of particles at $A \simeq 44$. It will be seen to be very similar to our treatment of the photodisintegration current.

The transformation of ^{28}Si into the iron peak could be imagined to occur in different ways. After a while, all the matter could be distributed with a peak around mass 36, then, later, around mass 44, and finally around mass 56. That is, one could imagine the transformation to evolve as a progressive wave does.

But it does not go that way. Because of the relative binding energies of the nuclei, the transformation rather takes the form of emptying a big container sitting at $A \sim 28$, into a big container sitting at $A \sim 56$, through pipes which have their smallest diameter at $A \sim 45$. The elements between $A \sim 36$ and $A \sim 50$ never become very abundant. The added binding energy of the nuclei in the iron peak compared to those with $A \sim 44$, always more than compensates the need for more nucleons to build them. As a consequence, the elements with $A \simeq 45$ have to carry a big flux (to fill the iron peak container) even though they are themselves quite unabundant. Since the flow of nucleons across a given nucleus is proportional to the number density of that nucleus, the large iron peak abundances are delayed by slow links at $A \simeq 45$.

By looking at the quasi-equilibrium abundances obtained by Bodansky et al.(1968), and the reaction rates of Truran et al. (1966) we have determined the point where nuclei cannot transport all the mass that they are fed from below, and the reaction rates

most important in crossing that point (we have recalculated, as described in section 2, only those reaction rates which were found most important). The network of those important reaction rates is shown in Fig. 2.

Except for ^{45}Ti, ^{45}Sc and ^{44}Ca, all the nuclei above mass 44 are in equilibrium either with the ^{28}Si or the iron group. The abundances of ^{45}Ti, ^{45}Sc and ^{44}Ca are determined by the flows trying to go from the ^{28}Si group to the iron group. The small abundances of ^{45}Ti, ^{45}Sc and ^{44}Ca being the reason for the lack of equilibrium between the ^{28}Si group and the iron peak, it is expected that in:

$$nX(^{44}\mathrm{Ti})\{^{44}\mathrm{Ti}(n\gamma)\} + \alpha X(^{41}\mathrm{Ca})\{^{41}\mathrm{Ca}(\alpha\gamma)\} + \alpha X(^{42}\mathrm{Ca})\{^{42}\mathrm{Ca}(\alpha n)\}$$

$$+ pX(^{44}\mathrm{Sc})\{^{44}\mathrm{Sc}(p\gamma)\} + pX(^{45}\mathrm{Sc})\{^{45}\mathrm{Sc}(pn)\}$$

$$+ X(^{46}\mathrm{Ti})\{^{46}\mathrm{Ti}(\gamma n)\} - X(^{45}\mathrm{Ti})\left[\{^{45}\mathrm{Ti}(\gamma n)\} + \{^{45}\mathrm{Ti}(\gamma\alpha)\}\right.$$

$$\left. + n\{^{45}\mathrm{Ti}(n\alpha)\} + \{^{45}\mathrm{Ti}(\gamma p)\} + n\{^{45}\mathrm{Ti}(np)\} + n\{^{45}\mathrm{Ti}(n\gamma)\}\right]$$

$$= \frac{dX}{dt}(^{45}\mathrm{Ti})$$

one can take $dX(^{45}\mathrm{Ti})/dt = 0$ and make a very small error, if one is interested only in the left side of the equation. [We have defined: $\{^{44}\mathrm{Ti}(n\gamma)\} = [\rho^2 N_A^2/A(n)A(^{45}\mathrm{Ti})]\langle\sigma v\rangle$.] This allows one to solve algebraically the three "rate" equations: the one above for the rates crossing ^{45}Ti and two similar ones for ^{45}Sc and ^{44}Ca. One can then obtain the following explicit expressions for $X(^{45}\mathrm{Ti})$,

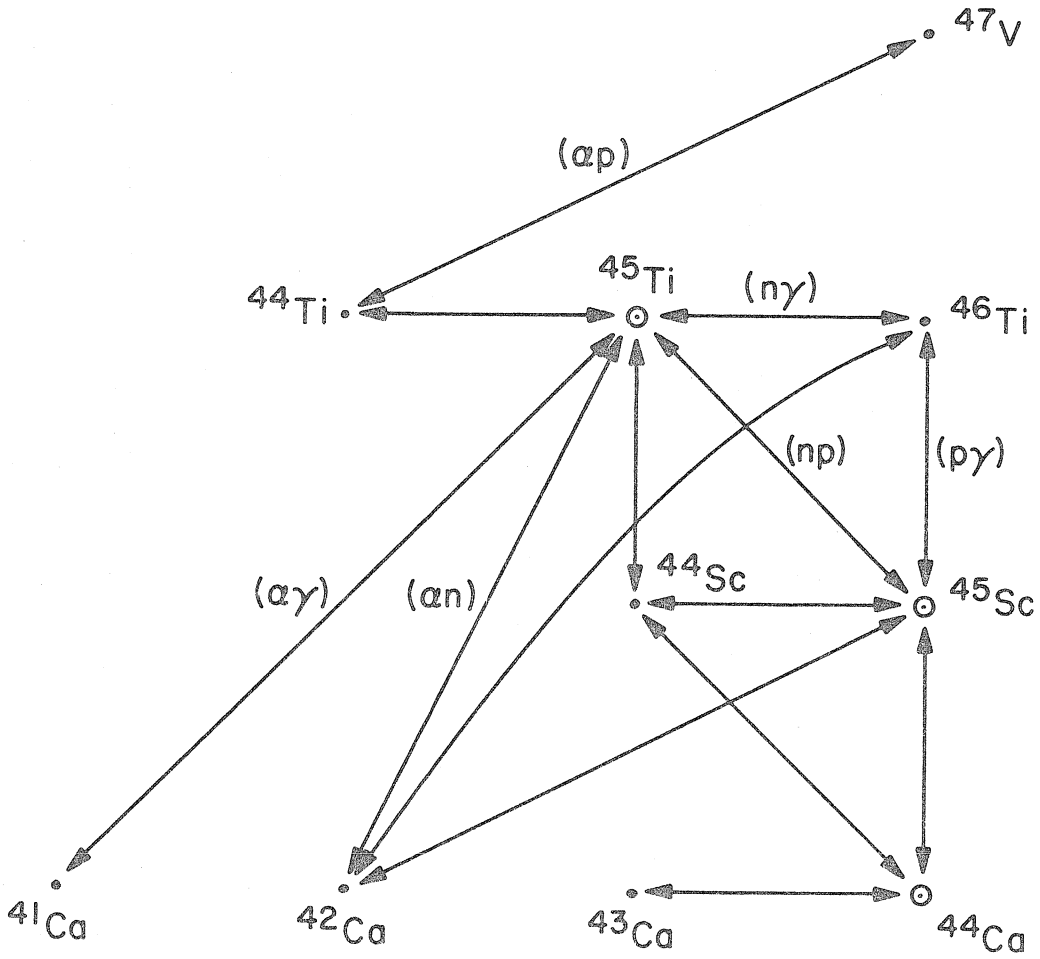
47V
(αp)
44Ti
45Ti
(nγ)
46Ti
(np)
(pγ)
(αγ)
(αn)
44Sc
45Sc
41Ca
42Ca
43Ca
44Ca

Fig. 2

Fig. 2. Reactions bridging the gap between the Si-group and the iron group. All other nuclei are in equilibrium with one or the other group. The small equilibrium abundance of those nuclei delays the flow of particles to the iron peak and makes reactions important.

$X(^{45}Sc)$, $X(^{44}Ca)$ and for the total upward flux:

$$a \equiv \{^{45}Ti(\gamma n)\} + \{^{45}Ti(\gamma\alpha)\} + \{^{45}Ti(\gamma p)\} + n\{^{45}Ti(n\alpha)\} + n\{^{45}Ti(np)\} + n\{^{45}Ti(n\gamma)\}$$

$$b \equiv -p\{^{45}Sc(pn)\}$$

$$c \equiv nX(^{44}Ti)\{^{44}Ti(n\gamma)\} + \alpha X(^{41}Ca)\{^{41}Ca(\alpha\gamma)\} + \alpha X(^{42}Ca)\{^{42}Ca(\alpha n)\} + pX(^{44}Sc)\{^{44}Sc(p\gamma)\} + X(^{46}Ti)\{^{46}Ti(\gamma n)\}$$

$$d = -n\{^{45}Ti(np)\}$$

$$e = p\{^{45}Sc(p\alpha)\} + \{^{45}Sc(\gamma n)\} + p\{^{45}Sc(pn)\} + p(^{45}Sc(p\gamma)\} + \{^{45}Sc(\gamma p)\}$$

$$f = -p\{^{44}Ca(p\gamma)\}$$

$$g = \alpha X(^{42}Ca)\{^{42}Ca(\alpha p)\} + nX(^{44}Sc)\{^{44}Sc(n\gamma)\} + X(^{46}Sc)\{^{46}Sc(\gamma p)\}$$

$$h = -\{^{45}Sc(\gamma p)\}$$

$$j = \{^{44}Ca(\gamma n)\} + p\{^{44}Ca(pn)\} + p\{^{44}Ca(p\gamma)\}$$

$$m = nX(^{43}Ca)\{^{43}Ca(n\gamma)\} + nX(^{44}Sc)\{^{44}Sc(np)\}$$

$$X(^{45}Sc) = \frac{agj - cdj - afm}{eaj - bdj - afh}$$

$$X(^{45}Ti) = (c - b\,X(^{45}Sc))/a$$

$$X(^{44}Ca) = (m - hX(^{45}Sc))/j$$

$$J_+ = [X(^{44}Ti)\alpha\{^{44}Ti(\alpha p)\} + X(^{42}Ca)\alpha\{^{42}Ca(\alpha\gamma)\}](1 - g)$$
$$+ X(^{45}Ti)n\{^{45}Ti(n\gamma)\} - X(^{46}Ti)\{^{46}Ti(\gamma n)\}$$
$$+ pX(^{45}Sc)\{^{45}Sc(p\gamma)\} - X(^{46}Ti)\{^{46}Ti(\gamma p)\} \quad (16)$$

where g can be defined as

$$g = \frac{\int J_+ dt}{\sum_{>>} n_{eq}(^{A}Z)} \quad (17)$$

($\sum_{>>}$ is a summation to be taken over all members of the iron group)

$$X_{eq}(^{A}Z) = K(A^{Z}, T, \rho)\alpha^{\delta_\alpha} p^{\delta_p} n^{\delta_n} X(^{28}Si) \quad (18)$$

$$X(^{A}Z) = gX_{eq}(^{A}Z) \quad (19)$$

$$n_{eq} = \frac{\rho N_A}{A} X_{eq}(^{A}Z) \quad (20)$$

$X(^{A}Z)$ is the fraction of the total nuclear mass in the form of a given element. For the elements of the iron group, we have also defined $X_{eq}(^{A}Z)$ which is the mass fraction there would have been in one element if the iron group and the ^{28}Si group were in equilibrium. For the members of the ^{28}Si group, $g = 1$ and $X(^{A}Z) = X_{eq}(^{A}Z)$. We also define

$$\delta_\alpha = (Z - 14)/2 \quad \text{if } Z \text{ is an even number} \quad (21)$$

$$\delta_\alpha = (Z - 15)/2 \quad \text{if } Z \text{ is an odd number} \quad (22)$$

$$\delta_p = Z - 14 - 2\delta_\alpha \tag{23}$$

$$\delta_n = A - 28 - 4\delta_\alpha - \delta_p \tag{24}$$

δ_α, δ_p and δ_n are respectively the number of α, p and n one must add to ^{28}Si to form the element ^{A}Z. We have also used

$$K(^{A}Z,T,\rho) = \left(\frac{A(^{A}Z)}{A(^{28}Si)}\right)^{5/2} A(^{4}He)^{-\frac{5}{2}\delta_\alpha} A(p)^{-\frac{5}{2}\delta_p} A(n)^{-\frac{5}{2}\delta_n} \frac{\omega(^{A}Z)}{\omega(^{28}Si)}$$

$$\times\ 2^{-(\delta_p+\delta_n)} (\rho N_A)^{\delta_\alpha+\delta_p+\delta_n} \left(\frac{M_u kT}{2\pi\hbar^2}\right)^{-\frac{3}{2}(\delta_\alpha+\delta_p+\delta_n)} \exp\left(\frac{Q(^{A}Z)}{kT}\right) \tag{25}$$

where

$$Q(^{A}Z) = B(^{A}Z) - B(^{28}Si) - \delta_\alpha B(^{4}He)$$

$B(^{A}Z)$ = the binding energy of ^{A}Z

M_u = the atomic mass unit

$A(^{A}Z)$ = the atomic mass in units of the atomic mass unit

$\omega(^{A}Z)$ = the partition function of ^{A}Z

We also have

$$\alpha = K(^{4}He,T,\rho)p^2n^2 \tag{26}$$

$$K(^{4}He,T,\rho) = \frac{1}{16}\left[\frac{A(^{4}He)}{(A(p)A(n))^2}\right]^{5/2}\left(\frac{M_u kT}{2\pi\hbar^2}\right)^{-9/2}\left((N_A\rho)^3 \exp\frac{B(^{4}He)}{kT}\right) \tag{27}$$

From equations 19 and 18 for $X(^{A}Z)$ and $X_{eq}(^{A}Z)$ it is

seen that the evolution of the abundances can be related to the evolution of $X(^{28}Si)$, α, p, n and g. To determine the evolution of the abundances, it is necessary to transform the fundamental time evolving quantities (the number of β-decays, the amount of mass liberated through ^{28}Si disintegrations, the number of nuclei crossing the $A \sim 45$ bottleneck) into α, p, n, $X(^{28}Si)$ and g. When added to the three time-integrated quantities, the conservation of the baryon number and the requirement of equilibrium between α, p and n (equation 26) will furnish us with the needed equations.

We then calculate the abundances of the different nuclei at all times, in order to calculate the time evolution of the β-decays, of the amount of disintegrated ^{28}Si and of the mass having passed through $A \simeq 45$. The abundances need to be known as a function of time to within a few per cent, in order to get the time integrated quantities to within a few per cent. A linear prediction-correction scheme has been devised to this end.

We start from the five basic equations

$$\sum_{\substack{\text{all} \\ \text{nuclei}}} X(^{A}Z) = 1 \quad * \tag{28}$$

$$\alpha = p^2 n^2 K(^4He, T, \rho) \tag{29}$$

$$\left(\frac{N-Z}{N+Z}\right)_{t=0} + 2\int \left\{ \sum_{\substack{\text{all} \\ \text{nuclei}}} \frac{X(I)}{A(I)} \beta(I) \right\} dt = \left\{ \sum_{\substack{\text{all} \\ \text{nuclei}}} \frac{2X(I)}{A(I)} [A(I) - 2Z(I)] + p - n \right\} \tag{30}$$

*This equation neglects the transformation of mass into energy.

where to simplify the writing, we have replaced ^{A}Z by I. $\beta(I)$ is the combined $\beta^{\pm}$-decay and e^- capture rates (positive for β^+ decay and e^- capture). Z and N are respectively the total number of "protons" and "neutrons" both inside and outside of the nuclei. $[(N-Z)/(N+Z)]_{t=0}$ is the neutron enrichment at $t = 0$. For instance, if all the matter were in the form of ^{29}Si at $t = 0$, then:

$$\left(\frac{N-Z}{N+Z}\right)_{t=0} = \left(\frac{15 - 14}{29}\right) = \frac{1}{29} = 0.035$$

N_A is Avogadro's number.

$$M_0 + \frac{1}{\rho N_A}\int 28 J_- \, dt = \sum_{>+>>} \frac{X(I)}{A(I)}\left(A(I) - 28\right) \tag{31}$$

To simplify the writing $\sum_{>}$ indicates that the sum should be taken over all nuclei of the ^{28}Si group, and $\sum_{>>}$ over all nuclei of the iron group. $\sum_{>+>>}$ then indicates that the summation should be taken over all nuclei of both groups.

We have also used $\langle A \rangle$:

$$\langle A \rangle \equiv \sum_{>+>>} X(I)\, A(I)$$

At $t = 0$:

$$\langle A \rangle_0 = \sum_{>+>>} X(I)A(I) \simeq 28(1 + M_0)$$

We have linearized the equations, subtracting the value they take at $t = t_1$ from their value at $t = t_1 + \Delta t$, replacing:

$$\int_{t=t_0}^{t_1+\Delta t} F(t)\,dt \rightarrow \int_{t=t_0}^{t_1} F(t)\,dt + F(t_1)\Delta t$$

$$\alpha(t_1+\Delta t) \rightarrow \alpha(t_1) + \Delta\alpha$$

$$p(t_1+\Delta t) \rightarrow p(t_1) + \Delta p$$

$$n(t_1+\Delta t) \rightarrow n(t_1) + \Delta n$$

$$g(t_1+\Delta t) \rightarrow g(t_1) + \Delta g$$

$$X(^{28}Si, t_1+\Delta t) \rightarrow X(^{28}Si, t_1) + \Delta X(^{28}Si)$$

We obtain five equations, linear in Δt, $\Delta\alpha$, Δp, Δn, Δg and $\Delta X(^{28}Si)$

$$\Big(\sum_{>+>>} \delta_n(I)X(I) + n\Big)\frac{\Delta n}{n} + \Big(\sum_{>+>>} \delta_p(I)X(I) + p\Big)\frac{\Delta p}{p}$$

$$+\Big(\sum_{>+>>} \delta_\alpha(I)X(I) + \alpha\Big)\frac{\Delta\alpha}{\alpha} + \sum_{>+>>} X(I)\,\frac{\Delta X(^{28}Si)}{X(^{28}Si)}$$

$$+ \sum_{>>} X(I)\,\frac{\Delta g}{g} = \frac{dL}{dt}\,\Delta t \qquad (33)$$

$$2\,\frac{\Delta n}{n} + 2\,\frac{\Delta p}{p} - \frac{\Delta\alpha}{\alpha} = 0 \qquad (34)$$

$$\left\{ \sum_{>+>>} \left[Z(I) - N(I) \right] \delta_n(I) \frac{X(I)}{A(I)} - \frac{n}{A(n)} \right\} \frac{\Delta n}{n}$$

$$+ \left\{ \sum_{>+>>} \left[Z(I) - N(I) \right] \delta_p(I) \frac{X(I)}{A(I)} + \frac{p}{A(p)} \right\} \frac{\Delta p}{p}$$

$$+ \left\{ \sum_{>+>>} \left[Z(I) - N(I) \right] \delta_\alpha(I) \frac{X(I)}{A(I)} \right\} \frac{\Delta \alpha}{\alpha}$$

$$+ \left\{ \sum_{>+>>} \left[Z(I) - N(I) \right] \frac{X(^{28}Si)}{A(^{28}Si)} \right\} \frac{\Delta X(^{28}Si)}{X(^{28}Si)}$$

$$+ \left\{ \sum_{>>} \left[Z(I) - N(I) \right] \frac{X(I)}{A(I)} \right\} \frac{\Delta g}{g} = -2 \left\{ \sum_{>+>>} \beta(I) \frac{X(I)}{A(I)} \right\} \qquad (35)$$

$$\left\{ \sum_{>+>>} \frac{X(I)}{A(I)} \delta_n(I) \left[N(I) + Z(I) \right] - 28 \sum_{>+>>} \frac{X(I)}{A(I)} \delta_n(I) + \frac{n}{A(n)} \right\} \frac{\Delta n}{n}$$

$$+ \left\{ \sum_{>+>>} \frac{X(I)}{A(I)} \delta_p(I) \left[N(I) + Z(I) \right] - 28 \sum_{>+>>} \frac{X(I)}{A(I)} \delta_p(I) + \frac{p}{A(p)} \right\} \frac{\Delta p}{p}$$

$$+ \left\{ \sum_{>+>>} \frac{X(I)}{A(I)} \delta_\alpha(I) \left[N(I) + Z(I) \right] - 28 \sum_{>+>>} \frac{X(I)}{A(I)} \delta_\alpha(I) + \frac{\alpha}{A(\alpha)} \right\} \frac{\Delta \alpha}{\alpha}$$

$$+ \left\{ 4 \sum_{>+>>} \frac{\delta_\alpha(I) X(I)}{A(I)} + \sum_{>+>>} \frac{\delta_p(I) X(I)}{A(I)} + \sum_{>+>>} \frac{\delta_n(I) X(I)}{A(I)} \right\} \frac{\Delta X(^{28}Si)}{X(^{28}Si)}$$

$$+ \left\{ 4 \sum_{>>} \frac{\delta_\alpha(I) X(I)}{A(I)} + \sum_{>>} \frac{\delta_p(I) X(I)}{A(I)} + \sum_{>>} \frac{\delta_n(I) X(I)}{A(I)} \right\} \frac{\Delta g}{g} = \frac{dM}{dt} \Delta t \qquad (36)$$

$$\sum_{>>}\left[\frac{\delta_n(I)}{A(I)}X(I)\right]\frac{\Delta n}{n}+\sum_{>>}\left[\frac{\delta_p(I)}{A(I)}X(I)\right]\frac{\Delta p}{p}+\sum_{>>}\left[\frac{\delta_\alpha(I)}{A(I)}X(I)\right]\frac{\Delta\alpha}{\alpha}$$

$$+\sum_{>>}\left(\frac{X(I)}{A(I)}\right)\left[\frac{\Delta X(^{28}Si)}{X(^{28}Si)}+\frac{\Delta g}{g}\right]=J_+\Delta t/[\rho N_A] \qquad (37)$$

where we have used

$$\frac{dL}{dt}=\frac{d}{dt}[X(^{12}C)+X(^{16}O)+X(^{20}Ne)] \qquad (38)$$

$$\frac{dM}{dt}=\frac{28J_-}{\rho N_A}-\frac{d}{dt}\left(12\frac{X(^{12}C)}{A(^{12}C)}+16\frac{X(^{16}O)}{A(^{16}O)}+20\frac{X(^{20}Ne)}{A(^{20}Ne)}\right) \qquad (39)$$

To simplify the calculations, dL/dt and dM/dt were calculated in the time step preceding the time step during which they were used.

The equations 33 to 37 are the prediction equations. They are used to give α, p, n, $X(^{28}Si)$ and g at $t+\Delta t$ when they are known at t. At each time step, the constants were calculated and the 5×5 matrix was inverted by the computer for $\Delta t = 1$. Since the equations are linear functions of Δt, $\Delta\alpha$, Δp, Δn, Δg and $\Delta X(^{28}Si)$, the maximum acceptable value of $\Delta\alpha$, Δp, ... $\Delta X(^{28}Si)$ can easily be used to determine the maximum Δt acceptable while maintaining the desired accuracy.

It would, in principle, be possible to choose small enough Δt's to keep the accumulated errors small. However the prediction equations for $\Delta\alpha,\ldots,\Delta X(^{28}Si)$ neglect the terms of higher than first order in the development of $(\alpha+\Delta\alpha)^n$ $(n\leq 8)$. Consequently,

the expression,

$$\alpha(t) = \alpha(0) + \int \frac{\Delta\alpha}{\Delta t}\, dt$$

is not accurate. Instead, it is preferable to control the accuracy through the evolution of the more physical quantities:

a) Conservation of baryon number

b) Sum of the weak interactions

c) Total number of nucleons liberated by the disintegration of ^{28}Si (from $t = 0$)

d) Strictly maintaining $\alpha = p^2 n^2 K(^4He, T, \rho)$

e) Sum of the nuclei having crossed the bottleneck at $A \sim 44$ (from $t = 0$).

We calculated:

$$M = \int \frac{dM}{dt}\, dt + M_0 \tag{40}$$

$$\frac{N - Z}{N + Z} = 2\int \sum_{>+>>} \beta(I)\, \frac{X(I)}{A(I)}\, dt + \left(\frac{N-Z}{N+Z}\right)_{t=0} \tag{41}$$

$$I_+ = \int J_+\, dt \tag{42}$$

and compared them to the equivalent quantities obtained through the prediction equations:

$$M' = \left\{ \sum_{>+>>} \frac{\delta_n(I)X(I)}{A(I)} + n + \sum_{>+>>} \frac{\delta_p(I)X(I)}{A(I)} + p + 4 \sum_{>+>>} \frac{\delta_\alpha(I)X(I)}{A(I)} + \alpha \right\} \tag{43}$$

$$\left(\frac{N-Z}{N+Z}\right)' = \left\{ -2 \sum_{>+>>} 2Z(I) - A(I) \quad + n - p \right\} \tag{44}$$

and

$$I'_+ = \rho N_A \left\{ \sum_{>>} \frac{X(I)}{A(I)} \right\} \tag{45}$$

Replacing the right-hand side of equations 33 to 37 by:

$$= 1 - \sum_{\substack{\text{all} \\ \text{nuclei}}} X(I) \tag{33'}$$

$$= 1 - \frac{\alpha}{p^2 n^2 K(^4He, T, \rho)} \tag{34'}$$

$$= \left[\left(\frac{N-Z}{N+Z}\right) - \left(\frac{N-Z}{N+Z}\right)' \right] \tag{35'}$$

$$= (M - M') \tag{36'}$$

$$= (I_+ - I'_+)/\rho N_A \tag{37'}$$

gives us the corrections $\Delta\alpha$, Δp, Δn, Δg, $\Delta X(^{28}Si)$ to satisfy conditions a) to e). Those correction equations were used to guarantee that whenever the X(I)'s were needed to calculate the time evolving quantities, they were known to sufficient accuracy to calculate the time evolving quantities with a 2% accuracy. The X(I)'s were not always "predicted" to that accuracy, but they were always corrected to that accuracy before they were used. Since the time integrated quantities control the evolution, the evolution is determined to a 2%

accuracy. The use of this prediction-correction method has the advantage of transferring the control of the evolution to physically evolving quantities which are monotonically varying functions of time. They are consequently much less subject to round-off and other errors.

4. A POSTERIORI JUSTIFICATION OF THE METHOD OF CALCULATION

We have outlined above the method of calculation we have used to study the transformation of ^{28}Si, ^{29}Si and/or ^{32}S into the iron peak. This method is based on a few postulates which we shall try to justify a posteriori. At the same time, we shall try to explain why quasi-equilibrium is a good approximation to this problem.

We shall see that, starting with ^{29}Si or ^{32}S brings on a temporary nonequilibrium regime which, on the time scale of the transformation of Si (via Mg) goes rapidly into the quasi-equilibrium solution. We shall also find that the flows needed to carry the transformation to the iron peak will cause but a small perturbation on the quasi-equilibrium calculations; that is the "permanent" regime is very close to quasi-equilibrium. Finally, the study of the reaction rates relating the Si and iron groups show that they rapidly capture protons and neutrons. However it is found that there exist fast cycles which transform ^{4}He into p and n, maintaining very closely the quasi-equilibrium abundances of ^{4}He, p and n.

It is easy to show that the reactions below $A \simeq 45$ are fast enough to maintain quasi-equilibrium in the permanent regime. As ^{28}Si disintegrates and liberates ^{4}He nuclei, the freed particles will tend to join the remaining ^{28}Si nuclei to form ^{32}S, ^{36}A, ^{40}Ca ... Comparing the rates shown in Table 5, we see that both the reactions $^{28}Si\ (\alpha\gamma)$ and $^{28}Si(\alpha p)$ can easily carry more ^{4}He than there is available. Equilibrium will then come very rapidly between ^{32}S,

TABLE 5

Reaction Rates for the Establishing of Equilibrium*

Target Nucleus	Reaction	$X(^{A}Z)$	Flux (react/sec/cm^3)	τ_γ (sec) (for reverse if it is photo ionization)
^{28}Si	$(\alpha\gamma)$	0.91	6.9×10^{34}	8.5×10^{-8}
	(αp)	0.91	2.2×10^{36}	--
	$(n\gamma)$	0.91	1.7×10^{35}	1.5×10^{-8}
^{29}Si	$(n\gamma)$	0.012	2.4×10^{33}	3.3×10^{-7}
^{30}Si	$(p\gamma)$	0.0046	8.2×10^{34}	1.1×10^{-8}
^{31}P	$(p\gamma)$	0.0043	9.0×10^{34}	8.0×10^{-8}
^{32}S	$(\alpha\gamma)$	0.034	2.7×10^{32}	4.0×10^{-7}
	(αp)	0.034	4.9×10^{34}	--
^{36}A	$(\alpha\gamma)$	5.8×10^{-4}	2.4×10^{29}	1.8×10^{-5}
^{36}A	(αp)	5.8×10^{-4}	3.0×10^{30}	--

* These calculations were done for $\rho = 10^7$ g/cm^3 and $T_9 = 5$. The number of α particles released per second is then 5×10^{33}.

^{28}Si and ^{4}He. The reactions ^{32}S($\alpha\gamma$) and ^{32}S(αp) will need to carry only a fraction ($\sim$ 2% at that stage of the evolution) of the liberated ^{4}He nuclei. They would be fast enough to carry all of it without disturbing equilibrium by more than 9%. Similarly, there is no difficulty in establishing or maintaining equilibrium for ^{40}Ca and ^{44}Ti. We would obtain similar results later on in the burning, or if we did the calculations for different T and ρ.

If one starts with ^{29}Si instead of ^{28}Si, how long will it take to establish quasi-equilibrium among the neutron rich nuclei? At $T_9 = 5$, the photodisintegration [(γn)] lifetime of ^{29}Si is 1.5×10^{-8}. That is, ^{28}Si, ^{29}Si and n will get into equilibrium within approximately 2×10^{-8} sec. However ^{30}Si will also absorb some of the neutrons. Its lifetime is approximately 3×10^{-7} sec. Equilibrium between ^{28}Si, ^{29}Si, ^{30}Si and n is then expected to be attained after 6×10^{-7} sec, much before any Si has had time to disintegrate (Fig. 5). If one starts with ^{32}S instead of ^{28}Si, similar arguments show that the temporary regime would last for 10^{-6} sec or so.

For quasi-equilibrium to be a good approximation, one also needs the equation

$$\alpha = K(^{4}\mathrm{He}, T, \rho)p^{2}n^{2}$$

to hold closely. The reactions

$$\alpha \rightleftharpoons n + (^{3}\mathrm{He} \rightleftharpoons p + (D \rightleftharpoons p + n))$$

are not expected to be fast enough to maintain equilibrium. However, we shall see below that, if the equilibrium does not hold at a given

t_o, fast cycles will develop to reestablish it rapidly. But before we look at such cycles, we shall study the source of the bottle-neck at $A \simeq 45$, where the main sink of p's and n's will be found. This will allow us to determine how fast the cycles must be if they are to maintain quasi-equilibrium.

As mentioned above, the low abundances of nuclei around mass 44 produce a bottle-neck in the flow of material to higher atomic masses in forming the iron peak. The efficient and accurate determination of the iron peak abundances early in the burning requires that we determine the important links beforehand. To that end, we have studied the incoming and outgoing fluxes in each nucleus around ^{44}Ti. If a nucleus receives more flow from below than it is able to carry upwards, that nucleus will be in equilibrium with ^{28}Si. If a nucleus is able to send more nuclei upwards than it receives from below, it will be in equilibrium with the iron peak. We have supposed quasi-equilibrium to calculate the abundances of the nuclei of interest. Using the rates for the special case $T_9 = 5$, $\rho = 10^7$ g/cc. $X(^{28}Si) = 0.85$, we have calculated the fluxes that each nucleus receives and those it would carry forward (see Table 6). These are over estimates of the fluxes, since some nuclei will not attain the quasi-equilibrium abundances, and since there will be some backward fluxes.

It is readily seen from Table 6 that ^{44}Ti and ^{44}Sc receive more flux from below than they can carry forward. They will be in equilibrium with what precedes. ^{45}Ti, ^{45}Sc and ^{44}Ca receive, in

TABLE 6

Fluxes around A = 44*

Element	Reaction	Flux from Si group (react/sec/cm^3)	Sum of the fluxes from Si group (react/sec/cm^3)	Flux to the iron group (react/sec/cm^3)	Sum of the fluxes to the iron group (react/sec/cm^3)
^{44}Ti	^{40}Ca(αγ)	3×10^{31}			
	^{43}Sc(pγ)	2.5×10^{31}	5.5×10^{31}		
	^{44}Ti(αγ)			3×10^{27}	
	^{44}Ti(αp)			10^{29}	
	^{44}Ti(nγ)			1.8×10^{30}	1.9×10^{30}
	^{44}Sc(pn)	1.8×10^{31}			
^{44}Sc	^{41}Ca(αp)	2×10^{30}			
	^{43}Ca(pγ)	10^{31}	1.2×10^{31}		
	^{44}Sc(nγ)			8×10^{28}	
	^{44}Sc(pγ)			10^{30}	
	^{44}Sc(αn)			2×10^{27}	
	^{44}Sc(αp)			2×10^{27}	1.1×10^{30}
^{44}Ca	^{41}K(αp)	5×10^{27}			
	^{43}Ca(nγ)	8×10^{27}			
	^{44}Sc(np)	10^{30}	10^{30}		
	^{44}Ca(pγ)			5×10^{30}	
	^{44}Ca(nγ)			10^{28}	5×10^{30}

TABLE 6 (continued)

Element	Reaction	Flux from Si group (react/sec/cm^3)	Sum of the fluxes from Si group (react/sec/cm^3)	Flux to the iron group (react/sec/cm^3)	Sum of the fluxes to the iron group (react/sec/cm^3)
^{45}Sc	^{42}Ca(αp)	1.4×10^{30}			
	^{41}K(αγ)	1.5×10^{27}			
	^{44}Sc(nγ)	10^{30}			
	^{44}Ca(pγ)	5×10^{30}	7×10^{30}		
	^{45}Sc(αγ)			5×10^{26}	
	^{45}Sc(αp)			5×10^{27}	
	^{45}Sc(αn)			1.2×10^{28}	
	^{45}Sc(pγ)			2.5×10^{31}	
	^{45}Sc(nγ)			1.6×10^{29}	2.5×10^{31}
^{45}Ti	^{41}Ca(αγ)	5×10^{29}			
	^{42}Ca(αn)	10^{30}			
	^{44}Sc(pγ)	10^{30}			
	^{44}Ti(nγ)	1.8×10^{30}	4×10^{30}		
	^{45}Ti(αp)			3×10^{28}	
	^{45}Ti(nγ)			1.8×10^{30}	1.8×10^{30}

TABLE 6 (concluded)

Element	Reaction	Flux from Si group (react/sec/cm^3)	Sum of the fluxes from Si group (react/sec/cm^3)	Flux to the iron group (react/sec/cm^3)	Sum of the fluxes to the iron group (react/sec/cm^3)
^{46}Ti	^{42}Ca(αγ)	6×10^{29}			
	^{43}Ca(αn)	1.4×10^{28}			
	^{43}Sc(αp)	3.5×10^{28}			
	^{45}Ti(nγ)	1.8×10^{30}			
	^{45}Sc(pγ)	2×10^{31}	2.2×10^{31}		
	^{46}Ti(αγ)			5×10^{29}	
	^{46}Ti(αp)			5×10^{28}	
	^{46}Ti(αn)			5×10^{29}	
	^{46}Ti(pγ)			10^{33}	
	^{46}Ti(nγ)			2×10^{31}	10^{33}

*Calculations done at $T_9 = 5$, $\rho = 10^7$ g/cm^3.

general, the same order of magnitude of flux from below as they are able to carry upwards. ^{46}Ti receives less flux from below than it is able to carry upwards. It will be in equilibrium with the iron group. ^{45}Ti, ^{45}Sc and ^{44}Ca will be in equilibrium neither with the Si group nor the iron group. We shall use the conserved current hypothesis to determine their abundances. The large flux that can be carried by the ^{45}Ti(np) reaction insures that ^{45}Ti and ^{45}Sc be in "equilibrium" with each other, but not with what precedes or what follows.

From the results in Table 6 and other similar results for different temperatures, densities and neutron enrichment, we have determined the reactions that would be most important in calculating the abundances of the iron peak. Our calculations of their rates have been described in section 2.

In the network of reactions we use (Fig. 2), it should be noticed that, whereas some of the alpha induced reactions go from nuclei in equilibrium with ^{28}Si to nuclei in equilibrium with the iron peak, the nucleon induced reactions always go to or/and from nuclei which are not in equilibrium with either group. If we supposed all nuclei in equilibrium with one or the other group, our calculated fluxes could be appreciably too large. For instance, if $g = 0$, and <u>if</u> ^{44}Ti(nγ)^{45}Ti(nγ)^{46}Ti is the main link, the conserved current hypothesis:

$$X(^{44}\text{Ti})n\{^{44}\text{Ti}(n\gamma)\} - X(^{45}\text{Ti})\{^{45}\text{Ti}(\gamma n)\}$$
$$= X(^{45}\text{Ti})n\{^{45}\text{Ti}(n\gamma)\} - X(^{46}\text{Ti})\{^{46}\text{Ti}(\gamma n)\}$$

gives

$$J_+ = \frac{X(^{44}Ti)n\{^{44}Ti(n\gamma)\}\ \frac{n\{^{45}Ti(n\gamma)\}}{\{^{45}Ti(\gamma n)\}} - X(^{46}Ti)\{^{46}Ti(\gamma n)\}}{1 + \frac{n\{^{45}Ti(n\gamma)\}}{\{^{45}Ti(\gamma n)\}}}$$

if $g = 0$ (so $X(^{46}Ti) = 0$),

$$J_+ = \frac{nX(^{44}Ti)\{^{44}Ti(n\gamma)\}x}{1 + x}$$

$$x = \frac{n\{^{45}Ti(n\gamma)\}}{\{^{45}Ti(\gamma n)\}}$$

whereas taking ^{45}Ti in equilibrium with the iron peak would have given:

$$J_+ = X(^{44}Ti)n\{^{44}Ti(n\gamma)\}$$

Neglecting the factor $x/(1+x)$ would introduce a systematic error which would be very large when x is small (x was found to be frequently ~ 1; neglecting x would then introduce an error of a factor of 2).

Our using only 15 reaction rates is a good approximation because the dividing line between those nuclei in equilibrium with the iron group and those in equilibrium with the ^{28}Si group is very thin. Except for ^{44}Ca, ^{45}Sc and ^{45}Ti all nuclei are strongly bound to one or the other group.

As is seen in Table 6 most of the current upward is frequently carried by $(n\gamma)$ or $(p\gamma)$ reactions. However the photodisintegration

of ^{28}Si gives α particles. How will the thermodynamic equilibrium between α, p and n be maintained in spite of the continuous consumption of p and n? Essentially the answer lies in the equilibrium existing between ^{28}Si and ^{44}Ti. If p or n or a combination of them is out of equilibrium, cycles will develop between ^{28}Si and ^{44}Ti to produce n and p. The equilibrium between ^{28}Si and ^{44}Ti could not be maintained without n and p having their equilibrium values. Since the alpha reaction rates $[(\alpha\gamma), (\alpha p), (\alpha n)]$ can easily carry the whole flux between ^{28}Si and ^{44}Ti, they will also, when need arises, generate cycles that will create p's and n's. These cycles will have to be fast enough to transform approximately 25% of the liberated ^{4}He into p's and n's, since an appreciable fraction of the flux past ^{44}Ti will be carried by p's and n's.

Consider, for instance, the cycle $^{28}Si(\alpha\gamma)^{32}S(\gamma p)^{31}P(\gamma p)$ $^{30}Si(\gamma n)^{29}Si(\gamma n)^{28}Si$ at $T_9 = 3$, $\rho = 2 \times 10^6$ g with 5% of ^{28}Si burned. If one calculates the abundances supposing equilibrium and then calculates the cycle using the rates in only one direction, one obtains:

$$X(^{28}Si)\alpha\{^{28}Si(\alpha\gamma)\} = 8.8 \times 10^{27} \text{ sec}^{-1} \text{ cm}^{-3}$$

$$X(^{32}S)\{^{32}S(\gamma p)\} = 4.3 \times 10^{29} \text{ sec}^{-1} \text{ cm}^{-3}$$

$$X(^{31}P)\{^{31}P(\gamma p)\} = 1.8 \times 10^{28} \text{ sec}^{-1} \text{ cm}^{-3}$$

$$X(^{30}Si)\{^{30}Si(\gamma n)\} = 1.8 \times 10^{23} \text{ sec}^{-1} \text{ cm}^{-3}$$

$$X(^{29}Si)\{^{29}Si(\gamma n)\} = 5 \times 10^{27} \text{ sec}^{-1} \text{ cm}^{-3}$$

where

$$\{Si^{28}(\alpha\gamma)\} = \frac{\rho^2 N_A^2}{A(^4He)A(^{28}Si)} \langle \sigma v \rangle$$

The "maximum" value of the slowest link in this cycle is about 10^{23} reactions sec^{-1} cm^{-3}. Under those circumstances alpha particles are being produced at the rate of 5×10^{22} sec^{-1} cm^{-3}, so that a single cycle converts into p's and n's the same order of magnitude of α's as are being produced. No difficulty should then be encountered in maintaining the equilibrium for the reaction $\alpha \rightleftharpoons 2p\,2n$.

It is also instructive to compare our calculations of the time evolution of the system to the exact solutions which have been obtained in some cases by Truran et al. (1966). They followed the time evolution of the mass fractions by using the reaction rates* joining the nuclei they were considering. They inverted a matrix having the same number of lines and rows as they consider elements. To keep round off errors to a minimum they used double precision. The process is accurate but somewhat computer-time consuming. It cannot easily be used for a general study of the kind undertaken here. However, it is very useful to check some of our assumptions and to verify our results. In a following section, we shall compare our results with dynamic calculations carried out by Truran where he followed the evolution of the mass fractions of the elements down to

*They included the $(\alpha\gamma)$, (αp), (αn), $(p\gamma)$, (pn) and $(n\gamma)$ reaction rates and their reverse.

temperatures where the reaction rates were slower than the dynamics. All mass fractions were then frozen.

Fig. 3 shows a comparison of our results with those of Truran at $\rho = 2 \times 10^7$ g/cc and $T_9 = 4$. The two methods are seen to give very similar results even at $t = 10^{-2}$ sec, before any ^{28}Si has burned. The most important difference seems to come from the 10% difference in the time scale at $t = 100$ sec. This is not an important difference since the reaction rates controlling the decay of ^{28}Si are not known to 10%. Our disagreeing could have been caused, for instance, by a different temperature variation of the weight factors of the nuclei involved in the ^{28}Si decay or by our neglect of ^{23}Na as a possible path for the decay of ^{24}Mg.

Perhaps more instructive is the comparison of our results at $T_9 = 3$ and $\rho = 2 \times 10^6$ g/cc. As can be seen from fig. 4 there is a very appreciable difference between our results (full line) and those of Truran even after 10^6 sec, when an appreciable fraction of ^{28}Si has burned. There is again a 10% difference in the time scale (that is the time to have burned a given fraction of ^{28}Si). However, our results represented by full lines are for 115 nuclei, including nuclei with $Z > N$. Truran has not included those nuclei. The dashed line results were obtained by excluding all nuclei for which $Z > N$. We also show results without the nuclei for $Z > N$ and without the nuclei for $Z = N$ if Z is odd. It is seen that the results are sensitive on which nuclei are included. It seems that quasi-equilibrium is established quite early but that the results of Truran

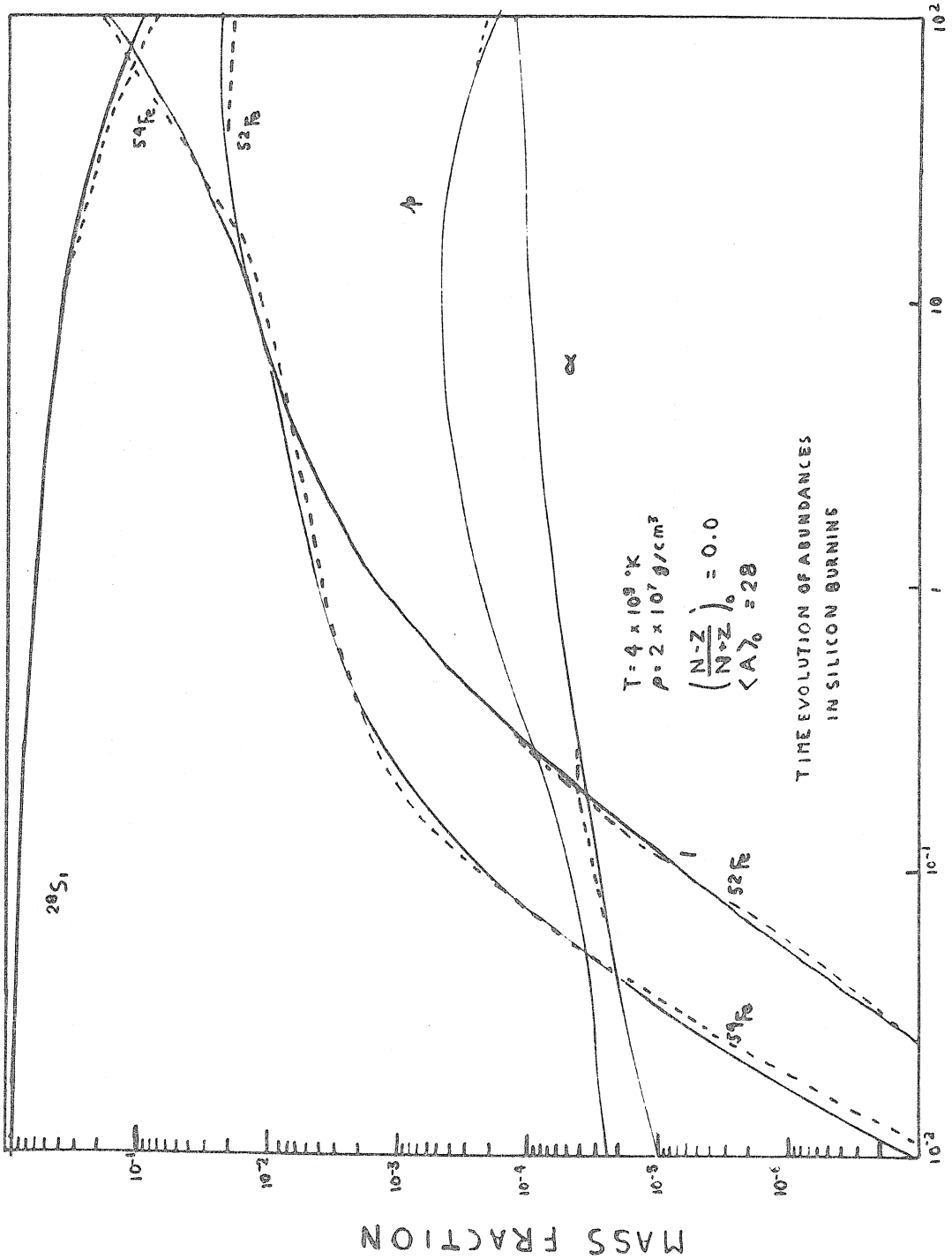
MASS FRACTION
TIME (SEC)
TIME EVOLUTION OF ABUNDANCES
IN SILICON BURNING
T = 4 x 10^9 °K
ρ = 2 x 10^7 g/cm^3
(N-Z/N+Z)_0 = 0.0
⟨A⟩_0 = 28
28Si
54Fe
52Fe
56Ni
α
p
n

Fig. 3

Fig. 3. Comparison of quasi-equilibrium calculations (full line), to the calculations of Truran (1969) (dashed line) at $T_9 = 4$, $\rho = 2 \times 10^7$ g/cm^3. Whenever the dashed line does not show, it is indistinguishable from the full line. The agreement is seen to be very good; the differences are much smaller than the uncertainties due to the uncertainties in the physical constants (notably the nuclear reaction rates).

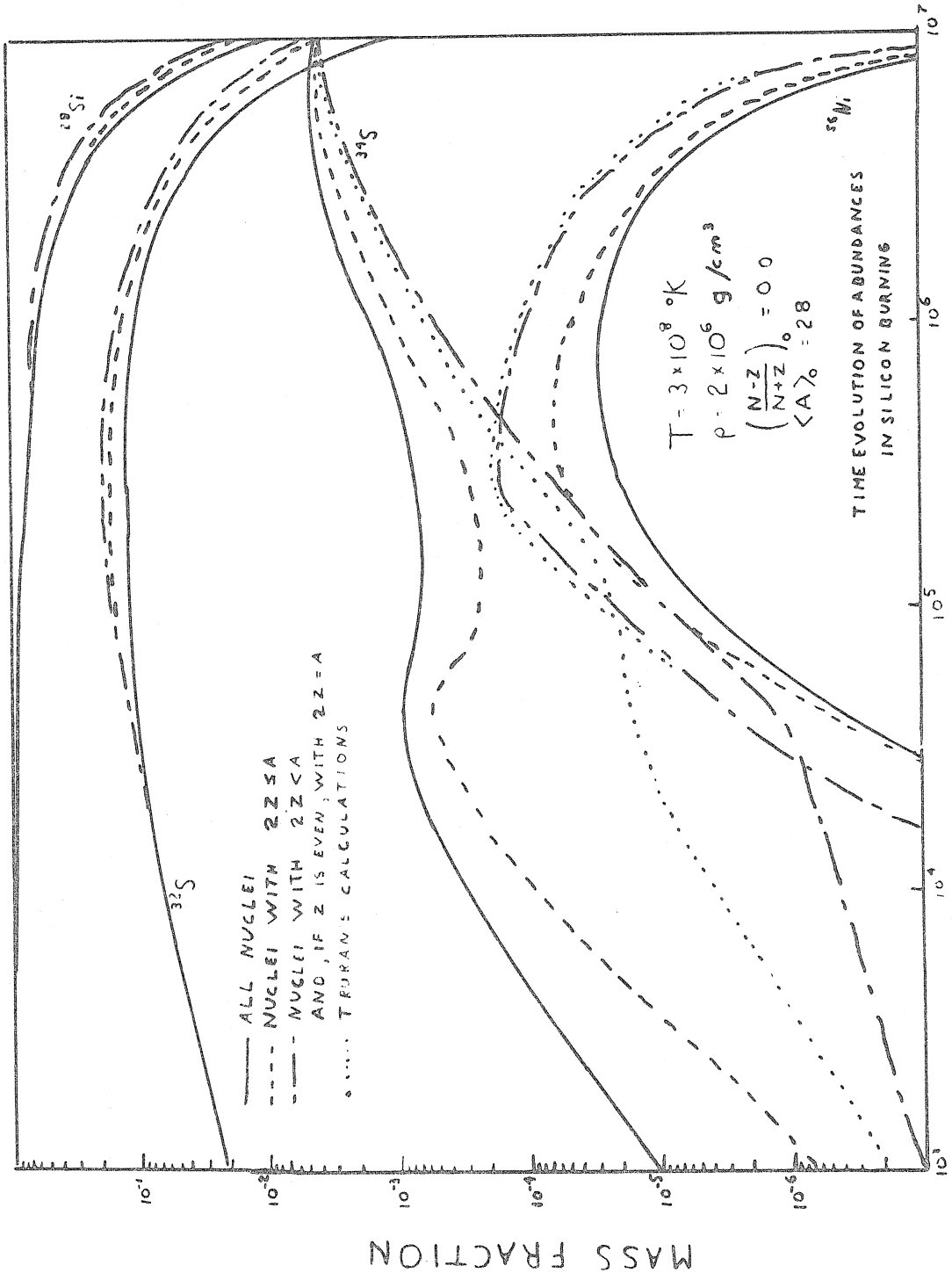
MASS FRACTION
TIME (SEC)
TIME EVOLUTION OF ABUNDANCES
IN SILICON BURNING
T = 3×10^8 °K
ρ = 2×10^6 g/cm^3
(N-Z/N+Z)_0 = 0.0
⟨A⟩_0 = 28
ALL NUCLEI
NUCLEI WITH 2Z ≤ A
NUCLEI WITH 2Z < A AND, IF Z IS EVEN, WITH 2Z = A
TRURAN'S CALCULATIONS
28Si
32S
34S
56Ni

Fig. 4

Fig. 4. Comparison of quasi-equilibrium calculations to the calculations of Truran (1969) at $T_9 = 3 \times 10^9$ °K and $\rho = 2 \times 10^6$ g/cm^3. The number of nuclei one includes in the network is seen to have important effects throughout the burning. Truran includes no nuclei with $2Z > A$ and if Z was odd no nuclei with $2Z = A$. The effect of the added nuclei is probably mainly felt through the $\beta^{\pm}$ decays and e^- capture and does not show at the higher temperatures.

and ours differ because of the different nuclei included in the network. The main difference between his results and ours, if we include only the nuclei he includes, probably comes from the accumulated beta decays. Whereas Truran includes beta decays only for those nuclei above K, we include beta decays (and positron decays and e-captures) for all the nuclei that we consider. There will have been a non-negligible number of beta decays even at $t = 10^3$ sec if we include beta decays from the nuclei with masses smaller than 39, but not if we do not.

5. THE FREEZING PROCESS

We have seen above that, with our method of solution, it was possible to solve correctly a "thought problem": the transformation of ^{28}Si, ^{29}Si, ^{32}S ... into the iron peak at a constant temperature. However, as the processed material is ejected from the star, it will cool down; there will come a point where the reaction rates will be slower than the dynamics. Can a constant temperature calculation represent such a process? More precisely, on what aspects of the history of the star are the observed abundances dependent? If they are dependent on the detailed dynamics, the quasi-equilibrium approximation will not be a good approximation: it neglects the details of the freezing which is where the dynamics appear in the abundances. If, however, the frozen abundances are relatively insensitive to the density and the temperature at which they have frozen, and if the photodisintegration rates are more temperature sensitive than the abundances are, then quasi-equilibrium will be an acceptable solution.

The final abundances will be seen below to depend mainly on the neutron enrichment and on the extent to which ^{28}Si burning has proceeded. The comparison with observed abundances depends on which zones of the star are ejected, what is the neutron enrichment in each of those zones and how much ^{28}Si has been burned in each of those zones. Since the rate of ^{28}Si burning is very temperature sensitive, it will be necessary to have closely spaced zones ($\Delta T_9 \sim 0.02$). The freezing will be found to be relatively unimportant. We shall study separately the temperature abundance of the reaction rates and of the

equilibrium abundances. It will turn out that the reaction rates will vary by orders of magnitude while the equilibrium abundances of the more abundant nuclei will vary by 20%, and those of the less abundant nuclei by factors of 2 or 3. Consequently, whatever be the dynamics speed, the matter will freeze at the same temperature, and the final abundances will not be very dependent on that temperature.

On Figs. 5 to 8 are found the time scales for ^{28}Si disintegration, for crossing the bottleneck at $A \sim 45$, for (γ,α), (γ, p) and (γ, n) reactions respectively. For nearly all the included cases, a $\Delta T_9 \sim 0.5$ change in temperature causes a two order of magnitude change in the time scale. However, variations in the time scale from reaction to reaction are much larger than that. The lifetimes for ^{4}He emission are up to five orders of magnitude smaller than those for ^{28}Si photodisintegration. The lifetimes of strongly bound iron peak nuclei are comparable to that of ^{28}Si. The lifetimes of proton and neutron emission cover the same range. They are smaller by 1 to 5 orders of magnitude than the time for the iron peak to get in equilibrium with ^{28}Si.

If one looks at the details of photodisintegration rates, one notices that the larger time scales are associated with the disintegration of the more strongly bound nuclei. The time scale varies by up to five orders of magnitude from nucleus to nucleus. If the dynamic time scale is $t \simeq 0.1$ sec, the more closely bound nuclei can be expected to freeze at $T_9 \simeq 3.8$, the less abundant and less closely bound ones at $T_9 \simeq 3.0$ or 2.6. A few nuclei, like ^{55}Co, may even freeze only at $T_9 \simeq 2.2$. Those nuclei related only through ^{4}He reactions

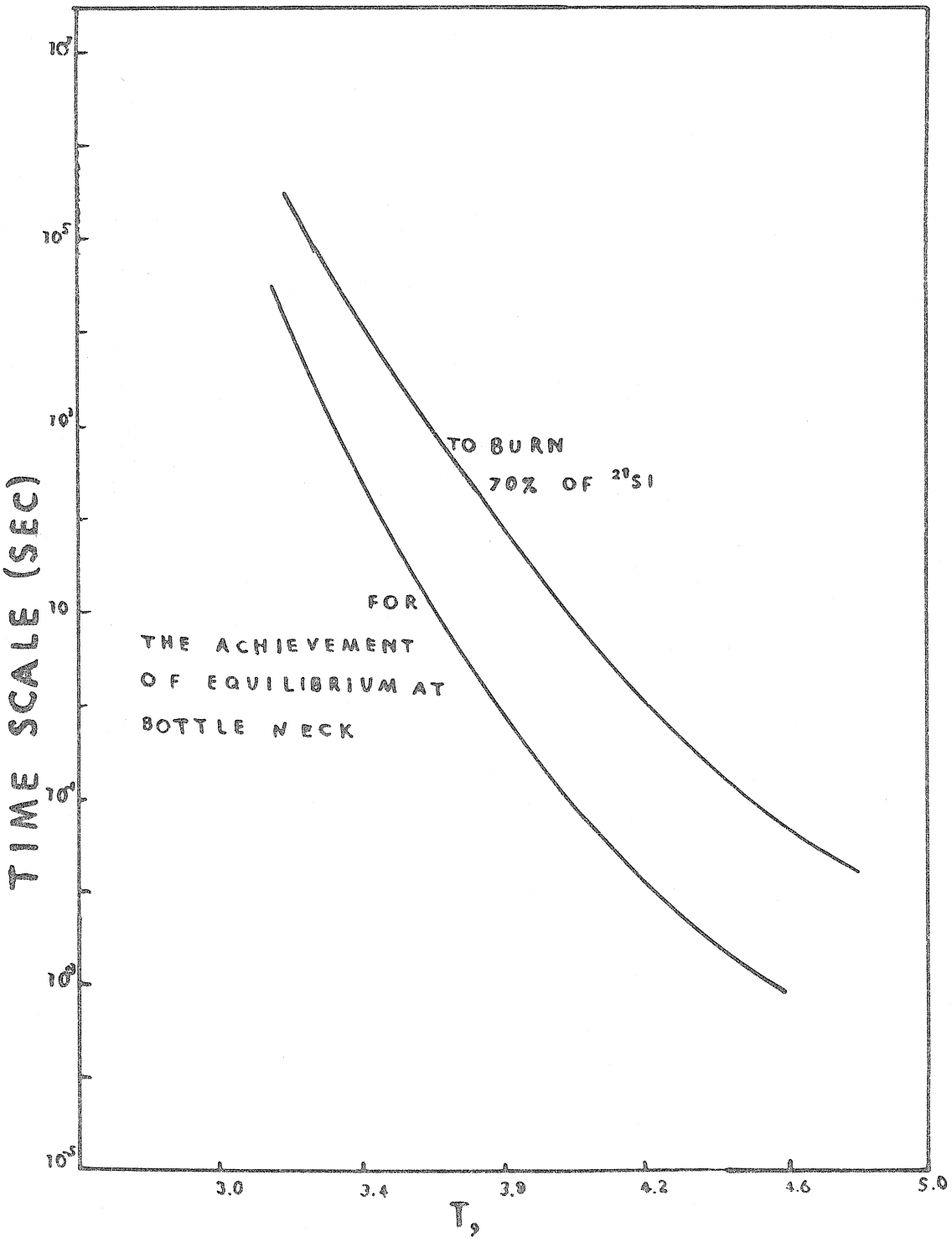
TIME SCALE (SEC)
10^7
10^5
10^3
10
10^{-1}
10^{-3}
10^{-5}
TO BURN
70% OF ^{28}Si
FOR
THE ACHIEVEMENT
OF EQUILIBRIUM AT
BOTTLE NECK
3.0
3.4
3.8
4.2
4.6
5.0
T_9

Fig. 5

Fig. 5. Temperature dependence of the time scale for Si burning and for achieving equilibrium between the Si group and the iron group. The time scale varies very rapidly with the temperature, so that it takes a large variation of the dynamic time scale to change the freezing temperature.

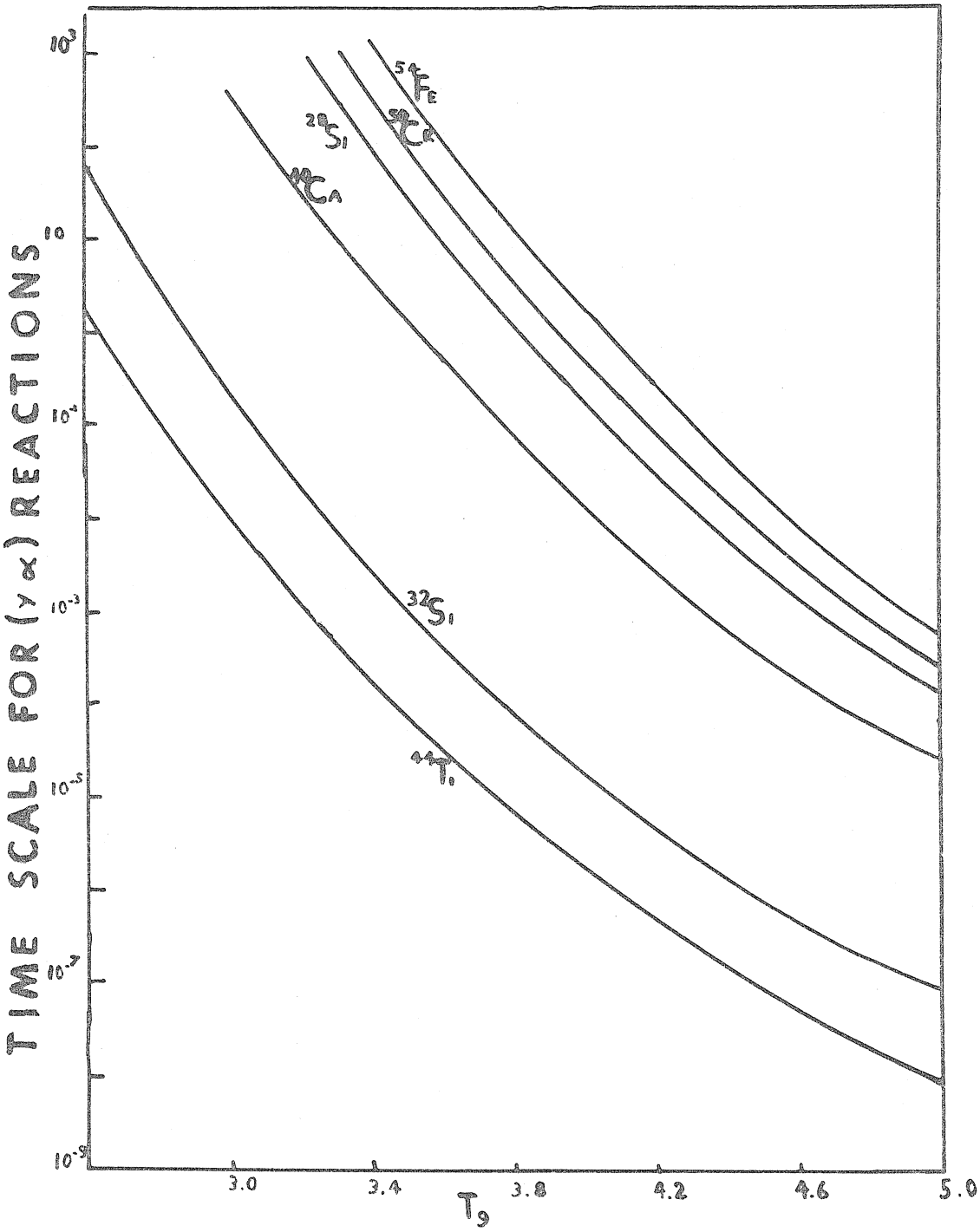
TIME SCALE FOR (γ α) REACTIONS
10³
10
10⁻¹
10⁻²
10⁻³
10⁻⁴
10⁻⁵
^{54}Fe
^{52}Cr
^{28}Si
^{40}Ca
$^{32}S_i$
^{44}Ti
3.0
3.4
3.8
4.2
4.6
5.0
T_9

Fig. 6

Fig. 6. Time scale for alpha photodisintegration. The time scale varies, at a given temperature, by up to 6 orders of magnitude from one reaction to the other. For a given reaction it varies by 6 orders of magnitude from $T_9 = 3.4$ to $T_9 = 5.0$. The freezing temperature will then vary from one reaction to another by $\Delta T_9 \simeq 1.6$.

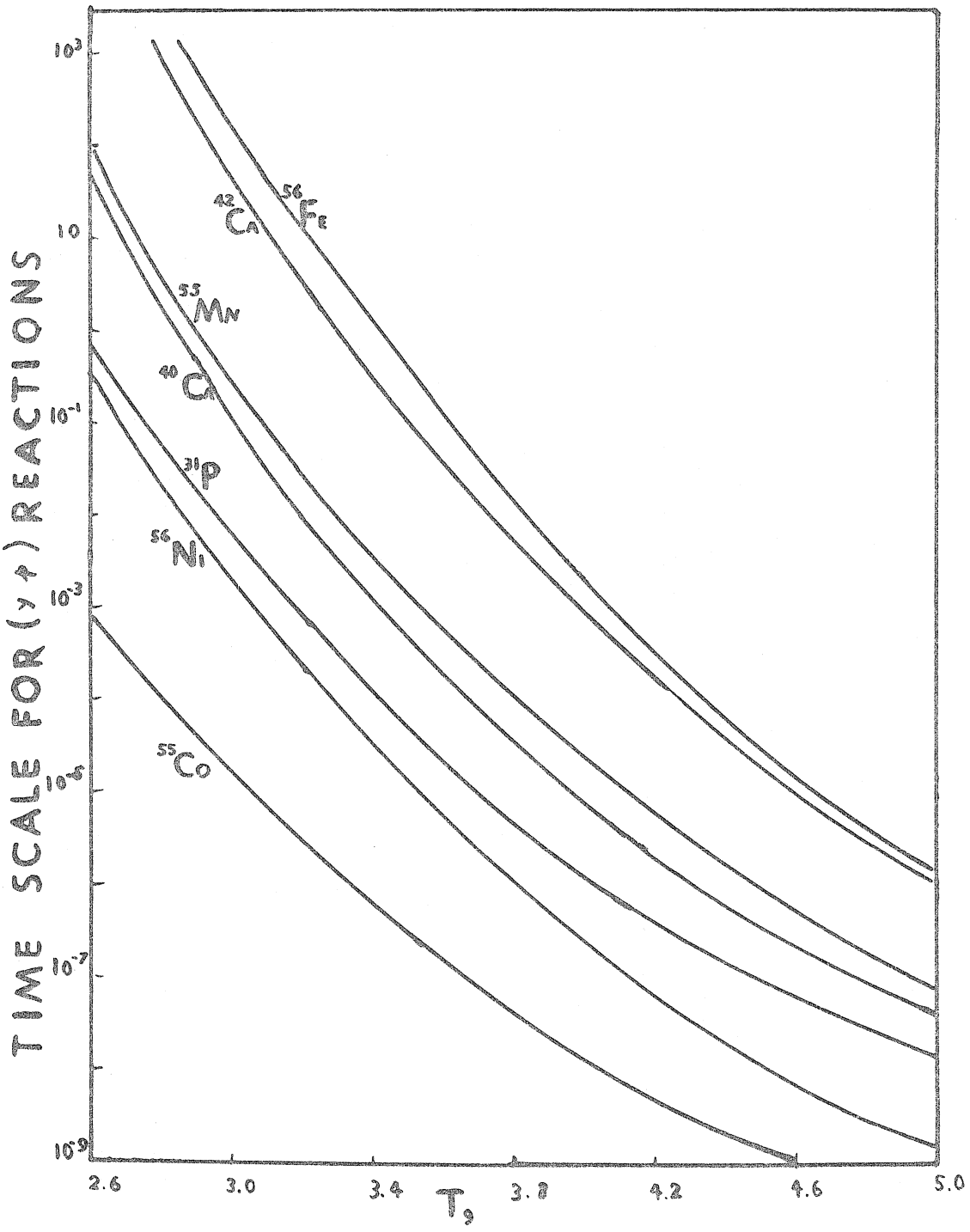
TIME SCALE FOR (γ,p) REACTIONS
10³
10
10⁻¹
10⁻³
10⁻⁵
10⁻⁷
10⁻⁹
⁴²Ca
⁵⁶Fe
⁵³Mn
⁴⁰Ca
³¹P
⁵⁶Ni
⁵⁵Co
2.6
3.0
3.4
3.8
4.2
4.6
5.0
T₉

Fig. 7

Fig. 7. Same as Fig. 6 but for proton disintegration. The time scales are some three orders of magnitude smaller for proton than for alpha emission.

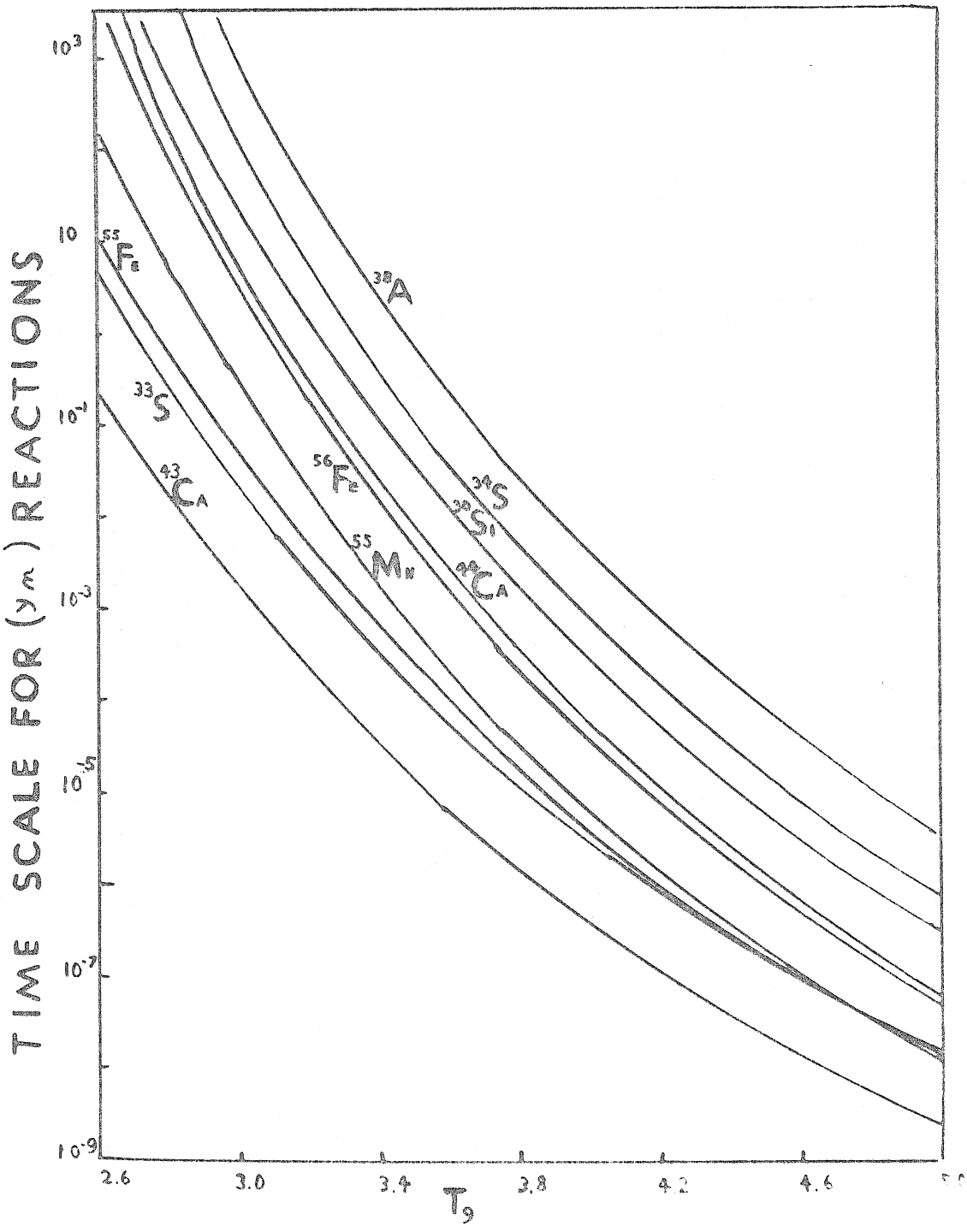
TIME SCALE FOR (γn) REACTIONS
10³
10
10⁻¹
10⁻³
10⁻⁵
10⁻⁷
10⁻⁹
55Fe
38A
33S
43Ca
56Fe
34S
30Si
55Mn
44Ca
2.6
3.0
3.4
3.8
4.2
4.6
T9

Fig. 8

Fig. 8. Same as Fig. 7 but for neutron photodisintegration.

probably will freeze slightly earlier than the others. It is clear, however, that there does not exist a well-defined freezing temperature. The equilibrium abundances at one given temperature will be a reasonable approximation to the frozen temperature only if the abundances are not sensitive to the temperature nor to the density. (Since there is no one moment in the dynamic evolution when all the abundances freeze, each will freeze at its own T, ρ.)

For dynamic time scales of 10^{-2} to 10^{-1} sec, the freezing of the ^{28}Si disintegration should occur between $T_9 = 4.4$ and $T_9 = 5.0$ (Fig. 5), and the freezing of the bottleneck at $4.0 \leq T_9 \leq 4.6$ (Fig. 5). The freezing of the individual nuclei should rather occur at $2.5 \leq T_9 \leq 4.0$. The freezing temperature will then depend on which aspect of the freezing is most important: the freezing of the photodisintegration flux, of the bottleneck or that of individual reactions.

We have mentioned above that there does not exist one, well defined freezing temperature, and, so, freezing density. The freezing will occur over a wide range of temperatures and densities. The accuracy of quasi-equilibrium calculations will be limited by the mass fraction changes over that range.

Comparing, in table 7, the mass fractions for $\rho = 10^7$ g/cc and $\rho = 10^9$ g/cm^3 shows how independent they are on the density, especially at $T_9 = 3.2$. This can be easily understood: the statistical factors that determine the relative abundances depend only on the temperature. For instance, suppose that only three nuclei are important: ^{52}Fe, n and ^{54}Fe. Then the equilibrium equations become:

TABLE 7

THE EFFECT OF THE DYNAMICS ON THE FROZEN ABUNDANCES

T_{90}	4.9*			4.8*				
ρ_0 (g/cm^3)	2×10^8			2×10^7				
T_9		3.8**	3.2**		4.2**	3.8**	3.8**	3.2**
ρ (g/cm^3)		10^7	10^7		10^9	10^9	10^7	10^7
Nucleon				Mass Fractions				
^{28}Si	0.44	0.44	0.44	0.285	0.285	0.285	0.285	0.285
^{32}S	.250	.255	.253	.21	.218	.212	.214	.210
^{54}Fe	.115	.106	.116	.116	.084	.092	.096	.107
^{56}Ni	.073	.053	.071	.25	.178	.216	.20	.25
^{36}A	.053	.056	.046	.050	.067	.060	.060	.048
^{40}Ca	.045	.039	.034	.056	.06	.055	.055	.045
^{58}Ni	.011	.010	7.8×10^{-3}	.011	.012	.011	.012	9.3×10^{-3}
^{52}Fe	6.4×10^{-3}	4.9×10^{-3}	3.6×10^{-3}	.012	.018	.014	.014	9.7×10^{-3}
^{55}Co	4.6×10^{-3}	2.2×10^{-2}	1.55×10^{-2}	6.2×10^{-3}	.05	.043	.043	2.8×10^{-2}
^{50}Cr	2.8×10^{-3}	3.2×10^{-3}	1.4×10^{-3}	1.4×10^{-3}	3.0×10^{-3}	2.1×10^{-3}	2.4×10^{-3}	10^{-3}
^{53}Fe	1.3×10^{-3}	1.3×10^{-3}	4.9×10^{-4}	8.4×10^{-4}	3.4×10^{-3}	2.1×10^{-3}	2.1×10^{-3}	7.7×10^{-4}
^{48}Cr	1.2×10^{-3}	5.1×10^{-4}	2.1×10^{-4}	1.9×10^{-3}	1.95×10^{-3}	1.3×10^{-3}	1.3×10^{-3}	4.4×10^{-4}
^{51}Mn	3.4×10^{-4}	1.3×10^{-3}	4.2×10^{-4}	2.5×10^{-4}	3.2×10^{-3}	1.9×10^{-3}	1.9×10^{-3}	6.0×10^{-4}
^{44}Ti	3.7×10^{-5}	1.2×10^{-4}	3.6×10^{-5}	4.0×10^{-5}	4.2×10^{-4}	2.3×10^{-4}	2.2×10^{-4}	6.2×10^{-5}

*Dynamic calculations of Truran (1969).

**Constant temperature calculations.

$$X(^{54}Fe) = f(T)(N_A\rho)^2 n^2 X(^{52}Fe) \tag{46}$$

$$X(^{54}Fe) + X(^{52}Fe) + p + n = 1 \tag{47}$$

$$\frac{2X(^{54}Fe)}{54} + n - p = (N-Z)/(N_A\rho) \tag{48}$$

If p and $n \ll (N-Z)/(N_A\rho)$, we can write:

$$X(^{54}Fe) = 27(N-Z)/(N_A\rho) \tag{49}$$

and

$$X(^{52}Fe) = 1 - X(^{54}Fe) \tag{50}$$

If $(N-Z)/(N_A\rho)$ is a constant, then $X(^{52}Fe)$ and $X(^{54}Fe)$ are independent of density, p and n are inversely proportional to ρ.

If $N-Z = 0$, we cannot neglect p any more in eq. 48. Actually one usually finds $n \ll p$, and

$$X(^{54}Fe) \simeq 27p$$

p, $X(^{54}Fe)$ and $X(^{52}Fe)$ are all functions of the density.

In our examples (Table 7), $(N-Z)/(N_A\rho)$ is much larger than the free proton mass fraction and the much smaller free neutron mass fraction. All the mass fractions are then independent of density. At $T_9 \simeq 4.6$ and $\rho = 10^7$ g/cm^3 this would not be the case, since then $p \gg (N-Z)/(N_A\rho)$. The equilibrium abundance would be density sensitive. However during the freezing process, the proton density would diminish and the point where $p \ll (N-Z)/(N_A\rho)$ would soon be reached. Since the photodisintegration lifetimes for $^{56}Ni(\gamma p)$ and $^{55}Co(\gamma p)$

are among the smallest, one can expect that quasi-equilibrium would be maintained among them at least down to $T_9 = 3.2$ (if the dynamic time scale ~ 0.1 sec). At that temperature, $p \gtrsim (N-Z)/(N_A\rho)$ only if $\rho \lesssim 10^4$ g/cm^3. [Actually if $(N-Z)/(N_A\rho) = 0.0$, the mass fractions are always density sensitive; there will always be a minimum value of $(N-Z)/(N_A\rho)$, for any T, ρ, for which the proton number density becomes important; our remarks above apply for $(N-Z)/(N_A\rho) \gtrsim 10^{-4}$; ^{12}C and ^{16}O burning are expected to produce more than 10^{-4} of neutron enrichment.] Whenever one makes quasi-equilibrium calculations one should always check whether $p \ll (N-Z)/(N_A\rho)$ and, if not, one should carry out the calculations at a lower temperature. During freezing, the proton density will usually be much smaller than $(N-Z)/(N_A\rho)$, and the variations of density during freezing will have no effect on the mass fractions.

The above remarks were made with respect to the free proton mass fraction. Similar remarks could be made relating to the free ^{4}He mass fraction.

Even though not as large as the temperature dependence of the reaction rates, the temperature dependence of the equilibrium abundances is not negligible. Its importance can be estimated by comparing the mass fractions at $T_9 = 3.2$ and at $T_9 = 3.8$ for a given amount of ^{28}Si left over (see Table 7). The mass fractions of the more abundant nuclei vary by factors of 1.2 or so. Those of the less abundant nuclei vary somewhat more (factors of up to 3). The reason is simple. Usually, over the range of temperatures of interest, the nuclei statistically most favored do not change as the temperature

changes: they are fixed by the neutron enrichment and by the amount of ^{28}Si having disintegrated. The free p and n mass fractions adjust to keep abundant the same abundant nuclei. The mass fractions of the less abundant nuclei will vary in so far as their statistical factors do not vary in the same way with temperature (and the abundances of p and n) as those of the most abundant nuclei (mainly because the more abundant nuclei have larger binding energies). The domineering effect of the most abundant nuclei can be seen by looking at Figs. 9 and 10. At $t = 0.0$, the most abundant nuclei all have $A \lesssim 44$; the equilibrium abundance of only three nuclei with $A \lesssim 44$ then varies by more than a factor of two while the temperature varies from $T_9 = 3.8$ to $T_9 = 3.2$; ^{40}K, ^{41}K and ^{32}Ca. When there is only $X(^{28}Si) = 0.115$ left (Fig. 10), the abundances of all nuclei with $A \lesssim 44$, except ^{28}Si, ^{32}S, ^{36}A and ^{40}Ca, vary by more than a factor of two. At $t = 0$, the neutron abundance is governed by the need for most neutrons to be in ^{30}Si, ^{34}S and ^{38}A. Those three nuclei are the most abundant neutron rich nuclei both at $T_9 = 3.2$ and at $T_9 = 3.8$. Their abundances do not change by more than 20%; they are fixed by the neutron enrichment of the material. When there is only 10% of ^{28}Si left, however, most of the neutron enrichment is absorbed in the iron peak. The mass fractions of the more abundant neutron rich nuclei in the iron peak are fixed but those of ^{30}Si, ^{34}S and ^{38}A vary considerably. However the mass fractions of ^{30}Si, ^{34}S and ^{38}A are then very small. After integrating over the different zones in a star, it is to be expected that most of the ^{30}Si, ^{34}S and ^{38}A will come from zones where they are abundant so where their mass fractions are

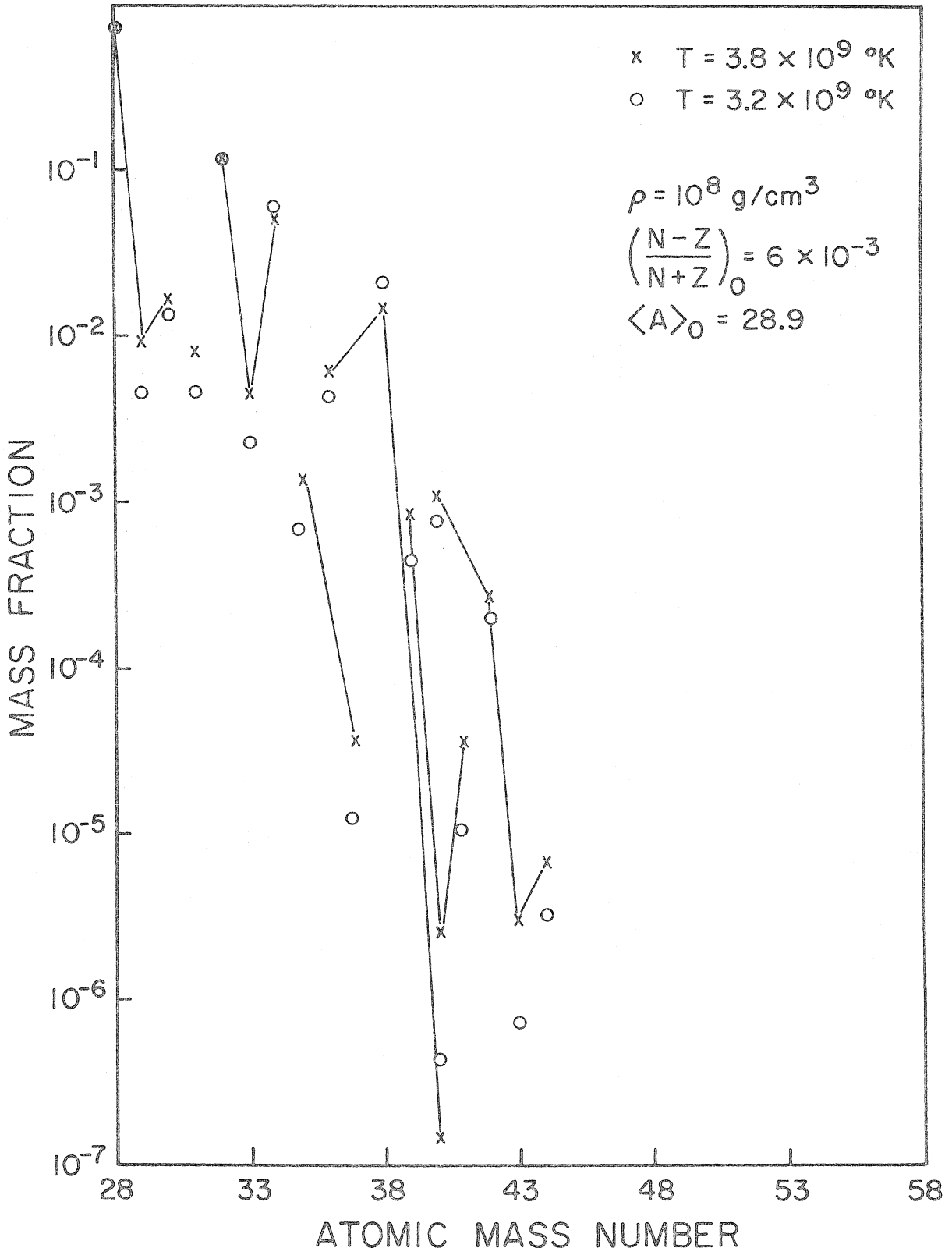
x T = 3.8 × 10^9 °K
o T = 3.2 × 10^9 °K
ρ = 10^8 g/cm^3
((N−Z)/(N+Z))_0 = 6 × 10^-3
⟨A⟩_0 = 28.9
MASS FRACTION
10^-1
10^-2
10^-3
10^-4
10^-5
10^-6
10^-7
28
33
38
43
48
53
58
ATOMIC MASS NUMBER

Fig. 9

Fig. 9. Variation of the equilibrium abundances with temperature. Before the disintegration of ^{28}Si the equilibrium abundances of elements with $A \lesssim 45$ is not very temperature sensitive: they govern the p, n and alpha abundances.

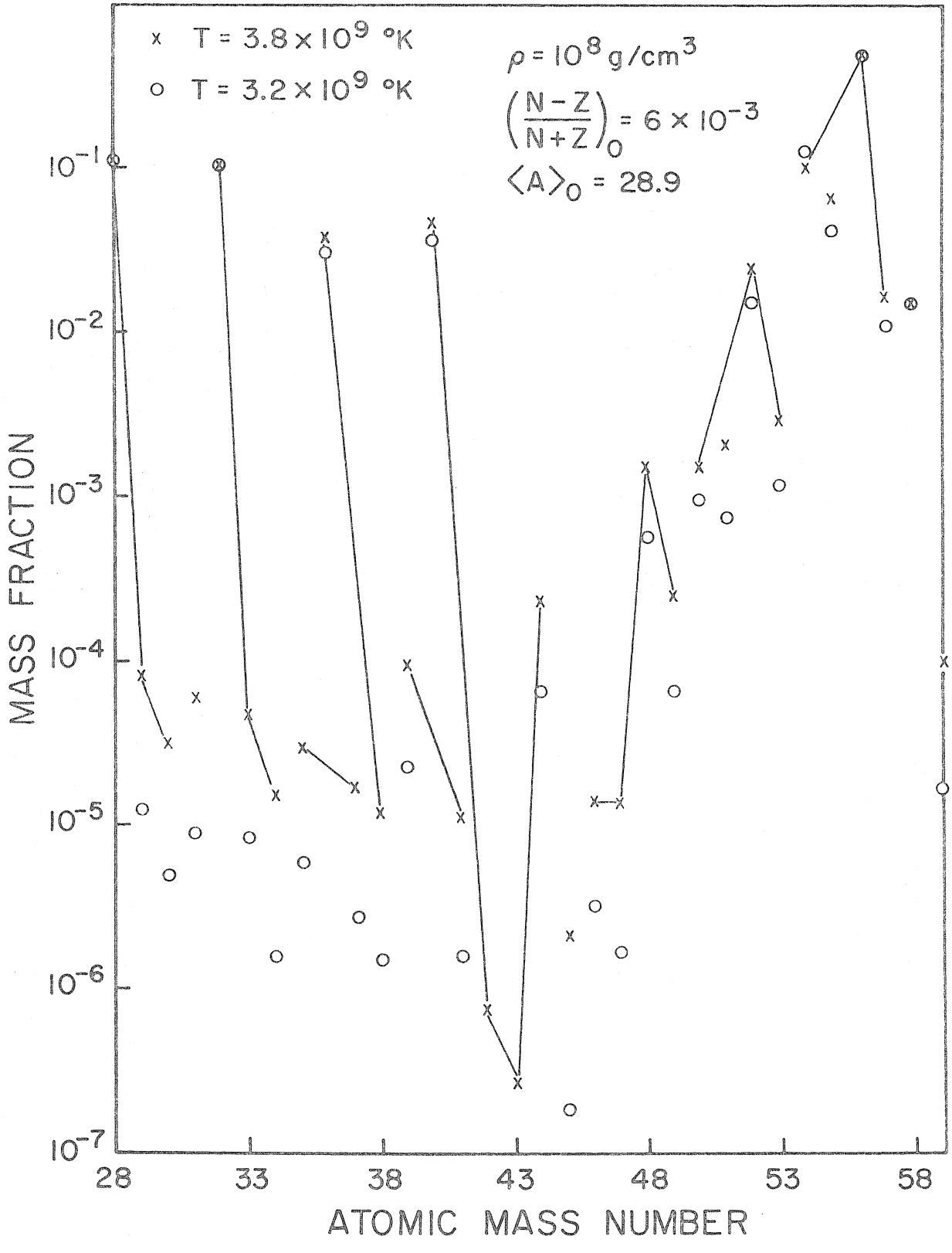
x T = 3.8 × 10^9 °K
o T = 3.2 × 10^9 °K
ρ = 10^8 g/cm^3
(N−Z)/(N+Z))_0 = 6 × 10^-3
⟨A⟩_0 = 28.9
MASS FRACTION
10^-1
10^-2
10^-3
10^-4
10^-5
10^-6
10^-7
28
33
38
43
48
53
58
ATOMIC MASS NUMBER

Fig. 10

Fig. 10. Variation of the equilibrium abundances with temperature. When there is only 10% of ^{28}Si left over, the abundances of n, p and α are controlled by the iron peak. The abundance of the iron peak elements is then insensitive to temperature, whereas that of low mass nuclei is very temperature sensitive. It turns out, however, that elements are mainly generated when their abundance is least temperature sensitive, since it is then that they are most abundant.

largely independent of temperature. This is true of most of the abundant nuclei. Their mass fraction depends on how much ^{28}Si has been burned and on the neutron enrichment, not on T nor ρ. As one integrates over the star, one integrates over how much ^{28}Si has been burned. The mass fractions of the important nuclei of the ejected material then depend only, within a factor of 1.3 or so, on the neutron enrichment. In a zone intermediate between the two already mentioned, Fig. 11 shows that $X(^{54}Fe)$ and $X(^{34}S)$ are strongly temperature dependent for a given $X(^{28}Si)$. This is because we are in the region where the control of the neutron enrichment shifts from the Si group to the iron group. Changing the temperature changes the value of $X(^{28}Si)$ at which it occurs. On a time scale of $\tau = 10^{-2}$ to 10^{-1} sec, it is necessary as can be seen from Fig. 5, to heat the material to $T_9 \simeq 4.4$ if one wishes to be left with $X(^{28}Si) = 0.80$. As the material cools with such a time scale, the bottleneck will freeze at $T_9 \simeq 4.2$. Whether the neutron density is fixed by the iron group or the Si group will depend on their relative influence at $T_9 \simeq 4.2$. Since whether the neutron density is determined by the Si group or the iron group changes appreciably the abundance of <u>all</u> neutron rich nuclei, $T_9 \simeq 4.2$ is the most important freezing temperature in those zones where $X(^{28}Si) \simeq 0.80$. In those zones where $X(^{28}Si) \lesssim 0.5$ the control of the neutron enrichment is always exerted by the iron peak. The freezing of the bottleneck is then not very important and the most important freezing temperature is that of the individual reactions, $3.0 \lesssim T_9 \lesssim 4.0$. Elements with $A \lesssim 45$ are mainly formed when

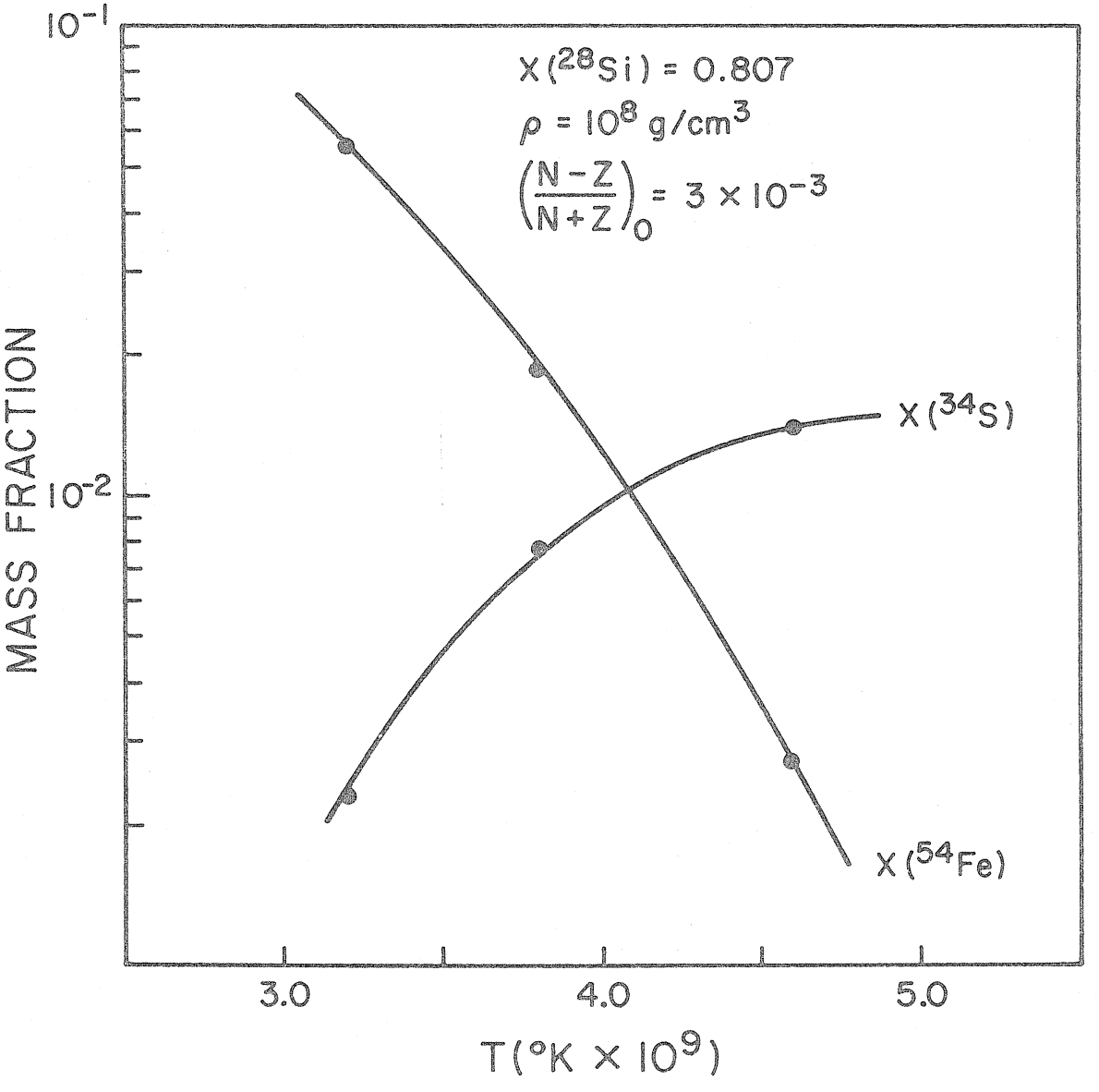
10^{-1}
10^{-2}
MASS FRACTION
$X(^{28}Si) = 0.807$
$\rho = 10^8$ g/cm^3
$\left(\frac{N-Z}{N+Z}\right)_0 = 3 \times 10^{-3}$
$X(^{34}S)$
$X(^{54}Fe)$
3.0
4.0
5.0
$T(^\circ K \times 10^9)$

Fig. 11

Fig. 11. Temperature dependence of elements that govern the neutron abundance when $X(^{28}Si) = 0.8$. The control shifts from the iron peak to the low mass elements as the temperature changes from $T_9 = 3$ to $T_9 = 5$. The abundance of all neutron-rich elements is then temperature sensitive. The important freezing temperature in that zone is then the freezing temperature of the bottleneck at $A \simeq 45$.

$X(^{28}Si) > 0.5$; the relevant freezing temperature for them is $4.0 \lesssim T_9 \lesssim 4.6$. The iron peak elements are formed when $X(^{28}Si) < 0.5$; the relevant freezing temperature for them is $3.0 \lesssim T_9 \lesssim 4.0$. One should then compare with observations, quasi-equilibrium results obtained at $3.2 \lesssim T_9 \lesssim 4.5$, expecting the low mass elements to be better fitted by the results at $T_9 \simeq 4.2$ and the iron peak elements by the lower temperature results. Note that since for $\Delta T_9 \simeq 0.6$, the equilibrium mass fractions vary by factors of 2 or less whereas the reaction time scales vary by 2 orders of magnitude; the time scale of the dynamics would have to vary by two orders of magnitude or so for differences by factors of 2 to appear, in the mass fractions of the unabundant nuclei (supposing burned the same mass fraction of ^{28}Si).

To verify these assertions, we have compared our calculations of partial-quasi-equilibrium abundances to the abundances obtained by Truran (1969), after freezing (Table 7). It is seen that the more abundant nuclei are determined by the quasi-equilibrium calculations (at $T_9 = 3.2$) to a factor of 1.2 or so. Most of the smaller abundances are determined to a factor of 2. Among the greater differences, that for ^{55}Co, for instance, can be related to the very small photo-disintegration time scale for $^{55}Co(\gamma p)$ (Fig. 7). It will consequently freeze at a lower temperature.

The observed abundances are seen to give only slim information on the past history of the material. They do tell us how much neutron enrichment the material has had. They also tell us that the material must have been through temperatures of $T_9 \simeq 4$ or 5 long enough for

^{28}Si to have been processed. The time it must have remained at such a high temperature depends on the temperature it went up to. The observed abundances should allow us to determine that time-temperature relationship.

To obtain, from stellar evolution models, the generated abundances, one needs to break the star into zones of thickness $\Delta T_9 \simeq 0.02$ (since such a temperature change already causes appreciable changes in the amount of ^{28}Si burned), to determine within a few per cent the number of beta decays in each zone, and to follow in each zone, the amount of ^{28}Si burned to a 1% accuracy. A change by a factor of 1.5 in the amount of ^{28}Si burned would change the observed abundances radically. To see this, note that the two calculations of Truran were compared in Table 7 to the same calculations of ours. The large differences in the ^{56}Ni abundances between the two cases considered by Truran, are seen to come from a factor of 1.2 in the amount of ^{28}Si burned. Considering the uncertainties existing in the experimental rates governing the ^{28}Si disintegrations (a factor of 1.5), it seems to us that the evolutionary models should be carried with two or three sets of the reaction rates to determine whether the transformation of ^{28}Si into the iron peak could possibly give the observed abundances in that particular zone of the star. The uncertainties involved in using the quasi-equilibrium approximation are much smaller than those introduced by the uncertainties in the reaction rates involved in ^{28}Si photodisintegration, and it seems to us that the method is quite appropriate. The above discussion applies to one particular zone of a star. If one integrates over many ejected zones, covering a great range in the

amount of ^{28}Si burned, (much larger than a factor of 1.5), the uncertainties in the photodisintegration rates become less important.

6. SUMMATION OVER MANY ZONES

If one wishes to study the partial burning of ^{28}Si, one cannot expect it to have occurred at only one temperature. It must have occurred in a finite object, with different temperatures in different zones. We shall present an approximation to summation over the different zones of the star. It cannot be expected to hold to 10% accuracy, but it will allow us to get insights into the effect of summing over zones at different temperatures.

The integration of the mass fraction for a given element, over the different zones in the star, can be written:

$$X(I) = \int_{M_1}^{M_2} X(I,M_r)\, dM_r \Big/ \int_{M_1}^{M_2} dM_r \qquad (51)$$

To get any further, we need to relate $X(I,M_r)$ to our calculations of $X(I,t,T_9)$. We need some hypothesis on the structure of the star. The simplest possible hypothesis is:

$$\frac{dM}{dT} = C \qquad (52)$$

where C is any constant and T is the peak temperature attained in each zone. As justified below, Eq. 52 would have to hold over a range $\Delta T_9 \simeq 2.0$. Then Eq. 51 becomes

$$X(I) = \int_{T_1}^{T_2} X(I,T)\, dT \Big/ \int_{T_1}^{T_2} dT \qquad (53)$$

All we need for our calculations to be reasonably accurate is the mass

temperature relation to be linear over a range $3.2 \leq T_9 \leq 4.6$ in the star. The proportionality constant C appears only in the value of the limits of integration. To relate to our calculations we finally make the hypothesis that the dynamics evolution goes on at the same rate, throughout all the zones of interest in the star. Then using Fig. 12* we find that an evolution that took t_o seconds at $T = T_o$, will take t_1 seconds at $T = T_1$:

$$t_1 = t_0 10^{(T_o - T_1)/0.26} \tag{54}$$

Or if we suppose that all the evolution took place in t_o sec at a temperature $T = T_o$, it is equivalent, insofar as the amount of ^{28}Si burned is concerned, to say it took place at $T = T_1$ but in t_1 sec. One then has

$$(\log_{10} e)\ \frac{dt}{t} = -\frac{dT}{0.26} \pm 25\% \tag{55}$$

and Eq. 53 becomes

$$X(I) = \int_{t_1}^{t_2} X(I,t)\ \frac{dt}{t} \ \Big/ \int_{t_1}^{t_2} \frac{dt}{t} \tag{56}$$

The limits of integration are dependent on the mass fractions of interest in the star and on the value of dM/dT. We shall treat t_1

*On Fig. 12 are plotted the lines of constant time in the plane of T vs. the photodisintegrated mass of ^{28}Si. Eq. 54 merely expresses that given a certain number of ^{28}Si disintegrations it will take ten times as long if the disintegration occurred at a temperature $0.26 \times 10^9\ ^oK$ cooler. Or on Fig. 12, the lines of constant time ($t = 10^n$, $n = -5, -4, \ldots, 3$) are each separated by a horizontal distance $\Delta T_9 = 0.26 \pm 0.06$.

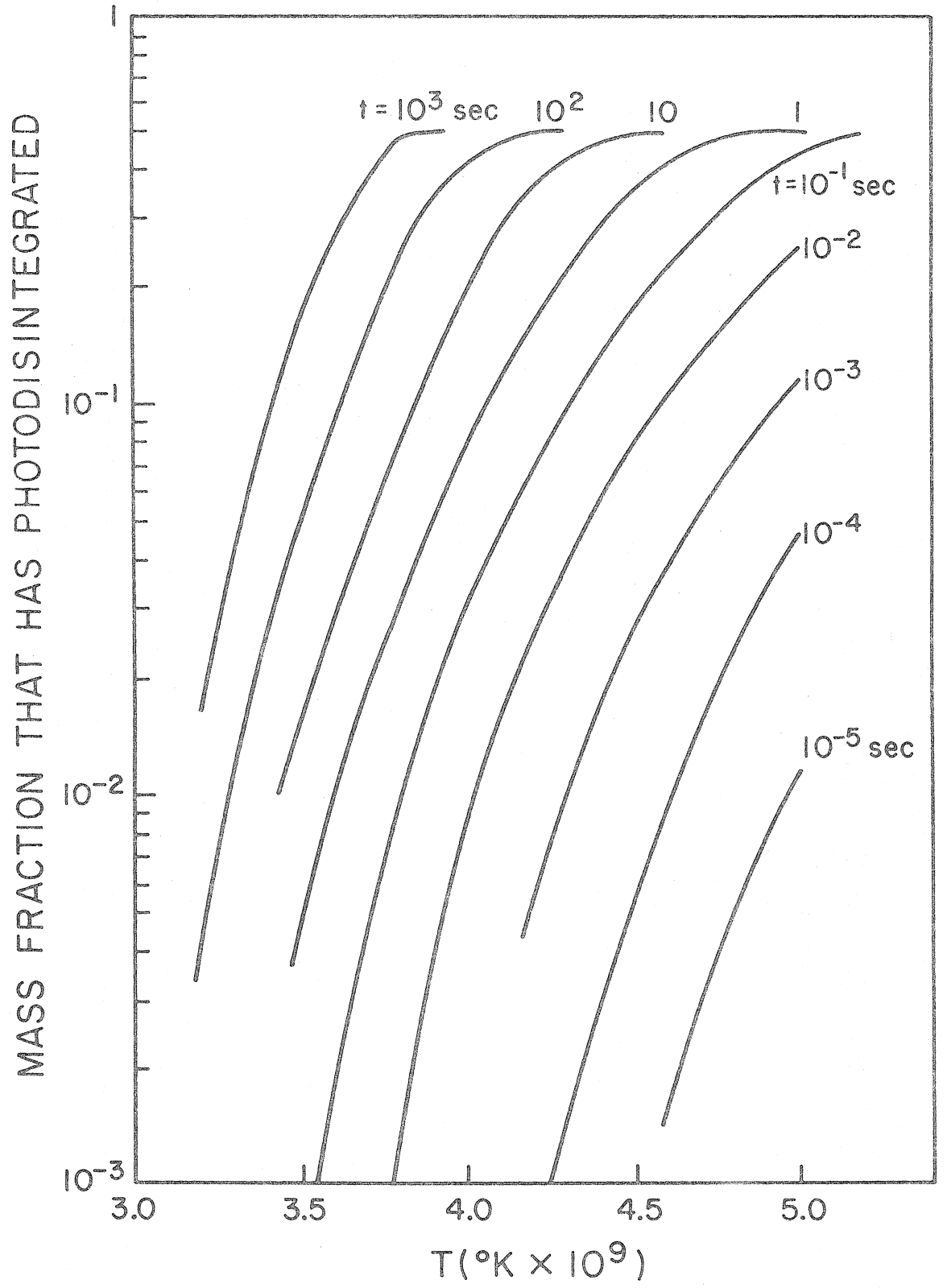
MASS FRACTION THAT HAS PHOTODISINTEGRATED
1
10^{-1}
10^{-2}
10^{-3}
$t = 10^3$ sec
10^2
10
1
$t = 10^{-1}$ sec
10^{-2}
10^{-3}
10^{-4}
10^{-5} sec
3.0
3.5
4.0
4.5
5.0
T(°K × 10^9)

Fig. 12

Fig. 12. Relation between time, temperature and the photodisintegrated mass fraction of ^{28}Si. All calculations were done including beta decays for $\langle A \rangle_0 = 28$, $((N-Z)/(N+Z))=1.2\times10^{-3}$. The time for a given mass fraction of ^{28}Si to disintegrate is seen to change by a factor of 10 if one changes the temperature by $\Delta T_9 = 0.26 \pm 25\%$ This allows us to approximate the burning in a star over a range in temperatures by the burning at a given temperature but over a range in time.

and t_2 as free parameters, determining them by requesting that $X(^{28}Si)$ and $X(^{56}Fe)$ be roughly equal to their respective observed mass fractions. The final result is not very sensitive on the limits of integration. If one increases t_2 by an order of magnitude, one should decrease t_1 by one order of magnitude or so, and one would still obtain the proper mass fraction for $X(^{28}Si)$ and $X(^{56}Fe)$. The optimum value of the ratio t_1/t_2 is then determined by the formation of ^{32}S, ^{36}A and ^{40}Ca which are produced mainly in the middle of the evolution.

The arbitrariness of the limits of integration is also related to the arbitrariness of the weight function dt/t. If the weight function were to be taken as (dt), this would correspond to:

$$\frac{dM}{dT} = C\ 10^{-(T_o - T)/0.26}$$

or it would mean that dM/dT varies from <u>any</u> constant by at least a factor of 10 over the range $\Delta T_9 = 0.26$. On the other hand the weight function dt/t^2 would correspond to

$$\frac{dM}{dT} = C\ 10^{(T_o - T)/0.26}$$

and again dM/dT would have to vary from <u>any</u> constant by a factor of 10 over the range $\Delta T_9 = 0.26$. Since such a strong variation of dM/dT seems rather unlikely, we can exclude weight functions like dt or dt/t^2.

To verify the sensitivity of our results on the exact shape

chosen for the weight function, we have made calculations using $dt/t^{1.2}$ instead of dt/t as our weight function. It turns out that by adjusting the limits of integration slightly, it is possible to obtain the same final result (within 20% or so for all elements) for the integration by using $dt/t^{1.2}$ or dt/t as the weight function. One needs merely, for $dt/t^{1.2}$, to use slightly larger values of both t_1 and t_2. It then seems that within reasonable limits, the weight function has little influence on our results. The arbitrariness of the weighing does not add any further arbitrariness than the arbitrariness of the limits of integration does.

7. NUCLEOSYNTHESIS OF ELEMENTS BETWEEN ^{28}Si AND ^{59}Co

We have seen above that, once the neutron enrichment and the mass fraction of decomposed ^{28}Si were fixed, the abundances were determined "uniquely" for most elements. Varying T and ρ was seen to have relatively little effect. Given the burned fraction of ^{28}Si, the abundances produced through Si burning in a star then depend only on the neutron enrichment. In general however, the neutron enrichment will increase while ^{28}Si burns. One needs to study the relative rates of neutron enrichment and of ^{28}Si burning. It will be found sufficient to study the evolution at $\rho = 10^8$ g/cc and for different values of T_9. The evolution at (ρ, T_9) can always be reasonably approximated by the evolution at $(10^8, T'_9)$. After determining how the abundances vary as a function of the relative rates of ^{28}Si burning and neutron enrichment, it will be found that the best fit to the observed abundances between ^{28}Si and the iron peak is obtained if the ^{28}Si burning is too fast for beta decays to occur. The neutron enrichment is then fixed by the original amount of neutron enrichment before ^{28}Si burning. It will be found to be within the range of neutron enrichment expected from explosive C burning. Under such circumstances, it will be found possible to obtain, within a factor of 3, the observed mass fractions of some 25 elements between ^{28}Si and the iron peak, including most of the neutron rich nuclei (except ^{36}S, ^{40}A, ^{46}Ca, ^{48}Ca, ...).

To determine the effect of changing (ρ, T_9) on the relative rates of beta decay and ^{28}Si burning, we have calculated the number

of beta decays and of ^{28}Si disintegrations per gram of material at different (ρ, T_9). We have found that the relative values of beta decays and ^{28}Si disintegrations at any (ρ, T_9) can be obtained from those at some $(10^8, T_9')$ (increasing T_9 by 0.2 to 0.4 for each order of magnitude increase in ρ). For instance, the evolution at $(10^6, 3.8)$ is approximated by that at $(10^8, 4.2)$ within 15% or so, since the abundances are determined by the amount of beta decays and of photodisintegrated ^{28}Si. Only the time scale changes. Then the study of the evolution of the abundances at any (ρ, T_9) can be replaced by the study at $(10^8, T_9)$.

The evolution of the abundances with time for different values of T_9 at $\rho = 10^8$ g/cc is shown on Fig. 13 to 15. We have included, in the value of the abundances for the stable nuclei, the contribution of the nuclei that beta decay after the matter has cooled down. For instance, the abundance shown for ^{56}Fe includes what is made in the form of ^{56}Ni.

For $T_9 \gtrsim 4.4$, beta decays become numerous enough for ^{54}Fe to be the dominant nucleus only after there has been a period in which ^{56}Ni has been the dominant nucleus. When ^{54}Fe becomes the most abundant nucleus, ^{58}Ni is also abundant, since ^{28}Si has all disappeared and the ^{4}He mass fraction is relatively high. It is then possible, by adding up mass fractions, to fit most nuclei between ^{28}Si and ^{58}Ni, including the neutron rich nuclei. This case will be discussed below at greater length.

For $3.5 \leq T_9 \leq 4.4$, the mass fractions in which ^{29}Si,

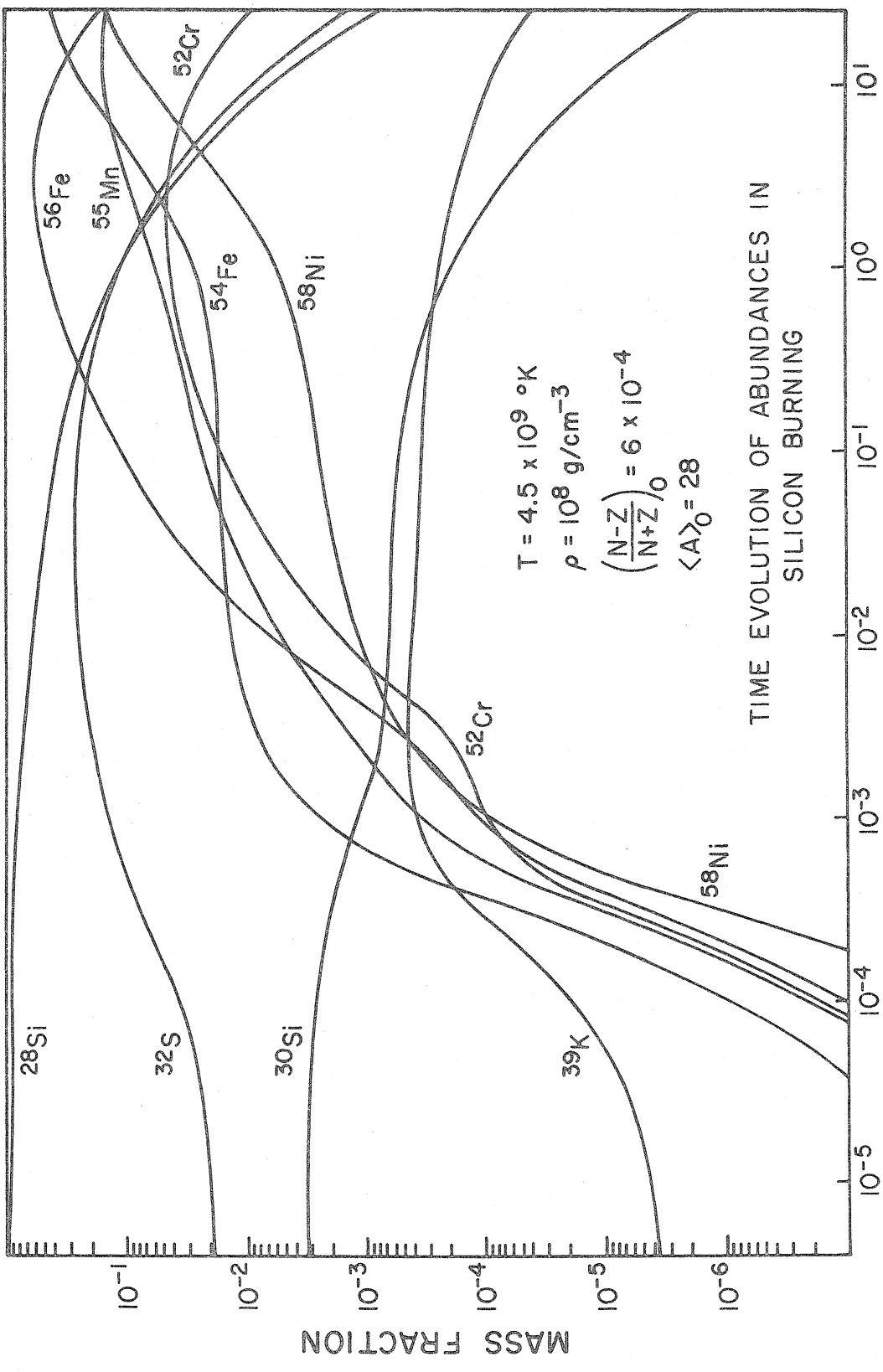
MASS FRACTION
TIME (SEC)
TIME EVOLUTION OF ABUNDANCES IN SILICON BURNING
T = 4.5 x 10^9 °K
ρ = 10^8 g/cm^-3
(N-Z)/(N+Z))_0 = 6 x 10^-4
<A>_0 = 28
28Si
32S
30Si
39K
52Cr
58Ni
56Fe
55Mn
52Cr
54Fe
58Ni

Fig. 13

Fig. 13. Time evolution of Si burning, including beta decays, at $T = 4.5 \times 10^9\ ^{o}K$, $\rho = 10^8\ g/cm^3$. At this temperature and density most of the ^{28}Si has disappeared before beta decays become numerous enough to transform ^{56}Ni into ^{54}Fe. The most abundant iron peak nucleus generated can then be ^{56}Fe (from ^{56}Ni) as observed.

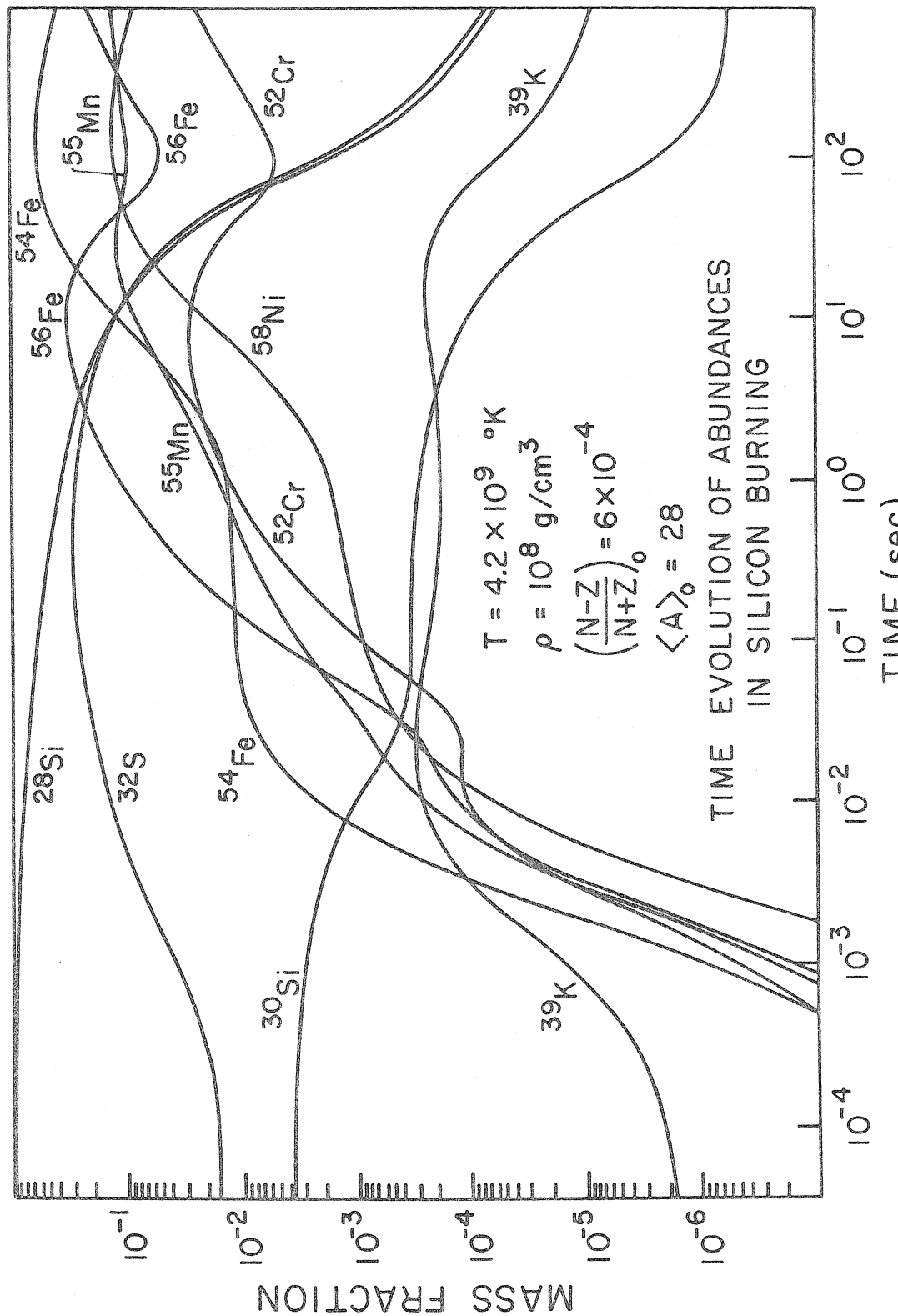
MASS FRACTION
TIME (sec)
TIME EVOLUTION OF ABUNDANCES
IN SILICON BURNING
T = 4.2 × 10^9 °K
ρ = 10^8 g/cm^3
(N-Z)/(N+Z))_o = 6×10^-4
⟨A⟩_o = 28
28Si
32S
54Fe
30Si
39K
55Mn
52Cr
58Ni
56Fe
54Fe
56Fe
55Mn
52Cr
39K

Fig. 14

Fig. 14. Time evolution of Si burning, including beta decays, at $T = 4.2 \times 10^9\ ^oK$, $\rho = 10^8\ g/cm^3$. In this case, ^{54}Fe rapidly becomes the most abundant nucleus. The iron peak generated then does not resemble the one observed.

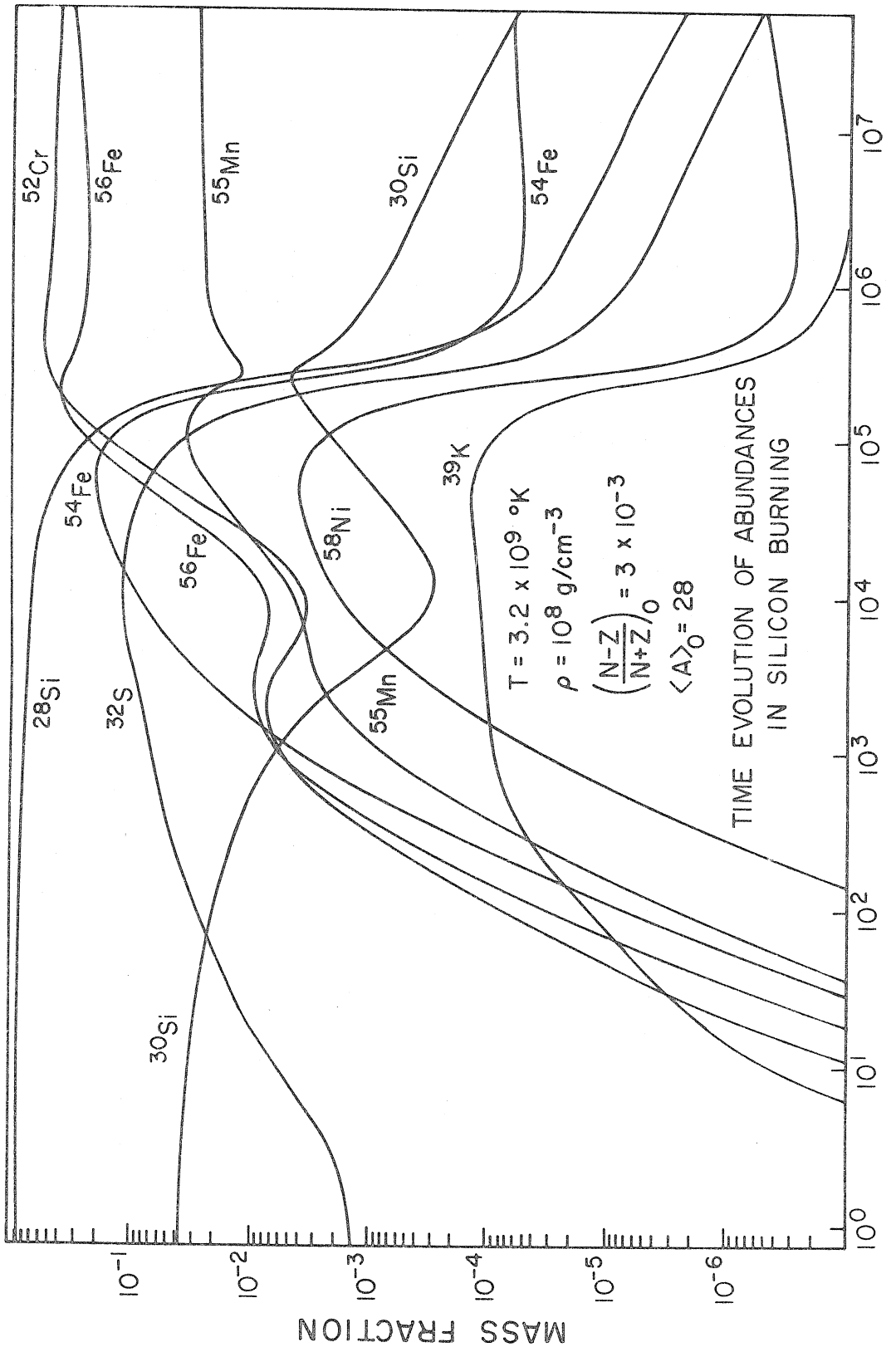
MASS FRACTION
TIME (SEC)
TIME EVOLUTION OF ABUNDANCES
IN SILICON BURNING
T = 3.2 x 10^9 °K
ρ = 10^8 g/cm^-3
(N-Z/N+Z)_0 = 3 x 10^-3
<A>_0 = 28
52Cr
56Fe
55Mn
30Si
54Fe
28Si
32S
54Fe
56Fe
58Ni
39K
55Mn
30Si

Fig. 15

Fig. 15. Time evolution of Si burning, including beta decays at $T = 3.2 \times 10^9\ ^oK$, $\rho = 10^8\ g/cm^3$. The most abundant iron peak element generated is here ^{52}Cr. Comparison of Fig. 13 to 15 points to the generation of the iron peak taking place at $T \gtrsim 4.5 \times 10^9\ ^oK$.

^{31}P, ... are made and those in which ^{56}Fe is made are separated by mass fractions in which ^{54}Fe is the most abundant nucleus. Using our $dM/dT = C$ approximation to sum over the contributions of the different masses, it is then impossible to obtain anything like the observed abundances. One always ends up with too much ^{54}Fe, too little ^{40}Ca, or something.

If $T_9 \lesssim 3.4$, the Cr isotopes will dominate the system for a large fraction of the evolution, before complete equilibrium is reached. It is again impossible to fit all nuclei between ^{28}Si and the iron peak if anything like the $dT/dM = C$ weighing function is appropriate.

It would be possible to obtain something close to the iron peak, except for ^{58}Ni, at equilibrium at $T_9 = 3.8$ as found by Burbidge, Burbidge, Fowler and Hoyle (1957). The elements between ^{28}Si and Ti would then have to be formed in a different process since a discontinuous relation is needed to eliminate the intermediate zones which would lead to abundances very different from the observed ones, but to keep the cooler zones to produce ^{28}Si ... and the hotter ones to produce the iron peak and since it is hard to imagine how one single process could lead to a discontinuous relation for dT/dM.

More generally, if we accept that few beta decays must have occurred during the formation of the elements of mass $29 \leq A \leq 60$, it places severe limitations on the minimum temperature at which the evolution must have taken place and on the corresponding maximum time during which the matter can have stayed and evolved at a

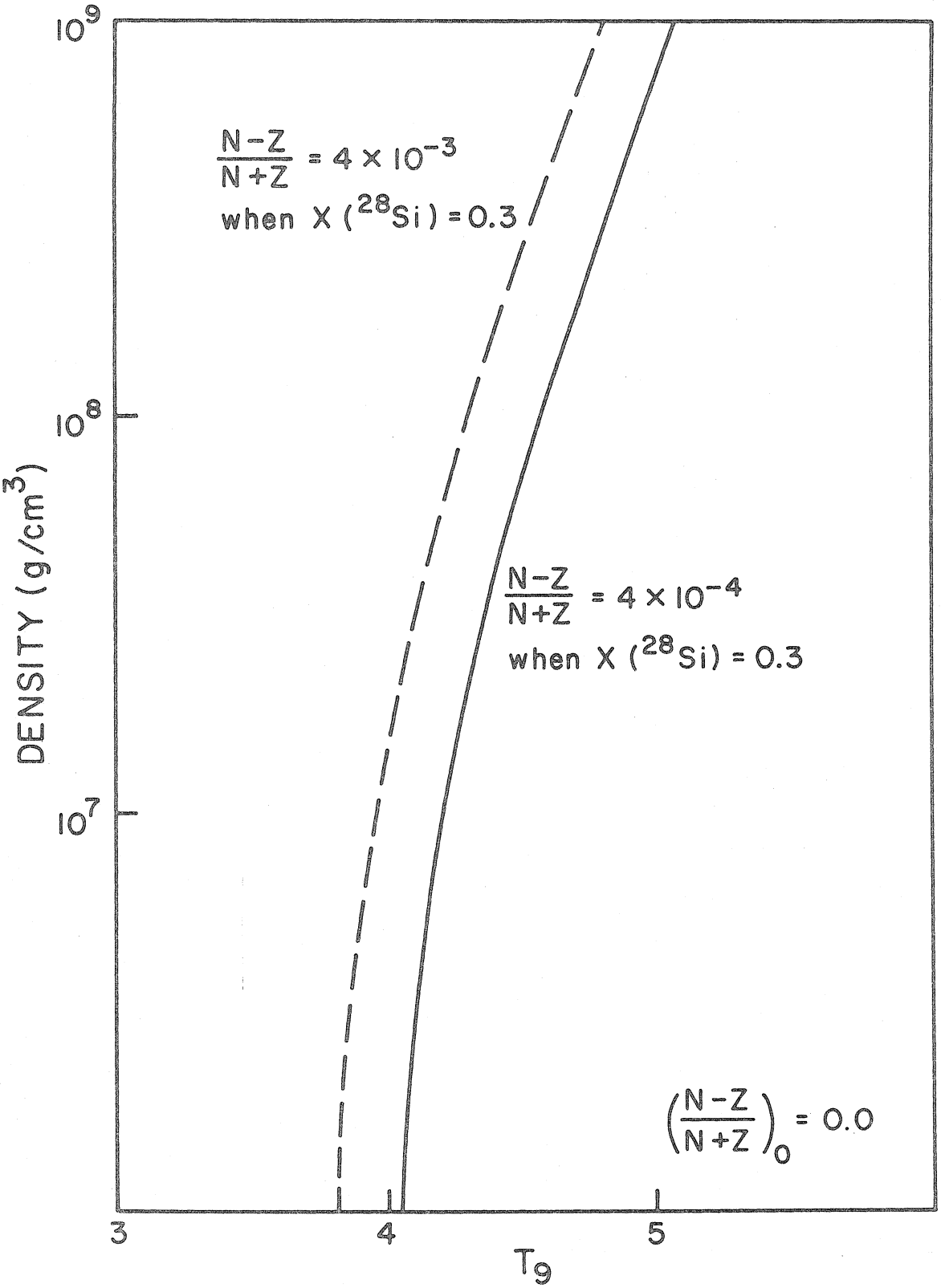
10^9
10^8
10^7
DENSITY (g/cm^3)
$\frac{N-Z}{N+Z} = 4 \times 10^{-3}$
when X (^{28}Si) = 0.3
$\frac{N-Z}{N+Z} = 4 \times 10^{-4}$
when X (^{28}Si) = 0.3
$\left(\frac{N-Z}{N+Z}\right)_0 = 0.0$
3
4
5
T_9

Fig. 16

Fig. 16. To the right of the full line, lies the region where Si burning must have occurred if the elements between ^{28}Si and ^{59}Co have been formed in a single process. To obtain the proper abundance of ^{29}Si, ^{30}Si, ... one needs as much beta decays to have occurred when very little ^{28}Si has been burned as when all has been burned thus imposing the plotted limit on the burning condition.

given density. To generate the iron peak, there must be zones in which the mass fraction of ^{28}Si is down to at most 30%. However, to best represent the low mass elements, there must have been as many beta decays for the matter that evolved little as for the matter that evolved more. Consequently, most of the beta decays should have occurred before ^{28}Si disintegration. Since something like $(N-Z)/(N+Z) = 5 \times 10^{-3}$ fits best the observations, much fewer beta decays than that must have occurred by the time the mass fraction of ^{28}Si is down to 30%. On Fig. 16 we have plotted the $T = f(\rho)$ for $\Delta(\frac{N-Z}{N+Z}) = 4 \times 10^{-4}$ (solid line) and for $\Delta(\frac{N-Z}{N+Z}) = 4 \times 10^{-3}$ (dashed line) coming from beta decays while ^{28}Si is reduced to 30% of its value at $t = 0$. Those curves determine a minimum temperature at which the evolution may have taken place at a given density. It seems to us that $\Delta(\frac{N-Z}{N+Z}) = 4 \times 10^{-4}$ is a more realistic limit, since burning 70% of the ^{28}Si is a minimum to obtain anything like the iron peak.

The minimum temperature at which the evolution may have taken place is then $T_9 \simeq 4.0$ and the corresponding maximum time scale is 10^2 sec (so long as you suppose the evolution to have taken place at densities $\geq 10^6$ g/cc). At $\rho = 10^8$ g/cc, the minimum temperature is around $T_9 = 4.5$ and the maximum time $\simeq 1$ sec. The values of the maximum time were obtained from Fig. 17. It was drawn by determining the time to burn 70% of ^{28}Si at the lowest temperature allowed at a given density.

We shall now investigate how successful can be the fitting of the observed abundances by summing over the zones, if the evolution

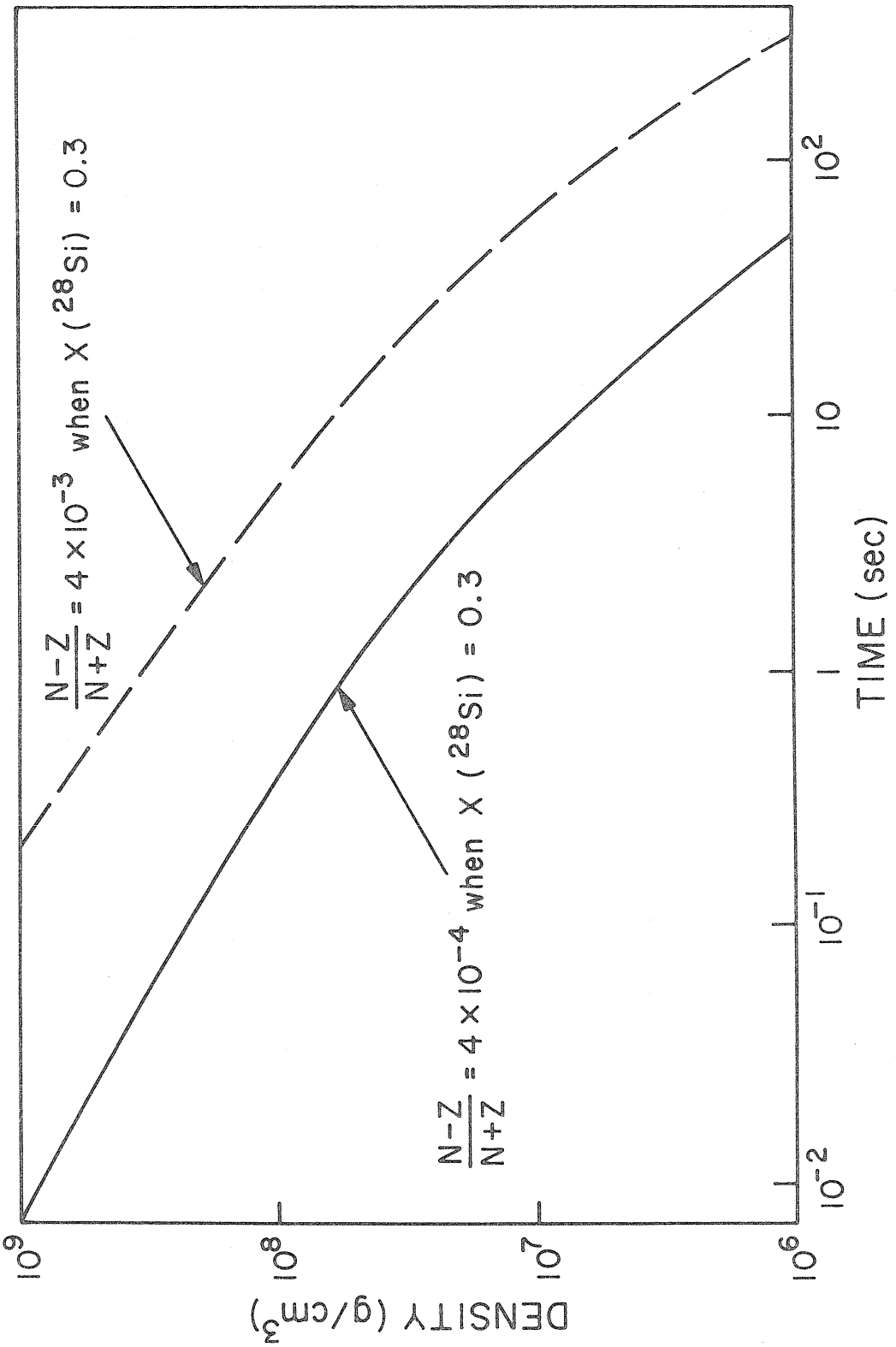
DENSITY (g/cm³)
10⁹
10⁸
10⁷
10⁶
TIME (sec)
10⁻²
10⁻¹
1
10
10²
(N-Z)/(N+Z) = 4 × 10⁻³ when X (²⁸Si) = 0.3
(N-Z)/(N+Z) = 4 × 10⁻⁴ when X (²⁸Si) = 0.3

Fig. 17

Fig. 17. The full line indicates the maximum time allowed for ^{28}Si to get down to 30% of its original value as a function of density. To the right of the full line too many beta decays would occur. The maximum time allowed at a given density corresponds to the minimum temperature plotted in Fig. 16.

took place at $T_9 \geq 4.4$ (see Fig. 13). One must bear in mind what this corresponds to in a real star: the burning lasted about 10 sec at $3.3 \lesssim T_9 \lesssim 4.6$. In the hottest zones ($T_9 \sim 4.6$) all of the ^{28}Si was burned. In those zones, there was appreciable β-decays, enough to transform some of the ^{56}Ni into ^{54}Fe and ^{58}Ni. In the cooler zones, no β-decays occurred; all the neutron enrichment comes from neutron enrichment during C and O burning. One then does not obtain quite enough ^{34}S, ^{38}A, ...

However, the evolution may well have taken place at a slightly higher temperature. As one raises the temperature, one diminishes the time scale, and essentially the same evolution takes place, except that, for a given amount of photodisintegrated ^{28}Si, the accumulated β-decays are less numerous. In other words, the size of the zones in the star in which ^{56}Ni is the most abundant nucleus increases. If the evolution takes place at $T_9 \gtrsim 5.0$, "no" β-decays need have occurred during Si burning in any of the zones of interest. One may then neglect β-decays during Si burning. As shown in Section 6, the evolution is then independent of temperature in so far that, if one increases T_9 by 0.26 but decreases the time scale by one order of magnitude in all zones and then sums over the zones, one obtains the same evolution. This has one important practical consequence: if one takes β-decays equal to zero during the evolution, one may study how freezing will affect the abundances after summing over the zones by carrying out the evolution at different T_9 and using the method described in Section 6 to sum over the zones (see Fig. 18 and 19 and Table 8).

It is then possible to obtain reasonable agreement with the obser-

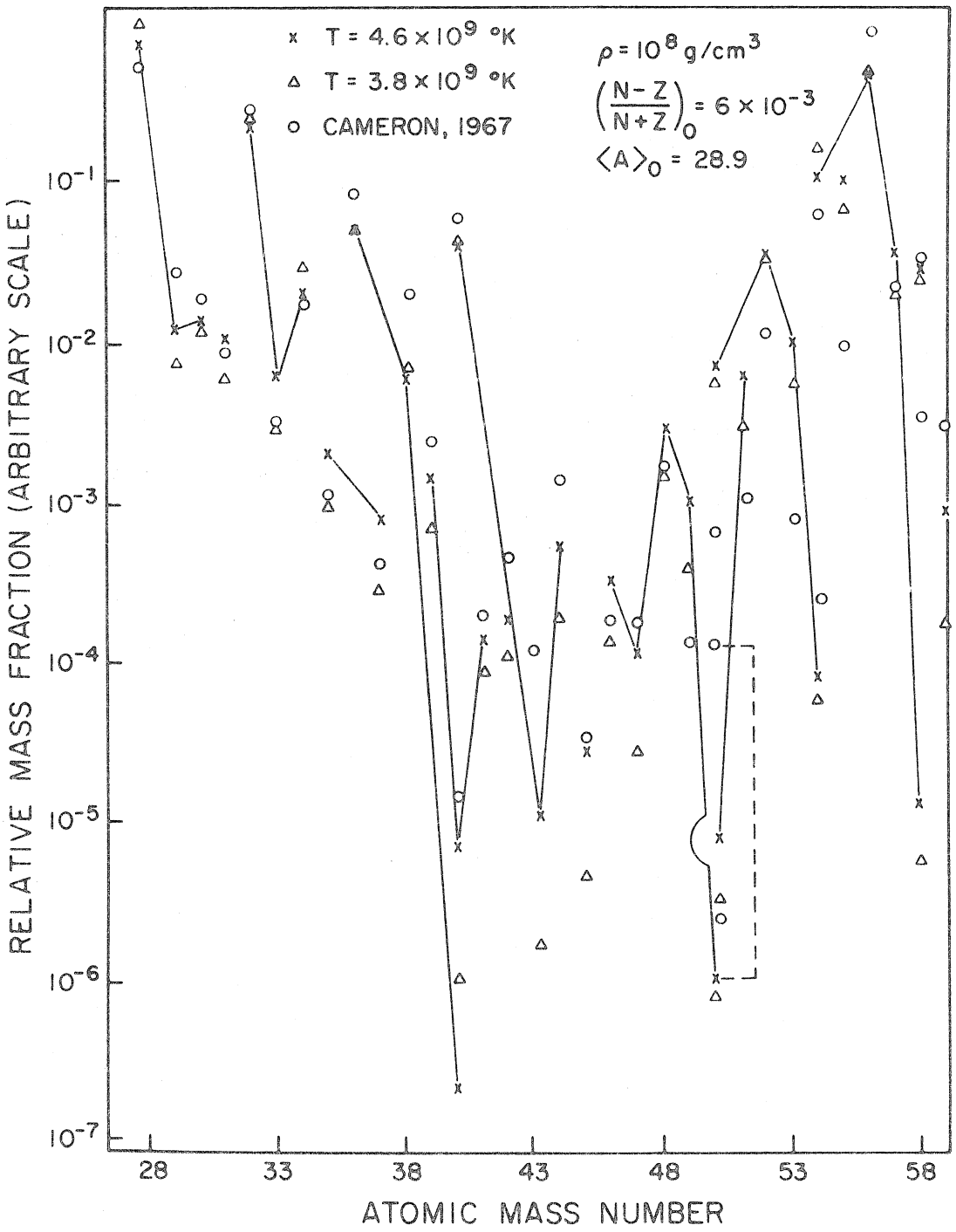
T = 4.6 × 10^9 °K
T = 3.8 × 10^9 °K
CAMERON, 1967
ρ = 10^8 g/cm^3
(N-Z)/(N+Z))_0 = 6 × 10^-3
⟨A⟩_0 = 28.9
RELATIVE MASS FRACTION (ARBITRARY SCALE)
10^-1
10^-2
10^-3
10^-4
10^-5
10^-6
10^-7
28
33
38
43
48
53
58
ATOMIC MASS NUMBER

Fig. 18

Fig. 18. Mass fractions of the observed and calculated abundances. At $T_9 = 4.6$ the summation was carried over Si having burned from 5×10^{-6} sec to 1.5×10^{2} sec corresponding to summation over zones with a range in temperature of $\Delta T_9 \simeq 1.8$. At $T_9 = 3.8$ the summation was carried over Si having burned from 1.5×10^{-2} sec to 2.5×10^{4} sec corresponding to summation over zones with a range in temperature of $\Delta T_9 \simeq 1.5$. The effect of changing the temperature is mainly felt around mass $A \simeq 40$, As discussed in Section 5. one would expect a higher freezing temperature for those elements. The neutron enrichment used here is an upper limit. A higher neutron enrichment would lead to too much ^{54}Fe.

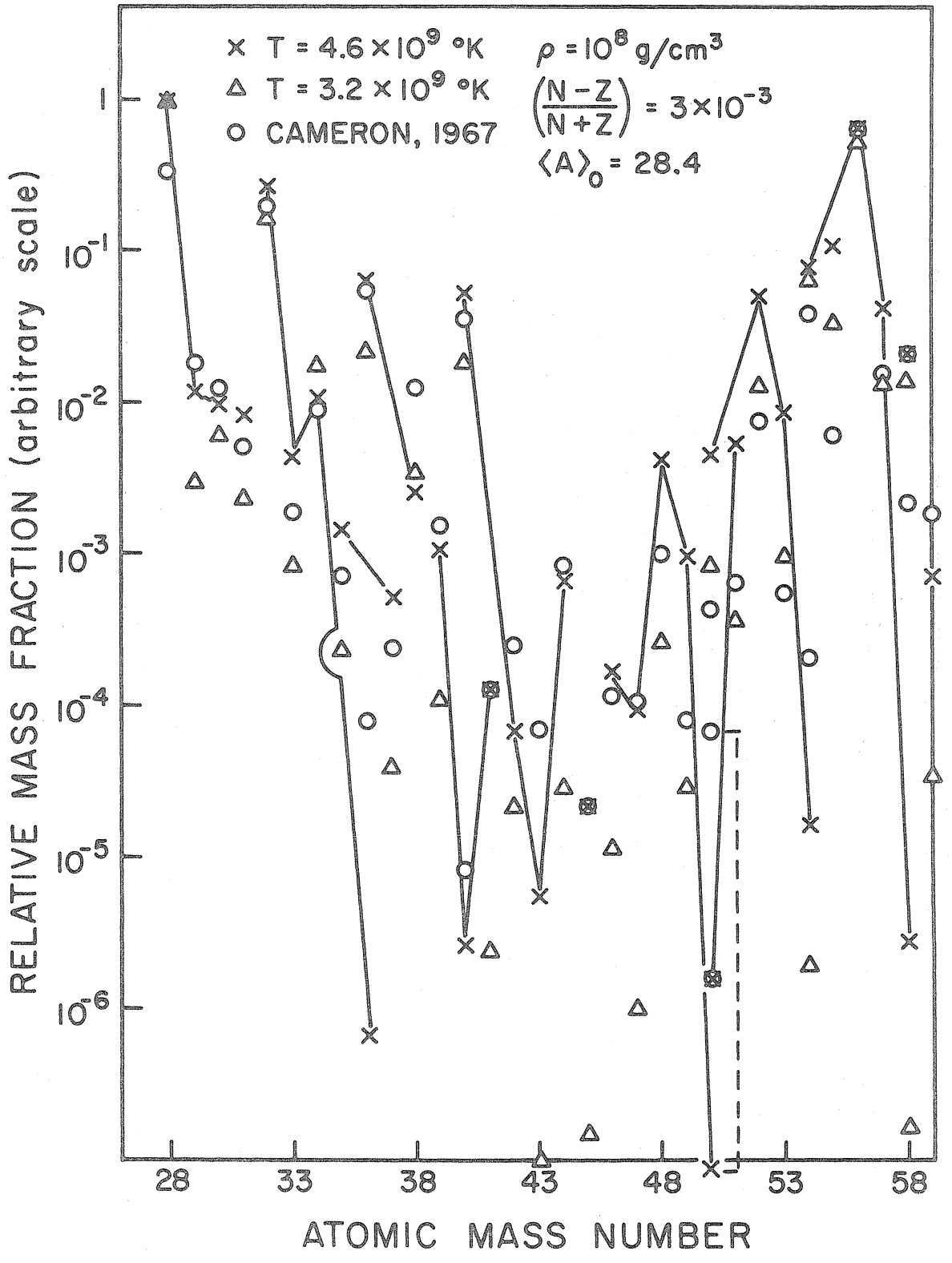
× T = 4.6×10⁹ °K
△ T = 3.2×10⁹ °K
○ CAMERON, 1967
ρ = 10⁸ g/cm³
(N−Z)/(N+Z) = 3×10⁻³
⟨A⟩₀ = 28.4
RELATIVE MASS FRACTION (arbitrary scale)
1
10⁻¹
10⁻²
10⁻³
10⁻⁴
10⁻⁵
10⁻⁶
28
33
38
43
48
53
58
ATOMIC MASS NUMBER

Fig. 19

Fig. 19. Mass fractions of the observed and calculated abundances. At $T_9 = 4.6$ the summation was carried over Si having burned from 4×10^{-6} sec to 4×10^{2} sec corresponding to summation over zones with a range in temperature of $\Delta T_9 \simeq 2$. At $T_9 = 3.2$ the summation was carried over Si having burned from 1 sec to 10^{10} sec corresponding to a range in temperature of $\Delta T_9 \simeq 2.5$. As discussed in Section 5 the higher freezing temperature should apply to low mass elements and the higher temperature to the iron peak elements. This is caused by the freezing of the bottle-neck at $A \simeq 45$ and so shows the importance of an experimental determination of the reactions involved (see Fig. 2). The neutron enrichment used here is a lower limit. A smaller neutron enrichment would lead to too much ^{28}Si.

vations. For instance at $T_9 = 4.6$, 25 out of 41 nuclei between ^{28}Si and ^{59}Co are fitted within a factor of 3.0. The better fitted nuclei are generally those which are least affected by the details of the freezing. The most abundant poorly fitted nucleus, ^{55}Mn, comes from the β-decay of ^{55}Co, which as seen previously has a very small life time for p emission (it goes to ^{54}Fe) and so, will freeze at a lower temperature than the other nuclei. Looking at Fig. 18 and 19 generally confirms what was said previously: those nuclei which control the ^4He and n abundances in the zones in which they are mainly generated are not much affected by the freezing process (^{29}Si, ^{30}Si, ^{32}S, ^{34}S, ^{38}A, ^{40}Ca, ..., ^{54}Fe, ^{56}Fe (from ^{56}Ni), ^{58}Ni ...). Those nuclei which are never the most abundant are most affected by the freezing: ^{35}Cl, ^{37}Cl, ^{40}K, ...

Comparing Fig. 18 to Fig. 19 shows that the observations would be better fitted if there had been more β-decays in the zones producing the low mass elements than in the zones producing the iron peak. Consequently the observed abundances indicate that the evolution took place at a temperature such that no β-decay occurred during Si burning, in any of the zones of importance in generating the abundances between ^{28}Si and ^{59}Co. This required a peak temperature, in the star, of $T_9 \gtrsim 5.0$, and an evolutionary time scale smaller than about 1.0 sec at $\rho = 10^8$ g/cc.

We have mentioned in Section 5 that the abundances we obtain were a function of the neutron enrichment, the fraction of ^{32}S to ^{28}Si when the burning starts, and the limits of integration. We shall now

discuss how varying those "free" parameters affects the abundances we obtain.

The effect of varying the limits of integration can be seen by looking at Table 8 (the lower limit was varied in this case). The lower limit of integration determines how much ^{28}Si, ^{29}Si, ... one obtains. The iron peak elements are not formed very early in the burning and the low mass elements are not formed very late in the burning. The ratio of the two limits of integration, and so the upper limit of integration is then fixed by the observed mass fraction of ^{56}Fe.

We have found that the mass fraction of ^{32}S at $t = 0$ essentially controls the abundance of ^{28}Si, ^{29}Si, ^{30}Si, and ^{31}P. The neutron enrichment (see Table 8) is more important, it controls ^{29}Si, ^{30}Si, ^{34}S, ^{38}A, ^{54}Fe, ^{58}Ni, ... To determine uniquely the abundances generated, evolutionary model calculations will have to determine the temperature reached in the ejected zones within $\Delta T_9 \simeq 0.1$ (a factor of 1.5 in the amount of ^{28}Si burned). This will lift the uncertainty contained in our limits of integration. In the zones in which little ^{28}Si has photodisintegrated, it will be necessary to know (within a factor of 2) the mass fractions of ^{32}S, ^{31}P and ^{28}Si coming from ^{12}C and ^{16}O burning. Finally, it will be necessary to know, in all the ejected zones, the neutron enrichment occurring during the C and O burning phases to within a factor of 1.5 or so.

With four free parameters, we are able to fit, within a factor of 3, the relative values of about 25 out of the observed 41 nuclei between ^{28}Si and ^{59}Co. Some of the nuclei are generated in zones where very little ^{28}Si has been photodisintegrated, others where it has

TABLE 8

The Effect of the Limits of Integration and of Neutron Enrichment

Nucleus	Ratio of the summed abundances**	Ratio of the summed abundances*	Nucleus	Ratio of the summed abundances**
^{28}Si	0.9	2.5	^{45}Sc	1.4
^{29}Si	2.4	3.6	^{46}Pi	3.8
^{30}Si	6.3	4.3	^{47}Ti	2.4
^{31}P	2.1	3.0	^{48}Ti	0.8
^{32}S	0.81	1.2	^{49}Ti	1.5
^{33}S	2.0	2.5	^{50}Ti	21.
^{34}S	5.8	3.5	^{50}V	2.5
^{35}Cl	1.8	2.8	^{51}V	1.5
^{37}Cl	1.8	2.3	^{50}Cr	4.0
^{36}Ar	0.8	1.0	^{52}Cr	1.5
^{38}Ar	5.0	3.1	^{53}Cr	4.0
^{39}K	1.7	1.6	^{54}Cr	20.
^{40}K	5.0	2.1	^{55}Mn	2.2
^{41}K	1.5	1.5	^{54}Fe	5.0
^{40}Ca	0.84	1.0	^{56}Fe	0.8
^{42}Ca	4.0	1.5	^{57}Fe	1.2
^{43}Ca	2.0	1.2	^{58}Fe	24.
^{44}Ca	0.9	1.0	^{58}Ni	5.0
			^{59}Co	3.

*The effect of extending the lower limit of integration by two orders of magnitude in time, corresponding to increasing the temperature range in the star by $\Delta T_9 \simeq 0.5$, for the case $T_9 = 3.2$, $\rho = 10^8$ g/cc, $((N-Z)/(N+Z))_o = 3 \times 10^{-3}$. For $A \geq 44$ the ratio is 1.

**The effect of increasing the neutron enrichment from $((N-Z)/(N+Z))_o = 1.2 \times 10^{-3}$ to 6×10^{-3} at $T_9 = 4.6$ and $\rho = 10^8$ g/cc.

completely disappeared. Some of the more poorly fitted nuclei (^{36}S, ^{40}A, ^{46}Ca, ^{48}Ca) are unabundant neutron-rich nuclei. They could easily have been generated by an exposure of the material to a small neutron flux. Of the other poorly fitted nuclei, some are sensitive to the freezing: for instance ^{55}Mn comes from ^{55}Co which has a very short lifetime to proton photodisintegration. It will then freeze at a lower temperature ($T_9 \simeq 2.5$). Of the better fitted nuclei, some (like ^{32}S, ^{36}A and ^{40}Ca) are nearly independent of any of our free parameters. They are always reasonably well fitted. The observed abundances between ^{28}Si and ^{59}Co then seem to be telling us that they were mainly generated in a quasi-equilibrium process. The modifications of the quasi-equilibrium results one may expect from the physics (like freezing) neglected in quasi-equilibrium calculations tend to make the agreement better. As expected (see Section 5) neutron rich nuclei between ^{28}Si and Ti are better fitted by the higher temperature calculations ($T_9 \gtrsim 4.2$) while the iron peak nuclei are better fitted by the lower temperature calculations ($T_9 \simeq 3.5$).

There is one characteristic of the burning which was not made evident previously but which may be important. On Fig. 13 it is seen that in some of the zones of the star over which we sum, ^{28}Si has completely disappeared. If the zone was burned at $T_9 \gtrsim 6.0$ and if it cooled after that, will complete equilibrium be maintained during the freezing? The first thing to freeze is the 7 $^{4}He \rightleftharpoons {}^{28}Si$ link. This freezes the total number of nuclei above ^{28}Si. As the matter cools, ^{4}He, p and n will try to add themselves to the available nuclei and, if the total number of nuclei above ^{28}Si is too small, will tend to increase the mass fraction

of the higher mass ($A \geq 56$) nuclei above the maximum values they could have in complete equilibrium. This is the type of situation necessary to produce more ^{58}Ni then ^{56}Fe, as noticed by Clayton and Woosley (1969).

Since in quasi-equilibrium calculations, the important parameters are the number of ^{28}Si having disintegrated and the neutron enrichment, it is possible, using quasi-equilibrium calculations, to study the property of the cooling described above. To this end, we have used the method described in Section 3 to calculate the photodisintegration of ^{28}Si, but we changed T and ρ in our equations as the evolution was progressing. The results of our calculations are shown on Fig. 20. The $T(t)$ and $\rho(t)$ relations we used correspond to explosion time scales. It is seen that, in some cases, the $7\alpha \rightleftharpoons {}^{28}Si$ flux freezes above $T_9 = 5$. At such temperatures, there is an appreciable mass fraction of free ^4He even at $\rho = 5 \times 10^7$ g/cc. As the matter cools down, the free ^4He nuclei tend to join with the available $^{28}Si \ldots {}^{56}Fe$. If, when the $7\alpha \rightleftharpoons {}^{28}Si$ reaction freezes there is more free ^4He than needed to transform the ^{28}Si, ^{32}S, ... into the iron peak, the final abundance has more ^{57}Ni, ^{58}Ni, ^{59}Co, ... than complete equilibrium would lead to. It is noteworthy that quasi-equilibrium always underproduces ^{58}Ni and ^{59}Co. It then seems that the observed abundances are telling us that some of the zones of the star were heated to temperatures $T_9 \gtrsim 6.0$. Under such circumstances, ^{58}Ni, ^{59}Co and possibly, at $\rho \lesssim 10^6$ g/cc. ^{60}Ni. ^{61}Ni, ... could be produced in the observed ratios.

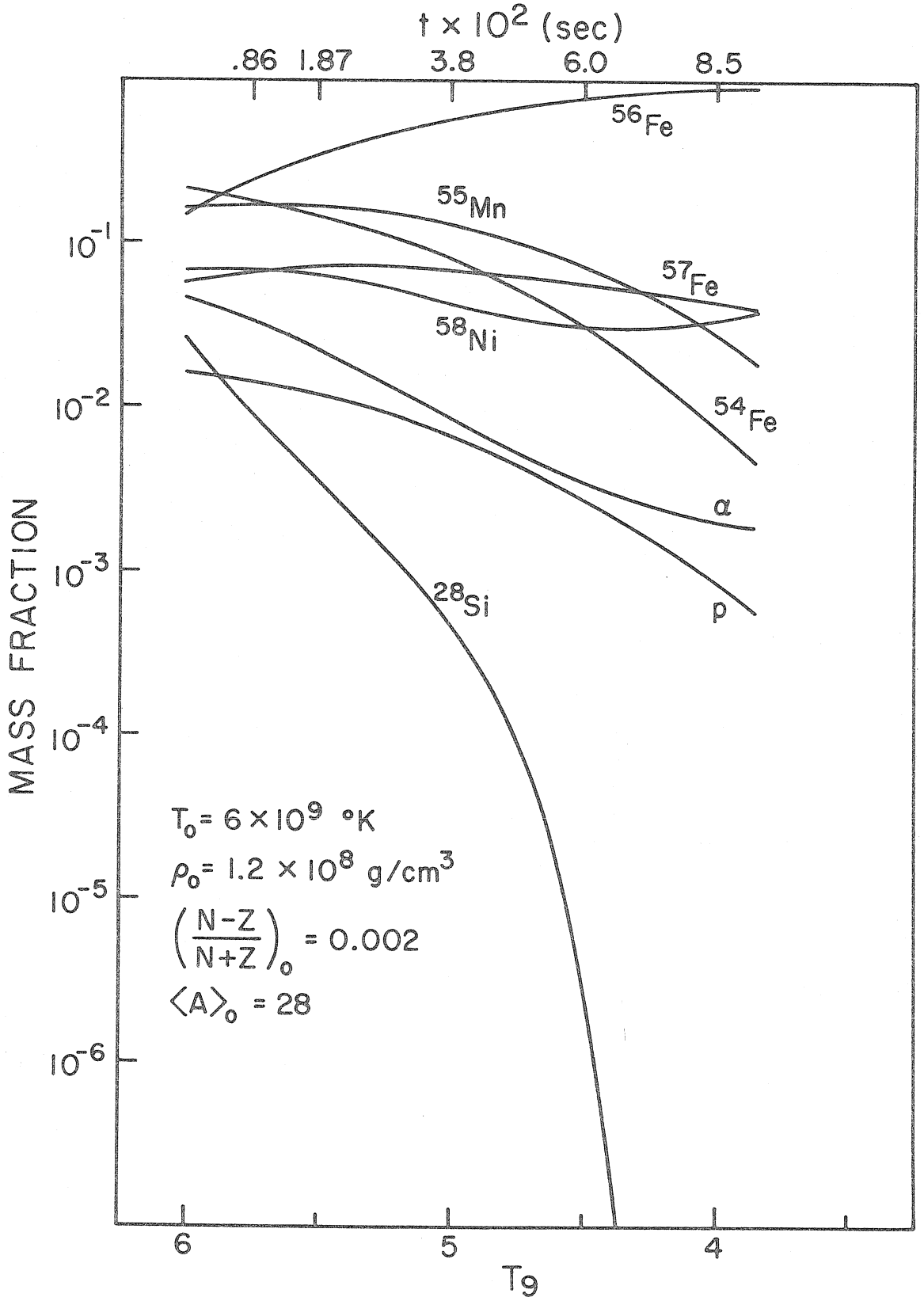
t × 10² (sec)
.86
1.87
3.8
6.0
8.5
56Fe
55Mn
57Fe
58Ni
54Fe
α
p
28Si
MASS FRACTION
10⁻¹
10⁻²
10⁻³
10⁻⁴
10⁻⁵
10⁻⁶
T₀ = 6 × 10⁹ °K
ρ₀ = 1.2 × 10⁸ g/cm³
(N-Z)/(N+Z))₀ = 0.002
⟨A⟩₀ = 28
6
5
4
T9

Fig. 20

Fig. 20. Time evolution of abundances with a dynamic profile. The time variation was taken to be $T_9 = 6 \exp(-t/0.21)$ and $\rho = 1.2 \times 10^8 \times (T_9/6)^{2.7}$. The freezing of the reaction $7\alpha \rightleftharpoons {}^{28}Si$ occurs above $T_9 = 5$ and after that, the ^{28}Si abundance falls below its equilibrium value. This leads to the production of ^{58}Ni, ^{59}Co and perhaps of ^{60}Ni, ^{61}Ni which are always under produced in equilibrium calculations. No difficulty was encountered in using our method of solution with time dependent temperature and density showing that it could be coupled with evolutionary stellar model calculations.

APPENDIX

Many of the nuclear reactions important for astrophysics proceed through a compound nucleus at sufficiently high excitation for the resonances to overlap, or, at least, for many resonances to lie in the energy interval where barrier penetration and Maxwell-Boltzmann factors make the reaction proceed. For those reactions the optical model will be a reasonable approximation for the nuclear physics involved in the particle channels, that is for the emission or absorption of p, n or α. However, it gives no information on the radiation channels (emission or absorbtion of a photon).

It is possible to write the cross section as (Fowler and Hoyle, 1964)

$$\bar{\sigma} = \sum \bar{\sigma}_\ell$$

$$\bar{\sigma}_\ell = 2\pi^2 \lambda\!\!\!^{-2}(2\ell + 1)(\Gamma_1\Gamma_2/D\Gamma)_\ell$$

$$= 2\pi^2 \lambda\!\!\!^{-2}(2\ell + 1)\left(\frac{(\Gamma_1/D)(\Gamma_2/D)}{\Gamma/D}\right)_\ell \qquad (1)$$

$$\frac{\Gamma}{D} = \sum \Gamma_i/D$$

The sums are to be taken over all open reaction channels in the nucleus of interest.

The optical model allows us to determine $(\Gamma_i/D)_\ell$ for the particle channels. But in the (n,γ), (p,γ) and (α,γ) reactions, one also needs $(\Gamma_\gamma/D)_\ell$. Recently a large number of $(n\gamma)$ reactions have been measured in the energy range of interest to astrophysics.

After obtaining an analytic expression for (Γ_γ/D), we fit free constants in that expression by comparing with the experimental results of Macklin and Gibbons (1965 and 1967).

Bethe (1937) has shown that, if the nucleus were a Fermi gas, the density of states would be observed to be:

$$\omega = \frac{C_1'}{(AE)^2} \exp\left(C_2'(AE)^{1/2}\right) \qquad \text{(E in Mev)} \qquad (2)$$

where for a Fermi gas:

$$C_1' = 1.7 \times 10^{-6} \text{ ev}^{-1}$$

$$C_2' = 0.92$$

Here, however, we shall treat C_1' and C_2' as arbitrary constants. A is the number of nucleons in the nucleus. E is the energy at which we are measuring the level density.

This energy is to be measured from the lowest possible level in a Fermi gas. By hypothesis, in a Fermi gas, there is no interaction between the particles. In the nucleus, the pairing and shell structure effects on the binding energy are ample proof of interaction between the nucleons. The interaction between the nucleons presumably lowers the position of the ground state compared to the excited states. Consequently, if one wants to calculate the level density at an energy B above the ground state of the nucleus, we shall use, in (2)

$$E = B' = B - \Delta \qquad (3)$$

where Δ is a correction for the pairing and shell effects.

Fig. 1 gives the variation of the position of the first excited level with neutron number, in even-even nuclei.* We interpret the dashed curve as giving a measure of the pairing of nucleons and of the effect of the deformation of nuclei on the level density (to abbreviate we will refer to the dashed curve as giving "the effect of pairing," keeping the effect of deformation implicit, in what follows). Then, the experimental points give, superimposed to the pairing energy, a measure of the energy needed to break the shell structure.

However exciting the first level does not require breaking completely the pairing or the shell structure. One rather expects that excitation of the first level would require, as a mean, a given fraction of the pairing or "shell structure" energy. So for an odd-odd nucleus, one expects:

$$\Delta_{oo} = C_3 \left[\sum_{i=1}^{4} \frac{E_{1i}}{4} - \delta(N) \right] \tag{4}$$

where E_{1i} is the excitation energy of the first level of the four even-even nuclei bracketing the odd-odd nucleus of interest, and $\delta(N)$ is the part of E_{1i} due to the pairing (read from the dashed curve in Fig. 1). $1/C_3$ is to be interpreted as the fraction of the "shell energy" broken, as a mean, in the first excited level.

For an even-odd or odd-even nucleus,

$$\Delta_{eo} = C_3 \left[\sum_{i=1}^{2} \frac{E_{1i}}{2} - \delta(N) \right] + C_4 \delta(N) \tag{5}$$

---

*Taken from Nuclear Data Sheets.

where the sum is to be taken over the two even-even nuclei bracketing the even-odd or odd-even nucleus, and where $1/C_4$ is interpreted as the fraction of the pairing energy required to excite the first level. For the even-even nuclei, exciting the first level breaks only one pair (the paired neutrons or the paired protons). To represent the pairing energy of the unbroken pair, we add a constant term to the expression for the even-odd or odd-even nuclei:

$$\Delta_{ee} = C_3[E_1 - \delta(N)] + C_4\delta(N) + C_5 \tag{6}$$

The constants are to be determined as explained below. But we first need an analytic expression for Γ_γ/D.

For magnetic or electric dipole transitions, one has (Blatt and Weisskopf, 1952), in the single particle model:

$$\Gamma_\gamma(B) = CR^2\int_0^B (B-E)^3 \frac{D(B)}{D(E)}\, dE$$

where the ground state is taken at $E = 0$; or since we need only Γ_γ/D:

$$\frac{\Gamma_\gamma(B)}{D(B)} = CR^2 \int_0^B (B-E)^3 \frac{1}{D(E)}\, dE \tag{7}$$

(2) into (7) gives:

$$\frac{\Gamma_\gamma}{D} = \frac{C_1''}{A_c^{3.333}} \int_0^X (X^2-x^2)^3 \frac{1}{x^3} \exp(x)\, dx \tag{8}$$

with

$$X = C_2'(A_c B)^{1/2}$$

and A_c = number of nucleons in the nucleus and $R^3 \propto A_c$.

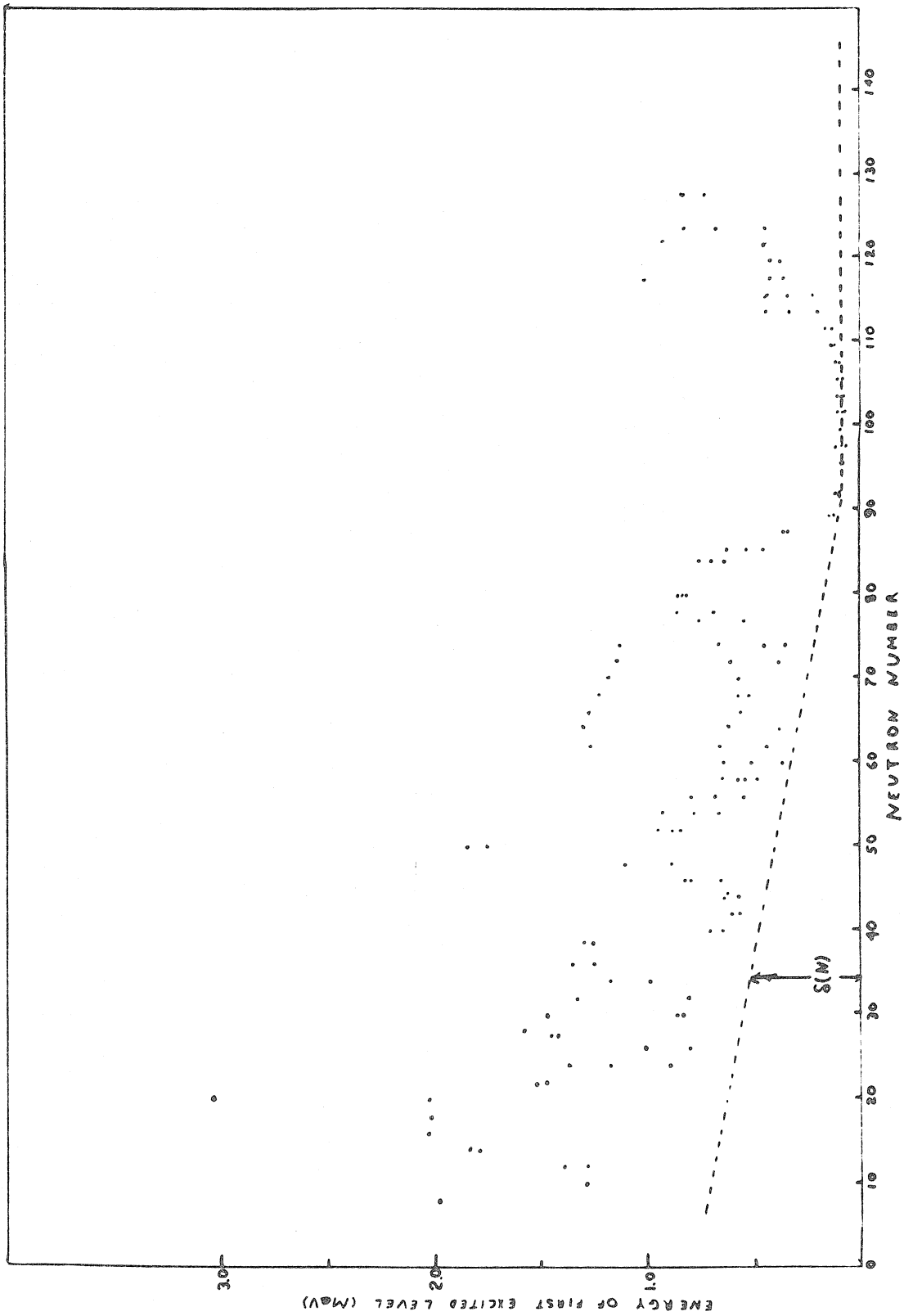
ENERGY OF FIRST EXCITED LEVEL (MeV)
3.0
2.0
1.0
0
10
20
30
40
50
60
70
80
90
100
110
120
130
140
NEUTRON NUMBER
δ(N)

Fig. 1

Fig. 1. Excitation energy of the first level above the ground state. The dashed line gives a measure of the effects of pairing and of deformation.

The integrand diverges at $x = 0$. However (2) cannot be an accurate representation of the level density as x goes to zero. Actually (2) does apply only for $d\omega/dx \gtrsim 0$. The lower limit at which (2) can be used is then $x = 4$. We approximate (8) by

$$\frac{\Gamma_\gamma}{D} = \frac{C_1''}{A_c^{3.333}} \int_4^X (X^2 - x^2)^3 \frac{1}{x^3} \exp(x)\, dx \qquad (9)$$

We integrate (9) by developing $1/x^3$ in series around X and keeping terms up to the fifth order. We then obtain:

$$\frac{\Gamma_\gamma}{D} = \frac{48\, C_1''}{A_c^{3.333}} e^X \left\{1 + \frac{6}{X} + \frac{70}{X^2}\right\}$$

$$\simeq \frac{48 C_1''}{A_c^{3.333}} e^{X + \frac{6}{X}} \qquad (10)$$

or

$$\log_{10}(\Gamma_\gamma/D) = -C_1 - 3.333 \log_{10} A_c + C_2 (A_c B)^{1/2} + 1.13/[C_2 (A_c B)^{1/2}] \qquad (11)$$

We have neglected the lower limit which to the fifth order contributes less than 20% if $X \geq 10$. (Note that if we go to higher orders in the development of $1/x^3$ both the upper and lower limits diverge. Only the difference between the two tends toward a well-defined limit.) By integrating (9) numerically for different values of X ($10 \leq X \leq 40$) we have verified that (10) estimates (9) within 20%.

We determine the systematic behavior of Γ_γ/D by comparing

our analytical result with the experimental values of $\langle \sigma v \rangle / v_T$ for the (n, γ) reactions, as given in Macklin and Gibbons (1965). To do that, however, we need $(\Gamma_n/D)_{\ell=0,1,2}$. For $(\Gamma_n/D)_{\ell=0}$ we have used the experimental values given in Newson (1965) for $54 \leq A \leq 208$. We have used "theoretical" values (Campbell et al. 1960) for $(\Gamma_n/D)_{\ell=1,2}$. Then (Fowler and Hoyle, 1964)

$$\frac{\langle \sigma v \rangle}{v_T} = \frac{2}{\pi^{1/2}} \int_0^\infty \sigma \, (E/kT) \exp(-E/kT) \, d(E/kT) \qquad (12)$$

Since $(\Gamma_n \Gamma_\gamma / \Gamma D)_\ell$ in (1) is a slowly varying function of E, estimating it at $E = kT$ gives a good approximation to (12). This gives an analytic expression with the help of which it is easy to determine the constants from the experimental data. We have used, to determine C_1 and C_2, the $(n\gamma)$ reactions leading to odd-odd compound nuclei for which $\Delta \sim 0$. Then the reactions leading to the odd-odd compound nuclei with $\Delta \neq 0$ were used to determine C_3. C_4 is then determined with the help of C_1, C_2, and C_3 by fitting reactions leading to even-odd compound nuclei. Finally C_5 is determined by using the even-even compound nuclei.

Once we have that first approximation to the constants, we can integrate (12) numerically, taking into account the variation of $(\Gamma_n \Gamma_\gamma / D\Gamma)$ with energy. We can then adjust the constants to get a best fit.

The final comparison is shown on Fig. 2. For $A \leq 176$, 6 cases lie outside a factor of 2.5. There were five reactions leading to even-odd compound nuclei for which the first level of only one

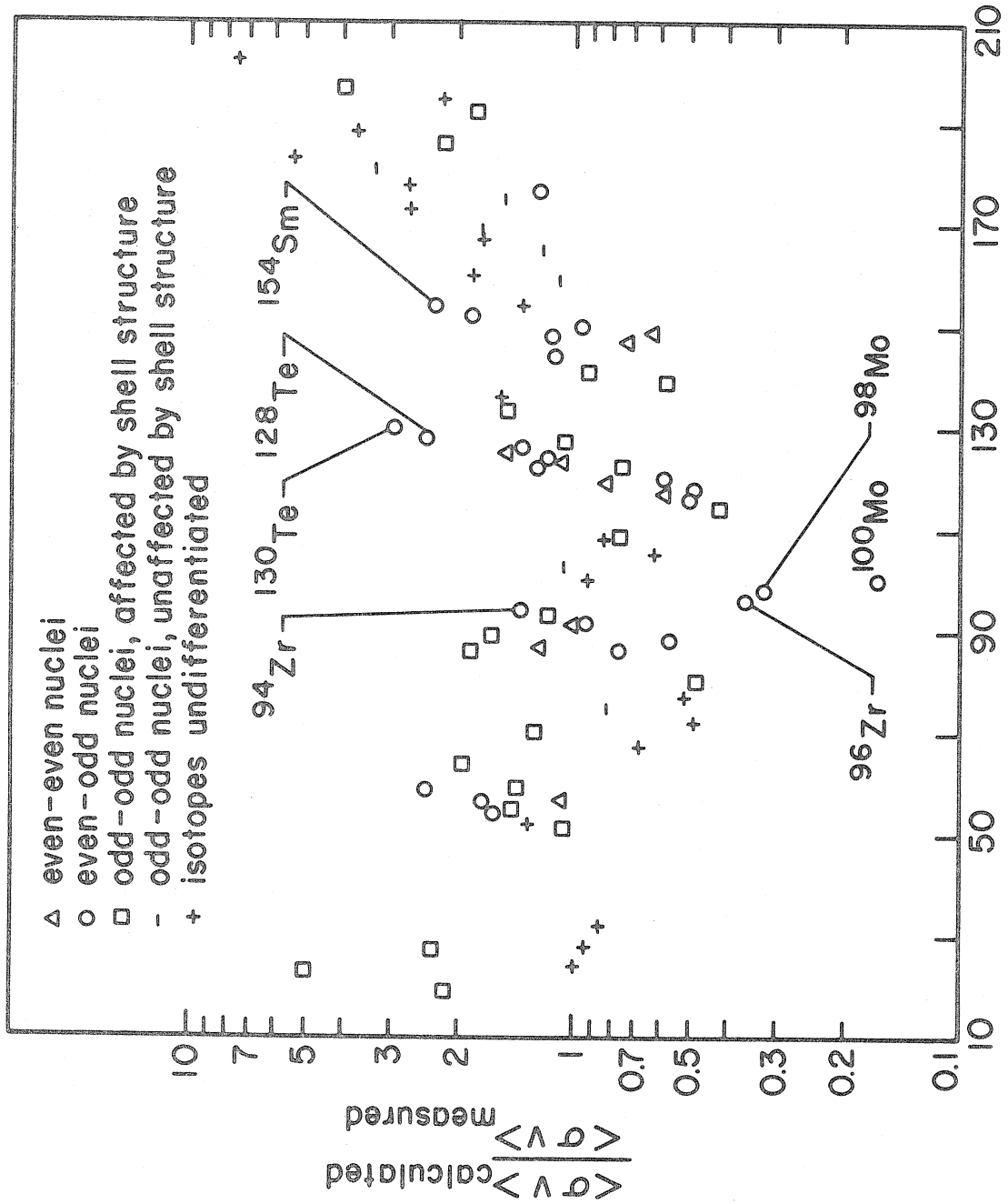
△ even-even nuclei
○ even-odd nuclei
□ odd-odd nuclei, affected by shell structure
- odd-odd nuclei, unaffected by shell structure
+ isotopes undifferentiated
94Zr
130Te
128Te
154Sm
96Zr
100Mo
98Mo
10
7
5
3
2
1
0.7
0.5
0.3
0.2
0.1
10
50
90
130
170
210
ATOMIC MASS NUMBER
⟨σv⟩calculated / ⟨σv⟩measured

Fig. 2

Fig. 2. Comparison of the calculated and experimental values (Macklin and Gibbons, 1965, 1967) of $\langle \sigma v \rangle$. For $A < 175$ there are about 70 measured cross sections. For six of these our calculated value is outside a factor of 2.5 from the measured value. Our calculations were done with $C_1 = 3.72$, $C_2 = 0.286$, $C_3 = 1.8$, $C_4 = 3.8$, $C_5 = 1.3$. The atomic mass numbers refer to the compound nuclei. The nuclei mentioned are, also the compound nuclei.

of the bracketing even-even nuclei were known: $^{94}Zr(n\gamma)$, $^{96}Zr(n\gamma)$, $^{100}Mo(n\gamma)$, $^{130}Te(n\gamma)$ and ^{154}Sm. These nuclei seem to be poorly fitted. These "systematic" formulas neglect the effect of the deformation of nuclei. For $A \leq 176$, it seems that the arbitrary constants adjust themselves to fit successfully the experimental results, without any consideration of deformation. But this might cause the divergence for $A > 176$. The poor fit for $A > 176$ might also be related to the effect of the two closed shells at lead. They start to be felt at $A \sim 173$ in the position of the first excited level.

REFERENCES

Bethe, H. A. 1937, Rev. Mod. Phys. 9, 69.

Blatt, M. and Weisskopf, V. F. 1952, Theoretical Nuclear Physics John Wiley and Sons, Inc., New York.

Bodansky, D., Clayton, D. D. and Fowler, W. A. 1968, App. J. Suppl. 16, 299.

Burbidge, E. M., Burbidge, G. R., Fowler, W. A. and Hoyle, F. 1957, Rev. Mod. Phys. 29, 547.

Campbell, E. J., Feshbach, H., Porter, C. E., Weisskopf, V. F. 1960, MIT (Nucl. Phys. Lab) Technical Report No. 73.

Clayton, D. D. and Woosley, S. E. 1969, to be published.

Clifford, F. E. and Tayler, R. J. 1965, Mem. RAS 69, 21.

Fowler, W. A. and Hoyle, F. 1964, Ap. J. Suppl. 91, 1.

Fowler, W. A., Caughlan, G. R. and Zimmerman, B. A. 1967, Ann. Rev. Astr. and Ap. 5, 525.

Fowler, W. A. 1968, private communication.

Hansen, C. J. 1966, unpublished Ph.D. Thesis, Yale University, New Haven, Connecticut.

Harchol, M., Jaffe, A. A., Miron, J., Unna, I. and Zionni, J. 1967, Nucl. Phys. A90, 459.

Hoyle, F. 1946, MNRAS, 106, 343.

Macklin, R. L. and Gibbons, J. H. 1965, Rev. Mod. Phys. 37, 166.

Macklin, R. L. and Gibbons, J. H. 1967, Ap. J. 150, 721.

Mattauch, J. H. E., Thiele, W. and Wabstra, A. H. 1965, Nucl. Phys. 67, 1.

Michaud, G., Scherk, L. and Vogt, E. W. 1969, to be published.

Newson, H. W. 1965, Proc. of the Int. Conf. on Study of Nuclear Structure with Neutrons, Antwerp (North Holland Publishing Co., Amsterdam).

Preston, M. A. 1962, Physics of the Nucleus, Addison Wesley Publishing Co., p. 150.

Truran, J. W., Cameron, A. G. W. and Gilbert, M. 1966, Can. J. Phys. 44, 563.

Truran, J. W. 1969, private communication.

Vogt., E. 1962, Rev. Mod. Phys. 34, 723.

Vogt, E., Michaud, G. and Reeves, H. 1965, Phys. Letters, 19, 570.

Vogt, E. 1968, in Advances in Nuclear Physics V-1, Edited by M. Baranger and E. Vogt (Plenum Press, New York) pp. 261-342.